Recent advances on magnetic carbon-related materials in advanced oxidation processes of emerging pollutants degradation

Elvana Çako [a,*], Kumaravel Dinesh Gunasekaran [b], Saravanan Rajendran [c], Anna Zielińska-Jurek [a,**]

[a] *Department of Process Engineering and Chemical Technology, Faculty of Chemistry, Gdańsk University of Technology, G. Narutowicza 11/12, 80-233, Gdańsk, Poland*
[b] *Trinity College Dublin, The University of Dublin, College Green, Dublin 2, D02 PN40, Ireland*
[c] *Department of Mechanical Engineering, Faculty of Engineering, University of Tarapacá, Avda, General Velasquez, 1775, Arica, Chile*

A B S T R A C T

Recently, carbon-related materials have been proposed to improve the charge separation of the photogenerated carriers in the semiconductor matrices' and surface properties. Carbon-related materials may act as co-catalysts, enhancing the pollutants adsorption on the surface, improving the charge carriers separation and photocatalyst stability and providing more active centres for photocatalytic reactions. This review summarizes recent advances in the preparation and environmental application of carbon-related materials. The focus was set on preparation of carbon-related materials and magnetic carbon-related photocatalytic materials with the property of easy separation after the purification process in an external magnetic field and their application for degradation of emerging pollutants not susceptible to biodegradation. The present studies identify four main groups of water pollutants: pesticides, pharmaceuticals, industrial chemicals, and heavy metals. Among them, pharmaceuticals and phenolic compounds represent a significant group of persistent organic pollutants. Some of the commonly used pharmaceuticals for human health, as well as disinfectants, are found in wastewater influents and effluents (after the purification process) almost in the unchanged form. Their detection in trace amounts (of about a few micrograms to hundreds of nanograms per litre) and removal become difficult but important because they put at risk the reuse of treated wastewater and the sustainability of water cycle management. Concerning levels of concentrations, these compounds are classified as hazardous due to possibilities of bioaccumulation, biomagnification and toxic impact on living organisms, even in trace amounts. Up to now, various methods have been reported in the removal of pharmaceuticals and phenolic compounds from aqueous systems.

Heterogeneous photocatalysis belonging to the group of advanced oxidation processes (AOPs) is one of the most promising methods used for the degradation of emerging pollutants. Introducing carbon-related materials modified by magnetic ferrites can significantly improve the efficiency of emerging contaminants' degradation. This review provides coherent information for future studies in the application of carbon-related materials and magnetic carbon-related materials for the removal of active pharmaceutical ingredients and phenolic compounds. Insights on pharmaceutical and phenolic compounds photodegradation in the presence of carbon-based materials combined with magnetic ferrites and their combination with SR-(AOPs) and Fenton-

---

* Corresponding author.
** Corresponding author.
E-mail addresses: elvana.cako@pg.edu.pl (E. Çako), annjurek@pg.edu.pl (A. Zielińska-Jurek).

type photocatalysis are for the first time discussed. Moreover, the effect of various parameters such as water matrice, pH, natural organic matter presence, and temperature were also discussed. Finally, the economic feasibility and consideration of photocatalyst recovery capability completed the concept and discussion on magnetic carbon-related materials.

1. Introduction

Rapid industrialization and population growth contribute to the deterioration of water quality through the discharge of hazardous pollutants. It was predicted that by 2022, the pharmaceutical industry would know a growth rate of 6.5 % per year, which means that a vast amount of pharmaceuticals are being produced due to increased consumer demand [1]. The pharmaceutical and biotechnology sectors were rated to have the highest ratio of research and development investment to net sales compared to other industrial sectors in the European Union in 2019, as presented in Fig. 1 (a) [2]. The trend predicts that the pharmaceutical industry will further grow in the upcoming years. With the intensification of climate change, more diseases and infections will affect societies [3]. The pharmaceutical industry is considered to be on the front line of challenges that the planet faces during transitory times. Despite the numerous advantages the pharmaceutical industry has provided humankind, it is worth mentioning that some detrimental and irreversible impacts

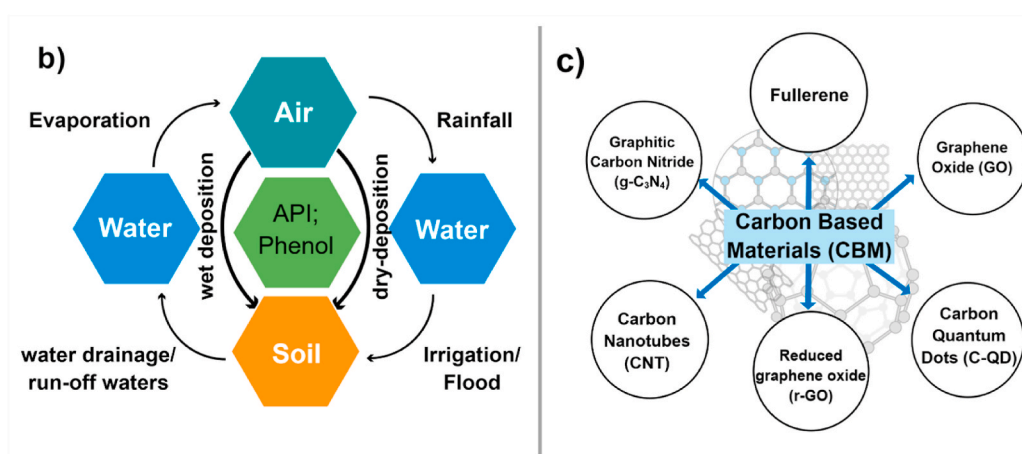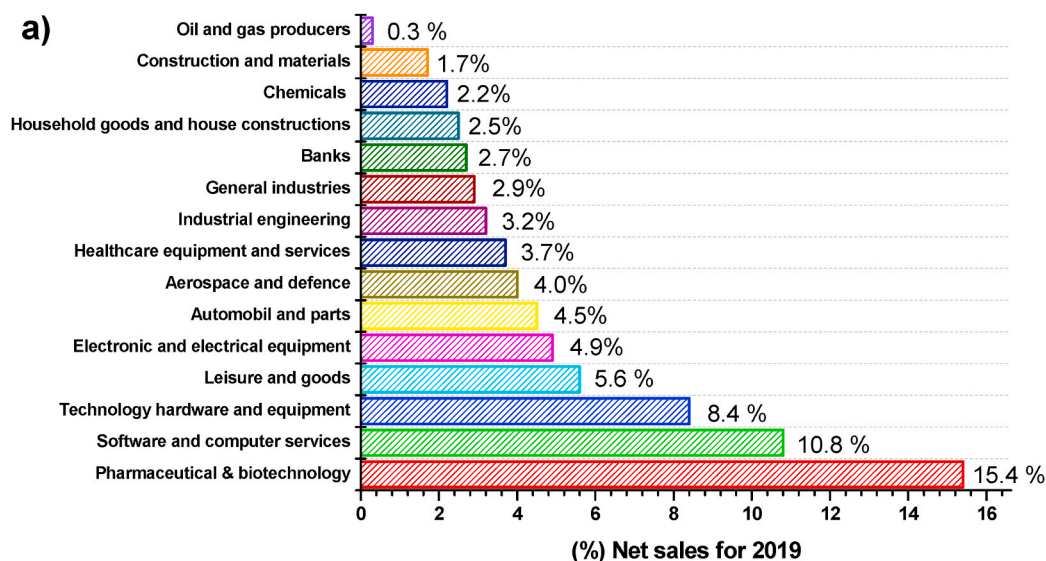**Fig. 1. a)** Ranking of industrial sectors, with data referred to 2500 companies worldwide in the EU (551), Japan (318), US (769), China (507), and the Rest of the World (355) [2]; **b)** Distribution cycle of active pharmaceuticals ingredients and phenolic compounds in the ecosystem; **c)** Carbon-based materials (CBM) used in photocatalysis for the removal of the selected group of pollutants.

Table 1
Pharmaceutical active compounds in wastewater systems in different countries.

Country	Source of Study	Class of Pharmaceutical compound	Active compound present	Concentration detected	Method of detection	Ref.
Poland	Warta river	Non-steroidal anti-inflammatory drugs Anti-inflammatory analgesic drug antibiotics antiepileptics	Ibuprofen Diclofenac Ketoprofen Naproxen	0.1346 µg/L 0.1851 µg/L 0.2327 µg/L 0.1046 µg/L	HPLC-ESI-MS/MS	[19]
Latvia	wastewater treatment plant in Riga	central nervous system stimulator analgesic antibiotic non-steroidal anti-inflammatory drug	Caffeine Acetaminophen Ciprofloxacin ibuprofen	12 µg/L 4 µg/L 200–400 ng/L 100–325 ng/L	HPLC-MS	[20]
USA	Water treatment plant, New Jersey USA	non-steroidal anti-inflammatory drug stimulants Antidepressants	Ibuprofen Caffeine iopamidol, trimethoprim	233 ng/L 0.2–24.4 ng/L 984 ng/L 232 ng/L	LC-MS	[21]
Costa Rica	Wastewater treatment plant	non-steroidal anti-inflammatory drug Stimulant Analgesic	Ibuprofen Naproxen Caffeine Acetaminophen	60 µg/L 64 µg/L 120 µg/L 14.9 µg/L	UHPLC-MS	[22]
China	Yellow river, Beijing	Analgesic Antibiotic non-steroidal anti-inflammatory drug	Acetaminophen Norfloxacin Ibuprofen	341.9 ng/L 382.3 ng/L 527.4 ng/L	HPLC-MS/MS	[23]

on living organisms and ecosystems have raised concerns. In recent years, it was reported that a considerable concentration of pharmaceuticals not susceptible to biodegradation is present in fresh waters, maritime, and wastewaters worldwide [4,5]. The major groups of concern of active pharmaceutical ingredients (API) belong to hormones, antibiotics, analgesics, antidepressants and anti-cancer drugs [6–8]. The mixture of pharmaceuticals and other contaminants in water bodies increases their toxicity to the ecosystem because more adverse effects can be observed in combination with other pollutants. It can be manifested in the form of substantial biological changes and extreme cases such as species extinction [9].

Around 4000 active pharmaceutical ingredients (API) are found to be used worldwide, from which 30–90 % of oral doses are excreted as active substances [10]. The concentration of organic pollutants in the environment is closely dependent on geographical and seasonal factors, and their mobility in soil is determined by the soil/water partition coefficient, differently called organic carbon adsorption coefficient (K_{oc}) [11]. Pharmaceuticals that tend to have low (K_{oc}), will pass in an aqueous system through drainage waters, while high (K_{oc}) pharmaceuticals will pass into water bodies through run-off waters [11]. The presence of pharmaceutical compounds and their concentration in the wastewater systems in different continents is presented in Table 1. In the previous studies the presence of pharmaceutical compounds in the influents and effluents of wastewater treatment plants (WWTPs) was described. For example, Pérez-Lemus et al. [12], Quesada et al. [13], Pesqueira et al. [14], and Spataro et al. [15] reported the presence of pharmaceuticals in a water environment. Moreover, various antibiotics, including sulfamethoxazole, erythromycin, triclosan, and trimethoprim, have been identified in the WWTPs influent situated in Southern California. Their concentrations ranged from 1.860 to 2.146 µg/L, 0.0167–0.278 µg/L, 0–0.410 µg/L, and 0.407–1.021 µg/L, respectively [16].

It has been reported that the release of pharmaceuticals into surface waters induced severe changes in the endocrine system of wild fish species [17]. The presence of different classes of pharmaceuticals has been found in many water bodies in relatively harmful concentrations. There are many ways that pharmaceuticals enter the aqueous systems. They are released through industrial effluents, hospital and veterinary waste discharges, human and animal excreta, treated sewage sludge, biosolids, and landfill leachates Fig. 2 (a) [18].

Phenolic compounds are the next group of compounds that are extensively found in the environment, as presented in Fig. 2 (b). They originate from natural and anthropogenic sources. Natural sources of phenol include the decomposition of inorganic matter, synthesis by microorganisms, and synthesis by plants [24–26]. Related to anthropogenic sources, phenol discharges from municipal, agricultural, domestic, and industrial effluents. Discharged effluents from various industries like petrochemical, pharmaceuticals, food processing, metallurgy, plastics, paint, agricultural, rubber, and textile industries are the main sources of phenol and its derivatives [27]. The presence of phenol in the environment has adverse effects on aqueous and terrestrial biota, and its estimated concentration has been reported to be in the range of 1–100 mg/L [28]. It was reported that 3.6 % of soil and groundwater contaminants constitute of phenol and its derivatives (European Environment Agency EEA, 2019) [29]. Interaction of phenol with other organic and inorganic compounds leads to the formation of other by-products, which can be more toxic than their parent molecule [30].

In this regard, it is necessary to provide advanced treatment methods of effluents containing trace amounts of persistent organic pollutants before their discharge in aqueous systems. The main group of treatment methods consists of conventional treatment and advanced oxidation processes. The conventional treatment methods are performed using the activated sludge microorganisms, coagulation, filtration, sand filtration, and electrokinetic remediation [31]. At the same time, advanced wastewater treatment
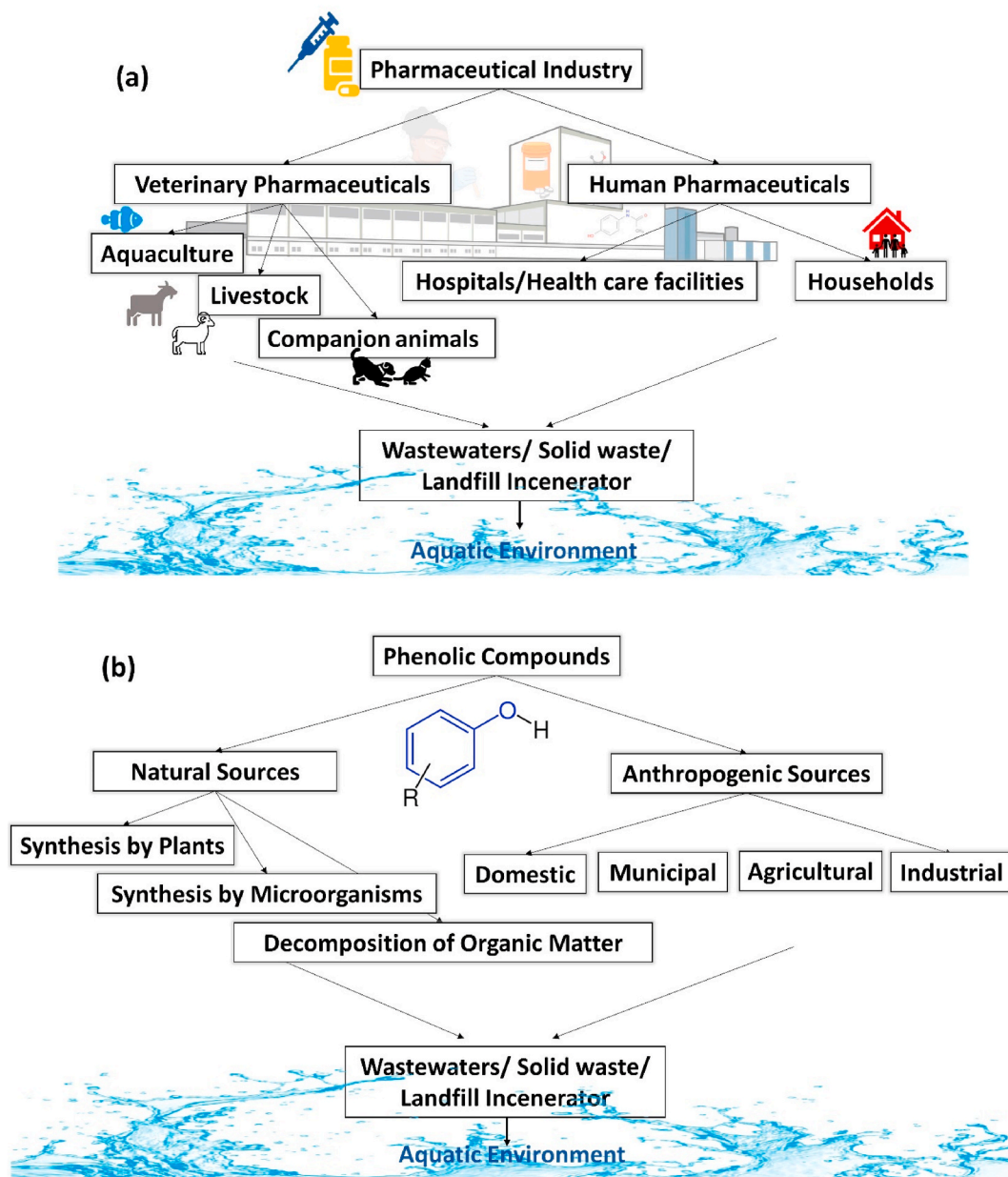
Fig. 2. a) Schematic presentation of pharmaceutical distribution in the environment. The figure was reproduced from the article [18]; **b)** Origin and migration of phenolic compounds through ecosystems.

processes consist of advanced oxidation processes, reverse osmosis, and membrane treatment.

Photocatalysis is one of the successful methods that consists of removing persistent organic pollutants, and it is also classified as green technology. The principle of photocatalysis is the generation of a photoinduced electron/hole (e^-/h^+) pairs through the photon excitation of a semiconductor [32]. Some photogenerated charge carriers will recombine, while others will migrate to the surface of the photocatalyst, participating in redox reactions with adsorbed organic molecules [33]. Photoexcited electrons are transferred from the valence band to the conduction band, while holes are unoccupied states within the valence band region of the material. The semiconductors that have more positive (VB) initiate oxidation reactions and generation of oxidation species, while more negative (CB) semiconductors demonstrate reduction properties [34].

The present review is focused on the application of photocatalysis for the remediation of wastewaters from pharmaceutical and phenolic compounds. The investigation of studies was concentrated on a timeframe of 13 years, from 2010 to 2023 (see in Fig. 3). The search of the literature was narrowed down from photocatalytic degradation of organic pollutants with carbon-related materials (CRM) to photocatalytic degradation of pharmaceuticals and phenolic compounds. Furthermore, the review is focused on the topic of
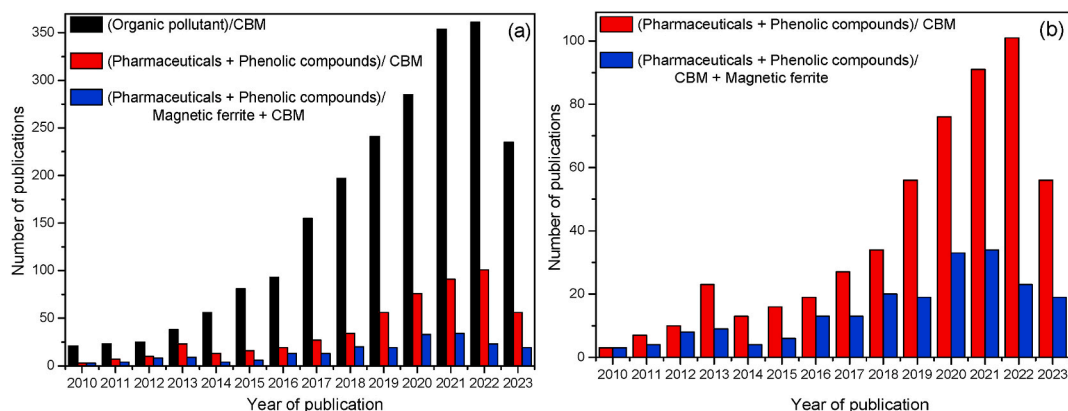
Fig. 3. Number of publications from 2010 to 2023 concerning removal of organic pollutants, pharmaceuticals and phenolic compounds with carbon materials and magnetic carbon-related materials. The information was collected from Web of Science (till September 2023).
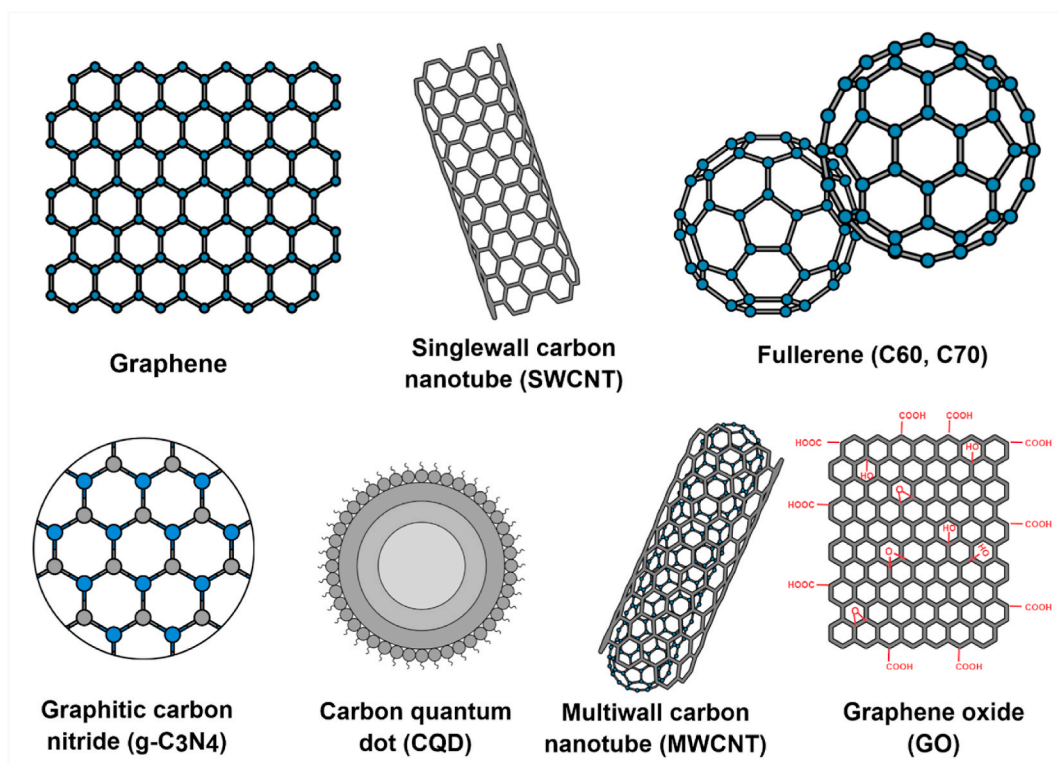

Fig. 4. Graphical presentation of different types of carbon-based materials.

photocatalytic degradation of pharmaceuticals and phenolic compounds using magnetic carbon-related materials, which consisted of a relatively law number of articles of around 212 as compared to 2024 for the search topic of photocatalytic degradation of organic pollutants with carbon materials. Therefore, pharmaceutical and phenolic compounds degradation using magnetic carbon materials provides space to further contribute with results regarding synthesis methods, improvement of properties, photocatalytic mechanism, effect of magnetic field and synergy of advanced oxidation processes combined with magnetic field.

Application of magnetic particles combined in the structure of heterocomposite with carbon-related materials (CRM) such as fullerenes, carbon nanotubes, graphene oxide, reduced graphene oxide, carbon quantum dots and graphitic carbon nitride (g-C_3N_4) for degradation of different pharmaceuticals and phenolic compounds in the aqueous phase was reported. Additionally, hybrid oxidation systems of sulfate radical-based advanced oxidation processes SR-(AOP) and Fenton-type photocatalysis were discussed.

2. Carbon-related materials

Recently, carbon-related materials have attracted much attention due to their significant structural and textural properties, superior thermal and mechanical stability, and the possibility of a wide range of applications, as shown in Fig. 3. Carbon-related materials come in a variety of forms, including zero-dimensional fullerenes (C60, C70), one-dimensional carbon nanotubes, two-dimensional graphene, graphene oxide (GO), reduced graphene oxide (rGO), carbon quantum dots (CQDs), and graphitic carbon nitride (g-C$_3$N$_4$) (Fig. 4). Carbon-related materials play remarkable roles in photocatalysis as cocatalysts and supporting materials due to their developed surface area, nontoxicity, cost-effectiveness, and abundance [35]. Moreover, carbon-based materials are applied in capacitors, batteries, electronics, membranes, heterogeneous catalysis, wastewater treatment, bioengineering, and drug delivery [36].

Fullerenes are hollow spherical carbon structures, synthesised for the first time by Eiji Osawa in 1970, using a graphite irradiated with a laser beam under a helium atmosphere [37,38]. Fullerenes with a general formula of C$_{20+2H}$, where H stands for hexagonal faces, consists of a few carbon units up to hundreds of carbon units, with the most common structures of 60-carbon units and 70-carbon units [38,39]. 60-carbon units (C$_{60}$), differently known as Buckminster fullerene, exhibit 5-fold symmetry and consists of a spherical shape that holds 12 pentagons and 20 hexagon rings, where each carbon particle is bonded with three carbon particles with sp^2 hybridization [40]. Due to their hydrophobic properties, fullerenes can be modified with polar functional groups to increase their solubility in water [41]. The activity of fullerenes can be improved through the chemical functionalization of their hollow cage with alkali and transitional metals [42,43], nonmetal [44], metal oxides [45]. The functionalization of fullerenes with other carbon-related materials such as graphitic carbon nitride, graphene, and carbon nanotubes was investigated. The heterojunction contributes to the preparation of hybrid materials with a defined morphology, improved redox properties, effective charge carriers separation, and increased transfer rate of photogenerated charges. Pi (π) conjugated photocatalytic materials are created when C$_{60}$ and g-C$_3$N$_4$ are combined, which accelerates the separation of photogenerated charges and decreases the bandgap energy of composite materials, making it photocatalytically active under visible light irradiation [46]. Ma et al. [47] reported that the morphology of g-C$_3$N$_4$ changed from flat to wrinkled when adding C$_{60}$, where C$_{60}$ is positioned upon the nitrogen junction with the carbon atom of fullerene. The role of nitrogen (N$_2$) of g-C$_3$N$_4$ in the C$_{60}$/g-C$_3$N$_4$ composite was explained by Li et al. [48], who reported that a type (II) heterojunction was formed between C$_{60}$ and g-C$_3$N$_4$, where C$_{60}$ molecules interacted with unsaturated N$_2$ of g-C$_3$N$_4$ causing a bending of g-C$_3$N$_4$ sheet which significantly improved charged transfer rate between two constituents. The combination of C$_{60}$ with graphene promotes suitable materials for energy storage, energy generation, and electronic devices. Molecular arrangement in such heterostructures defines the charge separation ability in the material. Ojeda-Aristizabal et al. [49] reported that C$_{60}$ orientation in the graphene layer was responsible for the charge transfer efficiency at the C$_{60}$/graphene interface. A combination of fullerene with different carbon allotropes like activated carbon, mesoporous carbon and carbon nanotubes can be applied in high-performance energy storage devices due to their electronic, electric, and textural properties [50]. Intercalation of fullerene with various carbon hybrids remains a challenge in the composite formation due to the high stability of C$_{60}$ that disrupts the layers of graphene and graphene oxide, low agglomeration, and the need to derivatize the constituents chemically to increase their solubility and assists the heterojunction formation [51].

Carbon nanotubes (CNT) with exceptional strength to weight ratio, chemical stability, thermal and electrical conductivity, large surface area and remarkable mechanical strength [52] are resistant materials, demonstrating 100 GPA of strength and 1000 GPA of stiffness [53]. CNT exists as one-dimensional material (1D), and based on the number of layers, it is divided into single-wall nanotubes (SWNT), double-wall nanotubes (DWNT) and multi-wall nanotubes (MWNT) [54]. The distinctive structure of carbon nanotubes (CNTs) consists of carbon atoms organised in a hexagonal lattice rolled into cylindrical tubes, where these layers are strongly held together through a delocalized electron cloud formed by sp^2 hybridization of carbon atoms [53]. The chemical and physical stability of CNTs is attributed to the strong carbon-carbon bonds. When exposed to potent oxidising substances or high temperatures, carbon nanotubes are oxidised. This procedure has the potential to modify the surface of CNTs by adding oxygen-containing functional groups like carboxyl (-COOH) and hydroxyl (-OH), contributing to their reactivity. Chemical functionalization of CNTs provides these materials with solubility and compatibility properties to ease their interaction with other materials [55]. The preparation methods of CNTs consist of the chemical vapour method, laser deposition, and arc discharge [56,56]. CNTs efficiency can be improved by modifying their structure with nonmetals, metals, and various semiconductors [57–60].

Graphene, graphene oxide (GO), and reduced graphene oxide (r-GO) are the next group of carbon-based materials. Graphene-based materials find applications in electronics, electrochemical sensors, energy storage, biosensors, and drug delivery systems [61–64]. A honeycomb lattice of zero, one, and three-dimensional graphene (0D, 1D, 2D, and 3D) are synthesised utilizing self-assembly techniques, vacuum filtration, thermal decomposition, chemical vapour deposition, solution dispersion technique and other [65,66]. Chemical functionalization of the graphene layer leads to the fabrication of graphene oxide (GO), a material with low conductivity properties. To overcome this drawback, reduced graphene oxide is introduced as an alternative. The first attempt of graphene oxide (GO) preparation dates back to 1859, when Brodie obtained GO through the oxidation of graphene by potassium chlorate (KClO$_3$) and nitric acid (HNO$_3$) at 60 °C [67]. In 1958, the Hummers' method was proposed as more efficient compared to Brodie and consisted of using KMnO$_4$, NaNO$_3$ and concentrated H$_2$SO$_4$ [68]. Nevertheless, this method was reported to release toxic gasses, and it was found necessary to improve it further. The modified Hummers' method replaced HNO$_3$ with a less corrosive acid of H$_3$PO$_4$, reducing the release of toxic gasses and increasing GO synthesis efficiency [69]. Later on, various different approaches were reported to synthesise photocatalytic active GO. Chemical functionalization of graphene enriched the structure with oxygen-containing functional groups, which impacted the dispersion rate, adsorption, and electronic properties of GO.

GO is the main precursor of reduced graphene oxide (rGO). Synthesis methods of reduced graphene oxide (rGO) include photochemical, thermal reduction, electrochemical reduction, microwave, chemical, and microbial techniques, which reduce the amount of oxygen in the functionalized (GO) layer [70]. The exceptional activity of GO and rGO can be achieved through modification of these

materials as GO/rGO [71] or as a modification with metal atoms (M) and metal oxides (MO), notably expressed as GO/M [72], GO/MO [73], GO/M-MO [74] and rGO/M [75], rGO/MO [76], and rGO/M-MO [77]. In combination with different semiconductors, rGO can provide properties like effective transport of photogenerated charges, improved separation of electron-holes pairs, increased adsorption rate toward the contaminant molecules, and the ability to immobilize and support the combined material [78]. Sodeinde et al. [79] confirmed that the presence of rGO increased the separation efficiency of photogenerated charge carriers and increased the adsorption capacity and conductivity of rGO/ZnO for the removal of chloramphenicol (CAP) antibiotic.

The next group of carbon-related materials is represented by carbon quantum dots (CQDs). CQDs are superbly used in photocatalysis for the degradation of pollutants in water, hydrogen generation, and CO_2 conversion [80–83]. CQDs can be prepared using top-down and bottom-up approaches. The top-down methods include chemical oxidation, ultrasonication, electrochemical techniques, arc discharge, and laser ablation. On the other hand, the bottom-up methods involve hydrothermal synthesis, solvothermal synthesis, microwave-assisted synthesis, pyrolysis, and plasma-based procedures for various applications [84]. They were first synthesised in 2004 during the purification process of single-walled nanotubes (SWNT) via electrophoresis [85]. Later, in 2006, CQDs were effectively fabricated by laser ablation of graphite powder and cement, and their fluorescence properties were significantly enhanced [86]. CQDs are extensively utilised in medical applications, biosensing, drug delivery, chemical sensing and photocatalysis due to their affordability, environmentally sustainable characteristics, and straightforward preparation techniques [87–90]. The internal structure of CQDs consists of a carbon core, while the outer surface of CQDs is made of graphene or graphene oxide sheets, which can be modified with highly water-soluble functional groups [91]. The CQDs exhibit fluorescence properties associated with bandgap transitions resulting from the presence of conjugated π-domains and surface defects within the CQD structure [92]. The fluorescence intensity depends on surface passivation, doping, pH and particle size. Surface passivation is a crucial factor in mitigating the contamination of CQDs. This process involves the application of a thin coating of organic molecules or polymeric materials to insulate the surface of CQDs.

Coated CQDs have demonstrated higher quantum yield and fluorescence intensity than non-coated CQDs. Pan et al. [93] observed that the fluorescence intensity of carbon quantum dots (CQDs) was enhanced through surface passivation using 1-ethyl-3-(3-dimethyl aminopropyl-carbodiimide (EDC). Additionally, the quantum yield of CQDs increased from 19 % to 41 % as the concentration of EDC increased from 2.5 to 25 mM. Elemental doping of CQDs with phosphorus (P) and nitrogen (N) led to the formation of a high quantum yield of 53.8 % of CQDs, which proved to have increased monodispersity, photoluminescence and stability in a wide range of pH [94]. Furthermore, the change in the pH significantly affected the quantum yield of CQDs. According to the findings of Jia et al. [95], it was observed that the fluorescence intensity of carbon quantum dots (CQDs) reduced by 90 % when the pH of the media increased from 4 to 8. This decrease in fluorescence intensity can be attributed to the deprotonation of carboxyl groups present on the surface of the CQDs, and the shift in the Fermi level. The utilization of CQDs in conjunction with magnetic materials has proven to be highly advantageous in the field of bioimaging, namely in the areas of fluorescence imaging, magnetic resonance imaging, and computed tomography. Nitrogen-doped CQDs embodied in magnetite probes (Fe_3O_4) exhibited fluorescence properties with a quantum yield of 21.6 % and superparamagnetic behaviour, which classified this material as a potential contrast agent for biomedical imaging of tumours [96].

Graphitic carbon nitride (g-C_3N_4) is an n-type semiconductor photocatalyst with a narrow bandgap of about 2.7 eV, photocatalytic activity and visible light absorption properties [97]. The structure of g-C_3N_4 consists of earth-abundant elements like carbon and nitrogen, which are integrated into the form of tri-s-triazine planes or heptazine rings [97]. Connections of tri-s-triazine units with planar amino groups contribute to the chemical stability of graphitic carbon nitride (g-C_3N_4) [98]. The highest photocatalytic activity of g-C_3N_4 is achieved by fulfilling physicochemical and electronic properties of photocatalysts such as high surface area, exposed reactive sites, low bandgap, solar energy harvesting towards Vis light spectra, and efficient charge carriers separation. Different types of structures like (0D) quantum dots [99], (1D) nanorods [100], nanowires [101], nanotubes, nanoparticles [102], hollow spheres [103], (2D) nanosheets [104], films [105] and (3D) hierarchical structures [106] were reported to meet the requirement of increased photocatalytic activity for g-C_3N_4. Further improvements of physico-chemical properties can be achieved through modification of g-C_3N_4 by coupling with other semiconductors [107,108], metal and non-metal doping elements [109,110], fabrication of mesoporous structure [111], and introducing magnetic properties [112]. Various methods are used for the preparation of g-C_3N_4-based photocatalysts like thermal polymerization [113], hydrothermal [114], sol-gel [115], chemical functionalization [116], ultrasonication-assisted exfoliation method [117], microwave and template-assisted method [118,119].

One limitation associated with the utilization of g-C_3N_4 as the sole semiconductor in the photocatalytic process is the elevated recombination rate of charge carriers. Consequently, it is recommended to employ the chemical functionalization technique to establish a heterojunction between two semiconductors possessing a reduced recombination rate of electron-hole pairs [116]. To overcome the g-C_3N_4 limitations, elemental doping, heterocomposite formation with broad and narrow band gap semiconductors, polymeric modification, and magnetic modification was investigated. The study performed by Hu et al. [120] showed that the incorporation of potassium (K) into g-C_3N_4 resulted in a particle size reduction, increased surface area, a narrower band gap, and an improved rate of separation of photogenerated charge carriers (e^--h^+). The concentration of precursors is a significant factor that influences the electrical characteristics of semiconductors. Previous research has indicated that the potentials of the conduction band (CB) and valence band (VB) in Na-g-C_3N_4 can be adjusted by controlling the sodium (Na) concentration [121]. Elemental dopants have the ability to function as trapping agents for photogenerated charges, hence impeding their potential for recombination. Tonda et al. [122] reported that Fe^{3+} species in iron-doped g-C_3N_4, acted as a trapping agent of e^--h^+ pairs and mediated their separation to efficiently reduce oxygen into superoxide radicals ($O_2^{\bullet-}$) and oxide hydroxyl ions (HO^-) into hydroxyl radicals ($HO^\bullet$). Furthermore, Zn served as a bridge between layers of g-C_3N_4, facilitating the separation of electron holes and preventing their recombination [123]. In the study performed by Chen et al. [124] it was reported that the formation of a type (II) heterojunction between g-C_3N_4 nanowires and B-TiO_2 tubes led to enhanced charge carriers separation. This improvement can be attributed to the charge trapping effect of pristine

g-C$_3$N$_4$ in conjunction with B-TiO$_2$. The combination of g-C$_3$N$_4$ and 2D TiO$_2$ in the form of S-scheme, yielded complete degradation of tetracycline (TC) [125].

Zinc oxide is a semiconductor that has been extensively studied for its application in the alteration of g-C$_3$N$_4$. Based on Scopus statistics, a total of 1965 research publications have been documented thus far pertaining to the combination of ZnO and g-C$_3$N$_4$. Notably, 958 of these articles specifically address the photodegradation of xenobiotics found in wastewater. Zinc oxide (ZnO) is classified as an n-type semiconductor with a wide bandgap of 3.2 eV. This material possesses numerous advantages, including anti-bacterial, photocatalytic, optical, and electrical properties as well as physical and chemical stability. Ismael et al. [126] investigated the effect of ZnO/g-C$_3$N$_4$ (10 %) on the photodegradation of 4-chlorophenol and methyl orange (MO). In the presence of composite, improved photodegradation was observed compared to the individual components of ZnO and g-C$_3$N$_4$. The ternary heterocomposite represents an additional category of junction phase development, enhancing the photocatalytic activity of g-C$_3$N$_4$.

The preparation of a ternary nanocomposite of ZnO-g-C$_3$N$_4$-GO was studied by Zhang et al. [127] for photocatalytic degradation of rhodamine B (RhB). It was found that the introduction of graphene oxide (GO) decreased the recombination rate of electron-hole pairs and enhanced the photocatalytic activity.

The subsequent category of materials investigated for heterocomposite synthesis with graphitic carbon nitride (g-C$_3$N$_4$) consists of narrow bandgap metal oxides. The appropriate bandgap values exhibited by tungsten oxide (WO$_3$) and g-C$_3$N$_4$ render these materials suitable for obtaining photoactive heterocomposites that can effectively harness visible light. Furthermore, the incorporation of silver (Ag) nanoparticles in the heterocomposite of WO$_3$/g-C$_3$N$_4$ resulted in enhanced photocatalytic activity, mostly attributed to their role as electron mediators and surface plasmon resonance properties [128]. When combined with TiO$_2$ and WO$_3$, the g-C$_3$N$_4$ is an electron mediator that improves the charge separation and facilitates their transfer to the interfacial site [129]. Additional narrow bandgap semiconductors, such as BiVO$_4$, Cu$_2$O, Ag$_2$O, and Co$_3$O$_4$, have been reported in the literature for the preparation of heterocomposite structures with g-C$_3$N$_4$ [130–133]. These composite materials have successfully removed many types of contaminants, including pharmaceuticals and organic dyes. The combination of g-C$_3$N$_4$ and WS$_2$ formed an electric field in the interface due to the positively charged surface of g-C$_3$N$_4$ and the negatively charged surface of WS$_2$ [134]. The generated electric field could direct the electrons (e$^-$) to the conduction band (CB) of g-C$_3$N$_4$, while holes (h$^+$) remain in the valence band (VB) of WS$_2$, preventing the recombination of electron-hole pairs. The phenomenon mentioned above was also noted in the resulting heterocomposite of g-C$_3$N$_4$/MoS$_2$, except that the holes (h$^+$) were localised in the valence band (VB) of g-C$_3$N$_4$, while the electrons (e$^-$) migrated to the conduction band (CB) of MoS$_2$ [135]. Moreover, polymers are another material used as platform supporters or membrane wrapping for g-C$_3$N$_4$-based heterocomposites. Z-scheme heterocomposite of g-C$_3$N$_4$/BiOI supported on β-phase PVDF (polyvinylidene fluoride) efficiently degraded above 94 % of tetracycline, demonstrating thus high permeability, self-cleaning ability, and stability [136]. PVDF and PAN possess respective complementary properties like high fouling, high hydrophobicity and low fouling, high hydrophilicity, which allows these materials to form double polymeric membranes and successfully support ZnO/g-C$_3$N$_4$ heterocomposite [137].

The techniques mentioned above are known differently as the chemical functionalization technique, which is employed as covalent and non-covalent functionalization of carbon materials. Covalent functionalization is defined as the covalent bonding of g-C$_3$N$_4$ and introduced chemical reactant, while noncovalent functionalization is attributed to electrostatic interactions, π-π bonding, hydrogen bonding, and van der Waals forces [138]. Covalent functionalization can be achieved by oxidation, hydroxylation, sulfonation, amidation, and surface defects, whereas noncovalent functionalization is an example of heterojunction formation of g-C$_3$N$_4$ and other semiconductors or metal oxides [139]. This technique allows us to develop modified g-C$_3$N$_4$-based heterocomposites in the form of 'Frustrated Lewis Pairs' and apply them for wastewater remediation. There is a lack of studies concerning the application of FLP-based carbon materials in the photodegradation of organic pollutants. Therefore, below, we are introducing the concept of 'Frustrated Lewis Pair' with regard to carbon-related materials modifications.

A Frustrated Lewis Pair (FLP) is a compound where the Lewis acid and Lewis base cannot interact due to steric hindrances and thus will separately react with a third molecule such as H$_2$, N$_2$, CO$_2$, or NO$_2$ [140,141]. FLPs have a wide range of applications, including CO$_2$ reduction, H$_2$ activation, N$_2$ fixation, organic synthesis, hydrogenation of unsaturated compounds, and pollutant removal [141, 142]. The catalytic mechanism of FLPs is strongly dependent on the surface/interface designs, which can be categorized into four types of configurations: a) solid Lewis acid and molecular Lewis base, b) molecular Lewis acid and solid Lewis base, c) solid Lewis acid and solid Lewis base, and d) introducing surface defects such as oxygen vacancies, bond breakages, and doping of solid platforms [143]. The most common solid materials used for Frustrated Lewis Pairs include polymers [144], zeolites [145], 2D materials such as graphene [146], graphitic carbon nitride [147], carbon nitride C$_2$N [148], C$_3$N [149], and metal organic frameworks [150]. Structure defects of carbon nitride favour the formation of a Frustrated Lewis Pair, as C and N-vacancies form the Lewis base. Some of the Lewis acid molecules used are B, Al, Ga, In, and Sn, while the Lewis base molecules are represented by C, N, O, S, P, and terminal hydroxyl groups (HO-) [151]. Surface defects of carbon nitride and exposed nitrogen sites served as a Lewis base platform when forming B-N/FLP and Al-N/FLP, where boron (B) and aluminium (Al) served as Lewis acids [149]. Defective boron carbon nitride (BN/FLP) was efficiently used in the organic synthesis of ammonia production [152]. These findings offer a potential alternative for developing efficient g-C$_3$N$_4$-based FLP and their application in photocatalysis and redox reactions.

3. Properties of magnetic carbon-related materials

Ferrite materials date back to the Neolithic period when humans observed stones (Lodestone-Fe$_3$O$_4$) that could attract iron [153]. The name ferrite refers to iron and derives from the Latin word 'Ferrum'. Ferrites find different applications as supercapacitors, solar cells, perovskite solar cells, electrodes for lithium-ion batteries, water splitting processes, and photocatalysis. Concerning ferrite properties like magnetic coercivity and the ability to hold magnetization, these materials are divided into two groups of soft ferrites
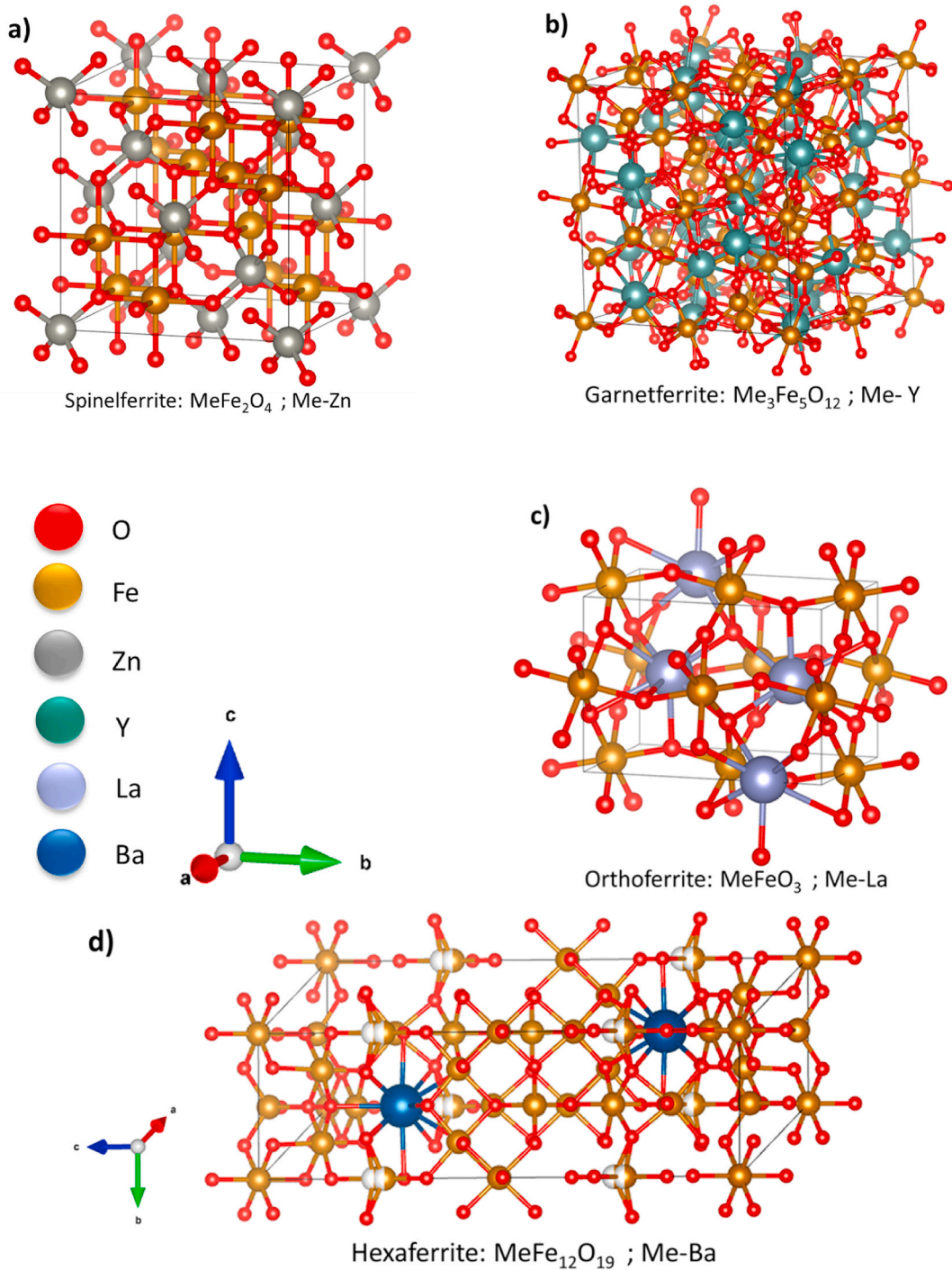
a)

Spinelferrite: MeFe$_2$O$_4$; Me-Zn

b)

Garnetferrite: Me$_3$Fe$_5$O$_{12}$; Me- Y

O
Fe
Zn
Y
La
Ba

c)

Orthoferrite: MeFeO$_3$; Me-La

d)

Hexaferrite: MeFe$_{12}$O$_{19}$; Me-Ba

Fig. 5. Crystal structures of different classes of ferrites. The structures of crystals were designed using VESTA and the crystallography open database.

and hard ferrites [154]. The crystal structure of ferrites is a very important feature and classifies them as spinel ferrites, garnet ferrites, hexaferrites, and orthoferrites, as presented in Fig. 5.

Spinel ferrite with a general formula of (MeO•Fe$_2$O$_3$; MeFe$_2$O$_4$; Me-Co, Zn, Fe, Cu, Ni, Mn, Mg), is characterized as face-centred cubic (FCC), where metallic cations are placed in the tetrahedral and octahedral sites [155]. Specifications of crystal structures of spinel ferrite classify it as normal spinel, inverse spinel, and complex spinel [156]. In normal spinel, Me (II) and Fe (III) are positioned in tetrahedral and octahedral sites, while in inverse spinel, half of Fe (III) cations are positioned in tetrahedral sites, and Me (II) and
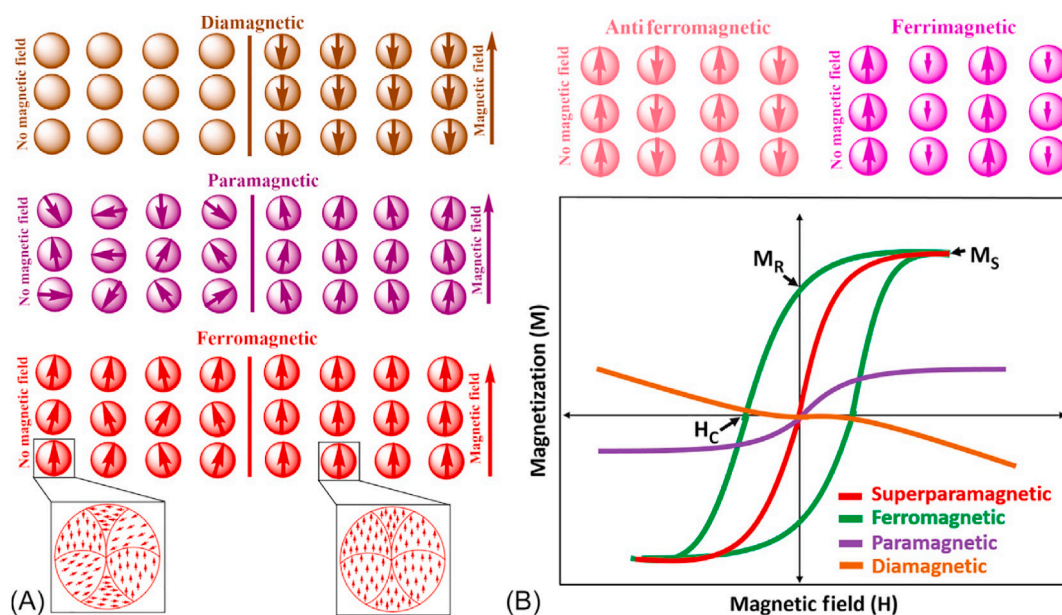
Fig. 6. Schematic presentation of magnetic properties of materials in the presence and absence of an external magnetic field (a), Hysteresis loop and demonstration of magnetic parameters like saturation magnetization (Ms), remanent magnetization (Mr), and coercive field (Hc) (b) [166].

remaining Fe (III) are located in the octahedral site [157]. In the case of complex spinel, both metal cations are allocated irregularly in tetrahedral and octahedral sites. Examples of normal, inverse, and complex spinel are known to be $ZnFe_2O_4$, $NiFe_2O_4$ and $MnFe_2O_4$, respectively. Garnet ferrite is the second class of ferrites with an overall formula of ($Me_3Fe_5O_{12}$; Me- Y, *Pm*, Sm, Eu, Gd, Tb) that demonstrate splendid chemical and structural stability due to uniform placement of cations in the tetrahedral and octahedral sites [158]. The third class of ferrites corresponds to hexaferrites with a chemical formula of ($MeFe_{12}O_{19}$; Me-Ba, Sr, Pb). Hexaferrites are ferrimagnetic materials that possess anisotropic properties related to the selective orientation of induced magnetization within the crystal [159].

Depending on their chemical formula and stacking sequence of three blocks, hexaferrites are classified into six types: M, W, X, Y, Z and U type [159]. Orthoferrites are a group of antiferromagnetic materials with a general formula ($MeFeO_3$; Me-Y and other earth rare metals) that crystallizes in orthorhombically distorted perovskite [160]. Based on magnetic properties, synthesised materials are classified as diamagnetic, paramagnetic, ferromagnetic, antiferromagnetic, superparamagnetic and ferrimagnetic, as presented in Fig. 6 (a) [161]. Atoms in diamagnetic materials have zero magnetic moments, which means that magnetization is in the opposite direction of the applied field [162]. Paramagnetic materials possess a magnetization in the same direction with the applied field, and magnetic moments are randomly oriented in atoms [163]. Ferromagnetic materials have strong magnetization from a parallel alignment of magnetic moments in atoms [164]. In antiferromagnetic materials, magnetic moments are antiparallel aligned in atoms, while ferrimagnetic materials possess higher saturation magnetization where magnetic moments are parallel and anti-parallel oriented [165]. The behaviour of magnetic material is characterised by magnetic parameters like saturation magnetization, remanent magnetization, and coercive field (Hc), which are analyzed from hysteresis loop (M − H) Fig. 6 (b).

Through chemical composition and preparation techniques, ferrites' properties can be modified. The method of ferrite preparation substantially affects morphology, particle size, stability, and surface area. For the preparation of ferrite materials, various synthesis techniques such as hydrothermal, solvothermal, sol-gel, combustion, co-precipitation, electrodeposition, sonochemical, spray pyrolysis, and microwave-assisted, also known as bottom-up method, and pulsed laser ablation and mechanical milling techniques, also known as top-down method can be utilised [167].

Combination of spinel ferrites (AB_2O_4) and orthoferrites ($RFeO_3$) with graphene oxide (GO), reduced graphene oxide (rGO), carbon quantum dots (CQD), graphitic carbon nitride (g-C_3N_4) and carbon nanotubes (CNT) using hydrothermal, solvothermal, co-precipitation, combustion methods was reported for wastewater treatment, water splitting, CO_2 conversion, and energy storage, see in Supporting Material Table (S1-S4). Zhang et al. [168] studied the photodegradation of tetracycline using iron (Fe) embedded carbon nanotubes. They confirmed that Fe/CNTs fabricated at 900 °C resulted in high photodegradation rates due to increased electron transfer efficiency and charge carriers separation. Heterocomposite formation between nitrogen-doped N-CNT and g-C_3N_4 exhibited high efficiency in the removal of tetracycline (TC) and organic dyes of rhodamine B (RhB) and methyl orange (MO) [169]. In this type of heterocomposite, N/CNT served as an electron acceptor for g-C_3N_4, inhibiting thus the recombination of electron-hole pairs. CNTs can be modified to obtain specific properties.

Magnetism is one of the features needed for the effective separation of photocatalysts from the reaction media. Magnetic separation of photocatalysts decreases the content of mass loss, thus contributing to good material recyclability. The magnetism of CNTs can be achieved through structure defects, vacancies, unpaired spin of carbon atoms and incorporation of magnetic compounds with CNTs
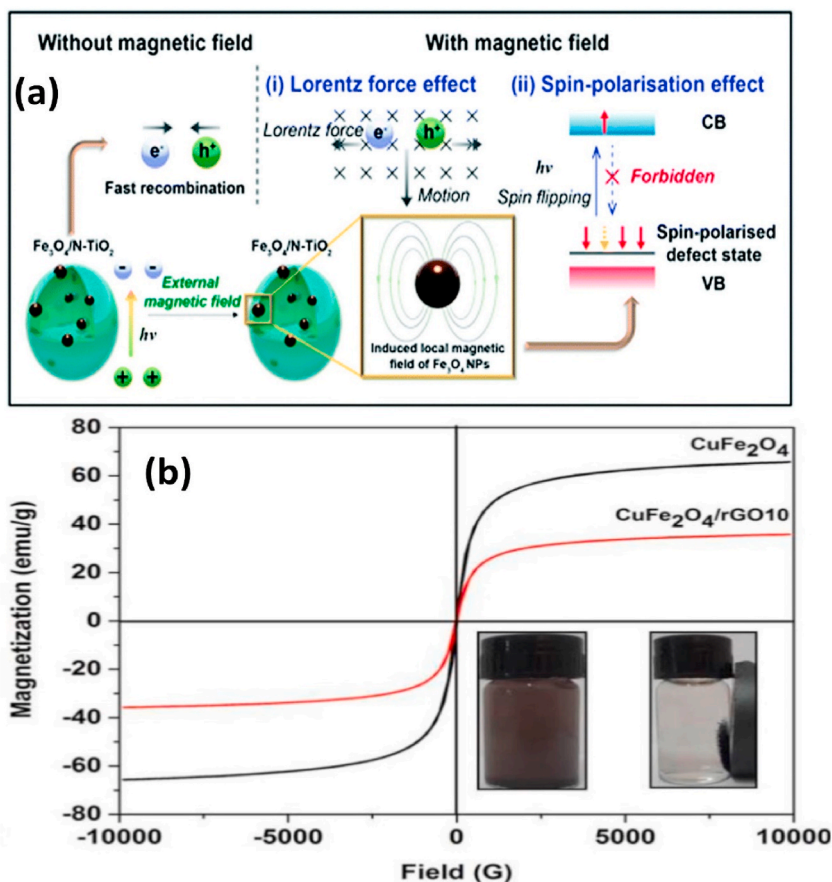
Fig. 7. Effect of the magnetic field in charge carriers separation (a) [190]; Magnetic properties and recyclability of $CuFe_2O_4$ and $CuFe_2O_4$/rGO (b) [179].

[170]. The characterization of the magnetic properties of heterocomposites consisting of magnetic ferrites and carbon materials is crucial for understanding the material behaviour and assessing its recyclability, see Fig. 7 (a, b). Deng et al. [171] synthesised carbon nanotubes and magnetite-modified CNTs to remove carbamazepine (CBZ). This type of material revealed high adsorption capacity, cost-effectiveness, high stability, and recyclability up to 6 cycles. The magnetic properties of ternary heterocomposite of g-C_3N_4/$ZnFe_2O_4$/rGO were investigated by Das et al. [172]. They confirmed the recovery ability of the heterocomposite, where a saturation magnetization (Ms) of 4.96 emu/g and the superparamagnetic behaviour of $ZnFe_2O_4$ were noticed. Nickel ferrite ($NiFe_2O_4$) loaded g-C_3N_4 was used for the total mineralization of oxytetracycline and remained stable for 10 photocatalytic degradation cycles, whereas the Ms value of 20.54 emu/g allowed the separation of the heterocomposite in an external magnetic field [173]. Higher saturation magnetization (Ms) value of 50.4 emu/g was obtained for $NiFe_2O_4$, whereas a lower Ms of 33.1 emu/g was noticed for the heterocomposite of $NiFe_2O_4$/MWCNT, due to non-magnetic nature of MWCNT [174]. The heterocomposite proved to be stable for five consecutive cycles, and a 20 % decrease in photodegradation efficiency was observed after the fifth cycle. A combination of $MnFe_2O_4$/GO resulted in a magnetically separable heterocomposite with Ms of 3.34 emu/g, while the Ms of pure $MnFe_2O_4$ was 55.58 emu/g [175]. Soft superparamagnetic material of bimetallic ferrite of $CuNiFe_2O_4$ with Ms of 29.17 emu/g, was successfully combined with g-C_3N_4, and a heterocomposite with Ms of 16.70 emu/g proved to be stable for four consecutive cycles [176].

Magnetic carbon-related materials expand their photocatalytic activity towards the visible light range. Heterocomposite of $ZnFe_2O_4$/g-C_3N_4 boosted its photocatalytic activity in the visible light region with absorption of a longer wavelength of 566 nm and band gap energy of 2.19 eV [177]. Combining g-C_3N_4 with $MnFe_2O_4$ increased the absorption properties in the UV–Vis region, while increasing the loading of $MnFe_2O_4$ (from 10 to 30 wt%) in the heterocomposite resulted in a narrower bandgap from 2.79 eV to 2.28 eV [178]. The physicochemical and magnetic properties of magnetic carbon-related materials are listed in Table 2.

Magnetic materials play a significant role in the development of heterocomposites by providing recyclability. Additionally, when subjected to an external magnetic field, these materials can influence the charge separation and surface reactions occurring on the photocatalyst. Photogenerated charge transfer can be influenced by three distinct effects: magnetoresistance effect, Lorenz force and spin polarisation, see in Fig. 7 (a). These factors collectively facilitate the efficient transfer of charge carriers to the interface.

It has been reported that in the presence of a magnetic field, the photocatalytic degradation of Congo red dye was significantly improved due to the magnetoresistance effect that facilitated the migration of charge carriers from the interface of $CoFe_2O_4$ and MoS_2
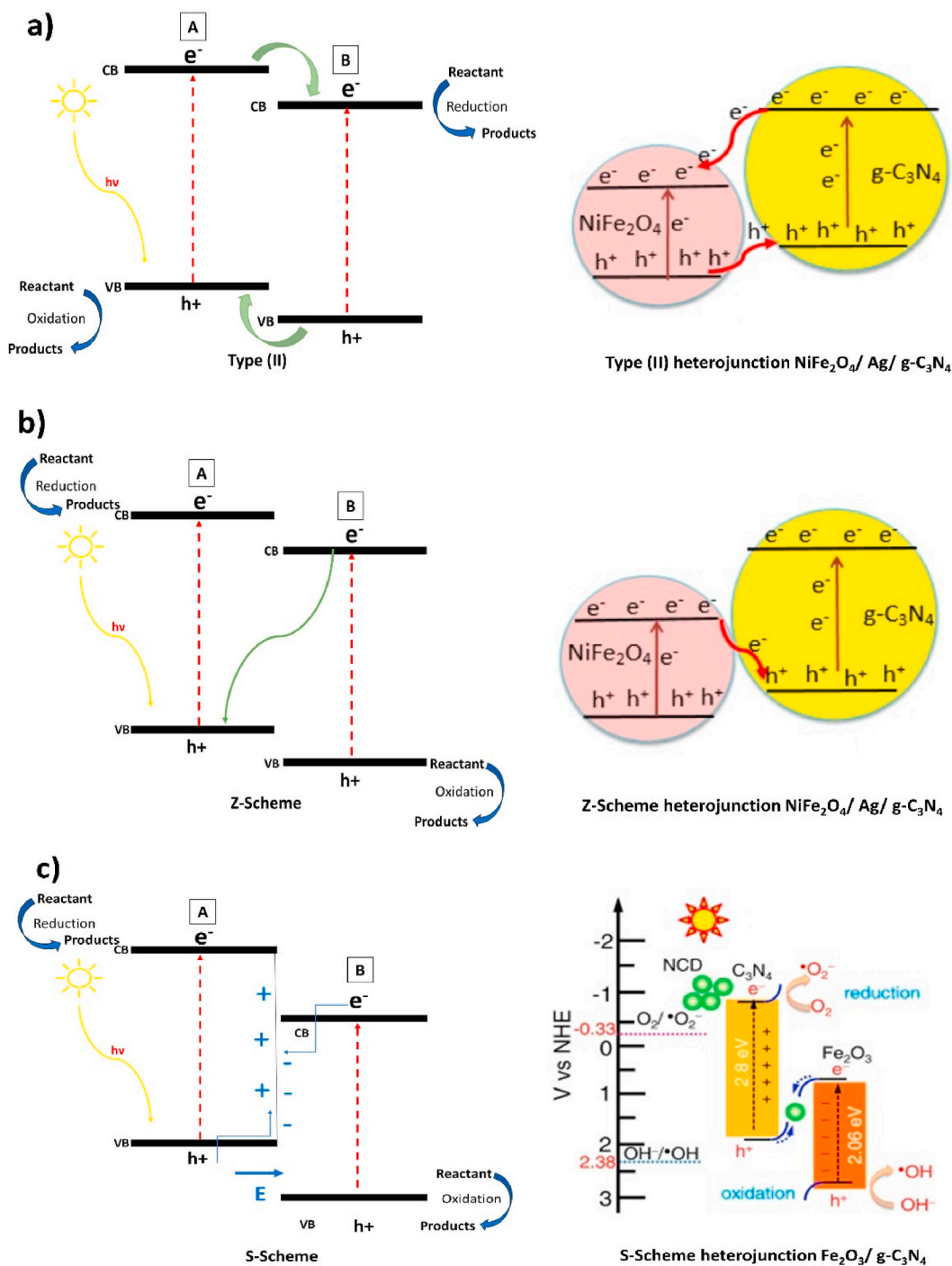
Fig. 8. Schematic illustration of the most common type of heterojunction between carbon materials and magnetic ferrites. Example of each type of heterocomposite formation such as type (II) and Z-scheme (a, b) [197], S-scheme (c) [198].

[186]. The removal of methyl orange (MO) using commercial TiO_2 was reported to achieve high efficiency for an applied magnetic field of 0.28 T [187]. Upon reaching the surface of TiO_2, photons undergo a process of absorption, wherein the energy carried by these photons is assimilated by the electrons residing in the valence band of TiO_2. This absorption event triggers a transition of the electrons from the valence band to the conduction band, resulting in the generation of photoinduced carriers, commonly referred to as electron-hole pairs. The use of a magnetic field effectively induces the Lorentz force, which facilitates the separation of electron-hole pairs, hence suppressing charge carriers recombination and enhancing the utilization efficiency of photoinduced carriers. Moreover,

12

Table 2

Saturation magnetization (Ms, emu/g) and bandgap energy (eV) values for magnetic carbon-related heterocomposites.

Photocatalyst	Ms (emu/g)	Bandgap energy (eV)	Ref
$ZnFe_2O_4$	4.96	2.25	[172]
$ZnFe_2O_4$/g-C_3N_4/GO (1.0 wt%)	2.69	2.38	
$ZnFe_2O_4$	–	1.95	[177]
$ZnFe_2O_4$/g-C_3N_4 (3.0 wt%)	–	2.19	
$NiFe_2O_4$	50.40	2.10	[174]
$NiFe_2O_4$/MWCNT	33.10	–	
$NiFe_2O_4$/g-C_3N_4	20.54	2.19	[173]
$MnFe_2O_4$	–	2.15	[178]
$MnFe_2O_4$/g-C_3N_4 (30 wt%)	–	2.28	
$MnFe_2O_4$	55.58	–	[175]
$MnFe_2O_4$/GO	3.34	–	
$CuFe_2O_4$	62	1.90	[179]
$CuFe_2O_4$/rGO	35	1.69	
$CuNiFe_2O_4$	29.17	1.51	[176]
$CuNiFe_2O_4$/g-C_3N_4	16.70	2.16	
$CaFe_2O_4$	–	1.90	[180]
$CaFe_2O_4$/g-C_3N_4	–	2.58	
$MgFe_2O_4$	11.30	2.27	[181]
$MgFe_2O_4$/TiO_2/GO	4.80	2.13	
$CoFe_2O_4$	87.30	<1.00	[182]
$CoFe_2O_4$/g-C_3N_4	76.60	1.40	
Fe_2O_3	–	1.98	[183]
g-C_3N_4/Fe_2O_3/	0.102	2.34	
$Bi_{25}FeO_{40}$	12.13	1.76	[184]
$Bi_{25}FeO_{40}$/rGO	12.05	1.52	
$BaFe_{12}O_{19}$	50	1.77	[185]
$BaFe_{12}O_{19}$/C_3N_4/Ag_2O	–	–	

the application of a magnetic field facilitates the alteration of spin states in molecules and reorganises the spin-polarized electrons. This leads to the alignment of the photocatalyst band structure, resulting in improved photodegradation of pollutants [188]. A significant degradation rate of antiviral agents of Ribavirin, Chloroquine Phosphate and Arbidol was reported by Wu et al. [189] due to the ferromagnetic alignment of photocatalyst and spin-oriented electrons in the presence of photocatalyst of α-Fe_2O_3/$Zn_{1-x}Fe_xO$, when the magnetic field of 100 mT was applied.

The surface reaction of a photocatalyst is influenced by the presence of a magnetic field, leading to enhanced exposure of active sites and improved degradation rate of selected contaminants [188]. The effect of magnetic field can be quantified by the following equations (1) and (2) [191]:

$$\eta_m = 1 - (A_{60min}/ A_0) \tag{1}$$

$$MFE = (\eta_m - \eta_{0T})/\eta_{0T} \tag{2}$$

where, the degradation rate of a pollutant in the absence of a magnetic field, denoted as (η_o), and the degradation rate of the same pollutant in the presence of a magnetic field of a specific magnitude (mT), denoted as (η_{mT}), are the variables of interest in this context. [A] stands for absorbance, and it can be replaced by concentration (C, mg·dm^{-3}) of pollutants. The positive result from equation (2) suggests that the presence of a magnetic field improves the photodegradation of contaminants. Conversely, negative results indicate that the magnetic field has a suppressive influence on the photodegradation of contaminants.

According to literature review survey, there is a lack of studies that describe the magnetic field effect in the photocatalytic process in the presence of magnetic carbon-related materials. Nevertheless, Li et al. [192] reported the photodegradation activity of α-Fe_2O_3/rGO for rhodamine B (RhB) degradation in an external magnetic field. When an external magnetic field was introduced to the photocatalytic system, the magnetic moments of α-Fe_2O_3 and rGO aligned parallel to the direction of the magnetic field. As a result, a greater number of photogenerated charges were transferred across the interface per unit time, leading to an increase in current density and a decrease in magnetic resistance (Mr). A negative value of Mr indicates an augmented quantity of photogenerated charges that participate in surface reactions within a certain time frame. The magnetic field plays a significant role in the surface reactions since it impacts the free radical pathway photodegradation reactions due to its effect on the lifetime of generated reactive oxygen species [193].

3.1. Types of heterojunctions between carbon materials and magnetic ferrites

Heterojunction formation between carbon materials and magnetic ferrites was realised in the form of type (II), Z-Scheme and S-scheme heterojunction (Fig. 8). In the context of type (II) heterojunctions, the conduction band (CB) of semiconductor A exhibits a higher positive potential compared to the conduction band of semiconductor B. Additionally, the valence band (VB) of semiconductor
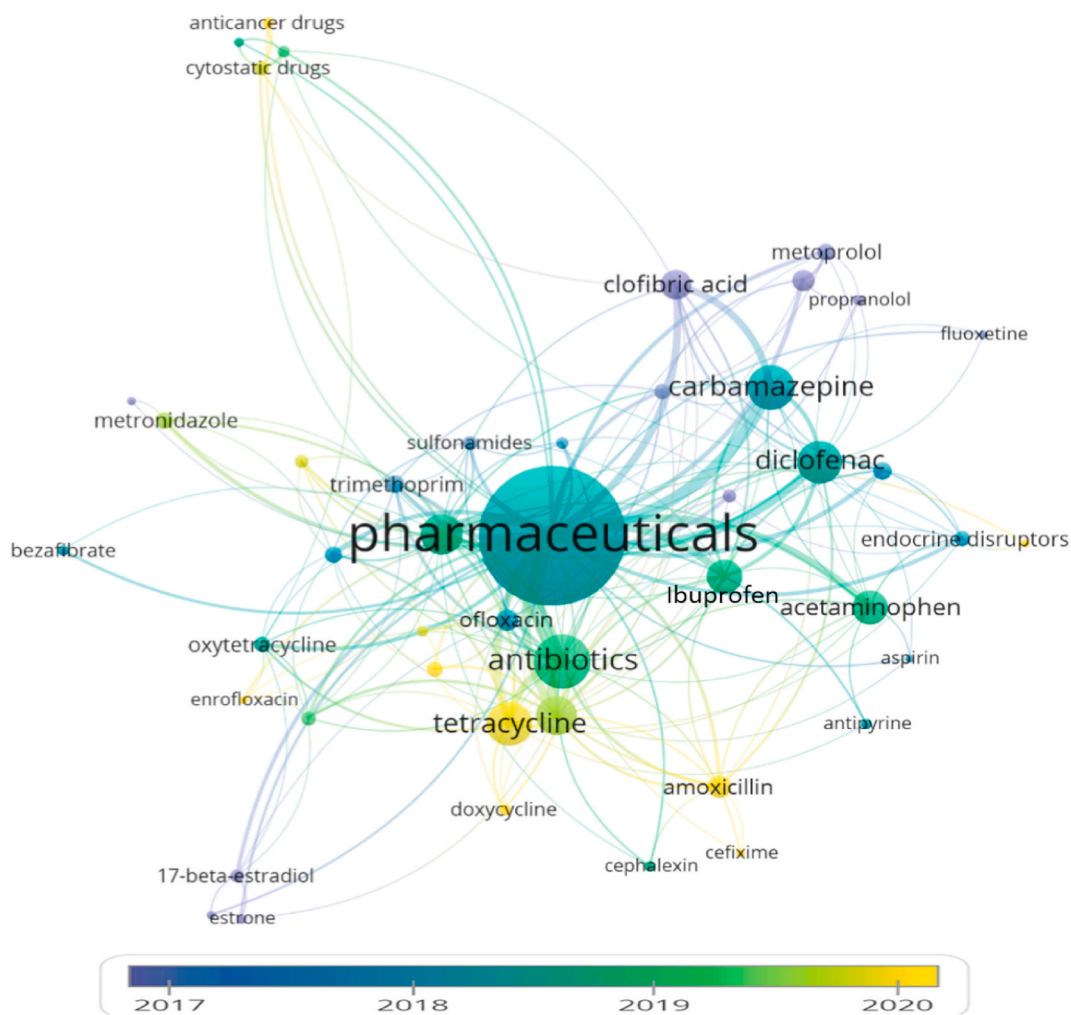
Fig. 9. Types of pharmaceuticals degradaded via carbon related materials assisted photocatalysis during a period of 2012–2023. The information was collected from Web of Science till September 2023.

A has a relatively less negative potential in comparison to the valence band of semiconductor B [194]. The transfer of electrons (e^-) will occur from semiconductor A to semiconductor B, whereas the transfer of holes (h^+) will take place from the valence band (VB) of semiconductor B to semiconductor A. Concerning S-scheme heterojunction, it is observed that the conduction band and valence band energy levels of semiconductor A are comparatively higher than those of semiconductor B. When two semiconductors come into contact, electrons from semiconductor A, which has a high Fermi level, are transferred to semiconductor B. As a result, the contact side of semiconductor A will acquire a positive charge due to the loss of electrons, while the contact side of semiconductor B will become negatively charged as it takes these electrons. The generation of an electric field occurs when subjected to light irradiation facilitates the transfer of electrons from the conduction band (CB) of semiconductor B towards the valence band (VB) of semiconductor A [195]. Within the Z-Scheme junction, the electrons that are excited by light absorption in the conduction band (CB) of semiconductor B will transfer to the valence band (VB) of semiconductor A. Subsequently, these electrons will get associated with the photogenerated holes (h^+) in semiconductor A [196].

Shi et al. [199] reported that formed type (II) heterojunction of $g-C_3N_4/ZnFe_2O_4$ resulted in 85 % tetracycline (30 mg dm^{-3}) degradation within 120 min of irradiation, whereas the rate constant of reaction was 0.0133 min^{-1}. Z-scheme heterojunction of superparamagnetic $Bi_2O_2CO_3$/carbon nanotube/$ZnFe_2O_4$ was successfully implemented for the effective removal of phenolic compounds. The highest degradation was observed for 2, 4 dimethyl phenol (DMT), followed by bisphenol, 2, 4-dichlorophenol (DCP) and 2, 4-dinitrophenol (DNP) with respective percentage degradation efficiency of 95 %, 93 %, 90 % and 80 % within 120 min of irradiation [200]. Double carbon material and Fe_2O_3 Z-Scheme of $Fe_2O_3/g-C_3N_4/GO$ was successfully used for photocatalytic removal of 3-methyl-4-nitrophenol [201]. High photodegradation efficiency of antibiotics of cefalexin and amoxicillin (20 mg dm^{-3}) was reported in the presence of S-scheme heterocomposite of $\alpha-Fe_2O_3/g-C_3N_4$. The high stability of this photocatalyst demonstrated its practical use towards wastewater remediation [202]. Increased efficiency in the S-scheme heterojunction is attributed to the internal electric field and Columbic forces, which are generated by the spontaneous movement of electrons from higher Fermi level semiconductor to lower
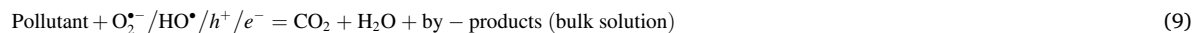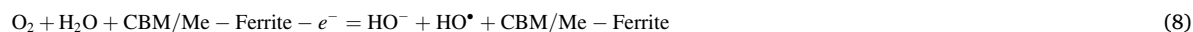
Fermi level magnetic ferrite as in the case of S-scheme heterocomposite of NiFe$_2$O$_4$/g-C$_3$N$_4$, used for cefalexin degradation [198].

4. Photocatalytic degradation of emerging pollutants using magnetic ferrites/carbon-related materials

The studies on magnetic carbon-related materials for the degradation of different groups of pharmaceuticals and phenolic compounds were described. The group of studied pharmaceuticals belong to antiepileptic drugs (carbamazepine), anti-inflammatory drugs (diclofenac, ibuprofen), analgesic (paracetamol), antimicrobial (sulphonamide), antibiotics (cefalexin, sulfamethoxazole), penicillin type antibiotics (amoxicillin, ampicillin), quinolone type antibiotics (ciprofloxacin, ofloxacin, norfloxacin, lomefloxacin) and B-blocker agent (propranolol hydrochloride) see in Fig. 9.

Reported phenolic compounds belong to phenol, 2,4 dimethylphenol, 4-chlorophenol and 4-nitrophenol. These types of xenobiotics were studied in the presence of magnetic carbon-related materials, where CRM were mainly g-C$_3$N$_4$, GO, rGO, CNT, MWCNT, CQDs, carbon allotropes (Fullerene, CNT, GO). Whereas, ferrite materials belonged to Fe$_2$O$_3$, Fe$_3$O$_4$, CoFe$_2$O$_4$, CuFe$_2$O$_4$, LaFeO$_3$, MgFe$_2$O$_4$, MnFe$_2$O$_4$, NiFe$_2$O$_4$, ZnFe$_2$O$_4$. Based on the previous studies, it was observed that reported heterocomposites were designed in the form of ferrite/CRM, ferrite/CRM/ferrite or CRM/ferrite/CRM.

The first group of ferrite carbon-related materials (CRM) belongs to ferrite-modified graphitic carbon nitride (g-C$_3$N$_4$), which was used for the degradation of pharmaceuticals. Mineralization of contaminants over g-C$_3$N$_4$ occurs through five steps. In the first two steps, contaminant molecules position themselves in the interface of g-C$_3$N$_4$ and aqueous phase, and then they will be adsorbed on g-C$_3$N$_4$. Generated reactive oxidation species like superoxide radicals O$_2^{\bullet-}$, hydroxide radicals (HO$^\bullet$) and photogenerated holes (h$^+$) will attack the pollutant molecules. During the photodegradation process, formed by-products are desorbed from the photocatalyst surface in the aqueous solution. The photodegradation route of the contaminant molecule is shown in the Eqs (3)–(9) [202,203].

$$hv + \text{CBM} / \text{Me} - \text{Ferrite} = \text{CBM} / \text{Me} - \text{Ferrite} \ (h^+ + e^-) \tag{3}$$

$$e^- + O_2 = O_2^{\bullet-} \tag{4}$$

$$O_2^{\bullet-} + e^- + 2H^+ \rightarrow H_2O_2 \tag{5}$$

$$H_2O_2 + e^- \rightarrow HO^\bullet + HO^- \tag{6}$$

$$Fe^{3+} + H_2O \rightarrow Fe^{2+} + HO^\bullet + H^+ + e^- \tag{7}$$

$$O_2 + H_2O + \text{CBM/Me} - \text{Ferrite} - e^- = HO^- + HO^\bullet + \text{CBM/Me} - \text{Ferrite} \tag{8}$$

$$\text{Pollutant} + O_2^{\bullet-}/HO^\bullet/h^+/e^- = CO_2 + H_2O + by - \text{products (bulk solution)} \tag{9}$$

The group type of CRM/ferrite/CRM heterocomposite, represented with rGO/Fe$_2$O$_3$/g-C$_3$N$_4$ photocatalyst, demonstrated a high removal rate of ciprofloxacin and terephthalic acid (20 mg dm^{-3}), and responsible oxidative species were found to be photogenerated holes, superoxide (O$_2^{\bullet-}$) and hydroxyl radicals (HO$^\bullet$) [204]. The ferrite/CRM/ferrite group of photocatalyst was represented through double orthoferrite modified carbon nitride of LaFeO$_3$/g-C$_3$N$_4$/BiFeO$_3$, where a high removal rate of ciprofloxacin (10 mg dm^{-3}) was noticed [205]. Type (II) heterocomposite of ZnFe$_2$O$_4$/g-C$_3$N$_4$ was reported to remove 85 % of tetracycline (30 mg dm^{-3}), through oxidative species of photogenerated holes (h$^+$), superoxide (O$_2^{\bullet-}$) and hydroxyl radicals (HO$^\bullet$) [206]. Z-Scheme heterocomposite of NiFe$_2$O$_4$/Ag/g-C$_3$N$_4$ was reported to effectively decomposed 92.1 % of tetracycline (20 mg dm^{-3}), whereas the oxidative species belonged to superoxide (O$_2^{\bullet-}$) and hydroxyl radicals (HO$^\bullet$) [197].

The next group of carbon-related materials combined with ferrites belong to graphene oxide, reduced graphene oxide, carbon dots and carbon allotropes. The type of formed heterocomposite is identified as CRM/ferrite. Iron oxide (Fe$_2$O$_3$), cobalt ferrite (CoFe$_2$O$_4$) and zinc ferrite (ZnFe$_2$O$_4$) were used to form the heterocomposite between ferrite/rGO. Configuration of Fe$_2$O$_3$/rGO resulted in higher than 90 % removal of tetracycline and ibuprofen in 140 min of irradiation [207]. Modification of reduced graphene oxide (rGO) with zinc ferrite (ZnFe$_2$O$_4$) resulted in 73.4 % ciprofloxacin (CIP) degradation in 60 min [208].

Next modification of zinc ferrite and carbon allotropes contributed to 91.36 % norfloxacin removal within 90 min of irradiation [209]. Fabrication of nickel ferrite (NiFe$_2$O$_4$) with carbon dots yielded the effective removal of tetracycline [210].

Furthermore, carbon nanotubes (CNT) and multiwall carbon nanotubes (MWCNT) were applied for the removal of pharmaceuticals and phenolic compounds. They were structured as ferrite/CRM heterocomposite. Modification of MWCNT with nickel ferrite resulted in improved removal of phenolic compounds such as phenol, o-nitrophenol and p-nitrophenol [211]. Degradation of 40 mg•dm^{-3} tetracycline in the presence of MnFe$_2$O$_4$/β-cyclodextrin/CNT was reported within 60 min of irradiation [212].

4.1. Photocatalytic degradation of xenobiotics using magnetic carbon-related materials and advanced oxidation processes

Heterogeneous photocatalysis, classified as an advanced oxidation process (AOP), involves the use of a semiconductor material capable of absorbing light to induce chemical transformations in the molecules of the reactants. It is considered an environmentally sustainable process due to its utilization of a photoactive solid photocatalyst and natural sunlight. The phenomenon of heterogeneous photocatalysis can manifest through a series of sequential steps. The processes involved in photocatalysis can be categorized as follows: a) the absorption of light, b) the excitation of charges, c) the movement of charged carriers towards the surface of the photocatalyst, d)

the commencement of reduction reactions through the photogenerated electrons (e−), and e) the initiation of oxidation reactions through the photogenerated holes (h$^+$) [213]. To achieve a highly active photocatalyst, it is necessary to fulfil the following criteria: a) efficient absorption of light across a broad range of solar light wavelength, b) appropriate positioning of the semiconductor's energy bands, c) minimal recombination rate of electron-hole pairs (e$^-$-h$^+$), and d) a large surface area with exposed active sites that promote redox reactions [214].

The discussed criteria can be achieved by photocatalyst fabrication and a combination of photocatalysis with advanced oxidation processes (AOPs). Sulfate-based radical advanced oxidation processes and (SR-AOP) and Fenton AOP are two of the alternatives used as additional sources of reactive oxidation species (ROS) such as hydroxyl (HO$^\bullet$), superoxide (O$_2^{\bullet-}$), singlet oxygen (^{1}O$_2$) and sulfate radicals (SO$_4^{\bullet-}$) for efficient degradation and mineralization of persistent organic pollutants. Persulfate serves as a general term for sulfate-based advanced oxidation processes (AOPs), which encompass peroxydisulfate (PDS; S$_2$O$_8^{\bullet-}$) and peroxymonosulfate (PMS; HSO$_5^-$) as specific examples. Peroxydisulfate salts (PDS) are present in three different forms, including ammonia (NH$_4$)$_2$S$_2$O$_8$, potassium K$_2$S$_2$O$_8$, and sodium Na$_2$S$_2$O$_8$ peroxydisulfate. Among these salts, sodium peroxydisulfate (Na$_2$S$_2$O$_8$) is considered to be more stable and environmentally benign when compared to the other two salts [215]. Na$_2$S$_2$O$_8$ is particularly attractive among many PDS salts due to its cost-effectiveness (0.18 USD/mol) and excellent solubility (556 g/L at 20 °C) [216]. Sulfate radical-based advanced oxidation processes (SR-AOPs) are regarded as even more effective alternatives to hydroxyl and superoxide radicals, primarily due to their higher redox potential of (E$_0$ = 2.5–3.1 V) compared to (E$_0$ = 1.9–2.7 V) for hydroxyl radicals (HO$^\bullet$) [217]. Peroxymonosulfate (PMS) exists as the triple salt of potassium peroxymonosulfate (2KHSO$_5$KHSO$_4$K$_2$SO$_4$) and is dissociated into the anion of peroxymonosulfate (HSO$_5^-$), which was first reported by Heinrich Caro and derived from Caro's acid or peroxysulfuric acid (H$_2$SO$_5$) [218,219]. PMS, also known as oxone is comparatively stable with a solubility of 250 g/L at 20 °C, is inexpensive, and is non-toxic [220]. The pH of reaction media defines the dissociation form of PDS and PMS, for instance, in acidic pH media, PDS dissociates in the form of (S$_2$O$_8^-$), while for pH lower than 9.4, PMS dissociates in the form of (HSO$_5^-$), further, for the pH value above 9.4 PMS dissociates as (SO$_5^{2-}$) [221]. In the pH range of 2–7, the predominant oxidative species are sulfate radicals (SO$_4^{\bullet-}$), while from pH 7 to 10, both sulfate (SO$_4^{\bullet-}$) and hydroxyl (HO$^\bullet$) radicals are present [222]. Several techniques are employed to activate persulfate, including thermal treatment [223,224], sonolysis [225], UV irradiation [226], UV–Vis irradiation [227], solar light irradiation [228], transition metal ions [229,230] and carbon-based materials [231].

Carbon materials are often regarded as a favourable option owing to their advantageous characteristics, including low toxicity, non-leaching properties, high abundance, stability, reusability, and large surface area [232,233]. The enhancement of the redox process is achieved through the modification of carbon materials using metal ions and their corresponding oxides. Furthermore, the utilization of metal ferrites in the form of magnetic nanocomposites surpasses the effectiveness of the PS-activated system. This superiority is observed in terms of improved PS activation, as well as the enhanced reusability and convenient recovery of the photocatalyst. Hence, an assessment was conducted to determine the impact of metal-ferrite/CBM triggered by PS on various types of antibiotics and phenolic compounds. Transition metals, including iron (Fe), cobalt (Co), copper (Cu), zinc (Zn), and manganese (Mn), have been found to successfully activate persulfate. Consequently, metal-ferrite-based photocatalysts are expected to be highly efficient in the removal of pharmaceuticals and phenolic compounds from wastewater. Series of magnetic ferro-spinel like iron (III) oxide (Fe$_2$O$_3$), iron (II, III) oxide (magnetite, Fe$_3$O$_4$), copper ferrite (CuFe$_2$O$_4$), cobalt ferrite (CoFe$_2$O$_4$), manganese ferrite (MnFe$_2$O$_4$), zinc ferrite (ZnFe$_2$O$_4$), nickel ferrite (NiFe$_2$O$_4$) and bimetallic ferrites (CuNiFe$_2$O$_4$) were used for PS activation. The reaction mechanisms of sulfate radical formation are presented in the following equations Eqs 10–15 [234,235]:

$$M^n + S_2O_8^{2-} \rightarrow M^{(n+1)} + SO_4^{\bullet-} + SO_4^{2-} \tag{10}$$

$$SO_4^{\bullet-} + M^n \rightarrow M^{(n+1)} + SO_4^{2-} \tag{11}$$

$$S_2O_8^{2-} + H_2O \rightarrow HSO_5^- + HSO_4^- \tag{12}$$

$$M^n + HSO_5^- \rightarrow M^{(n+1)} + SO_4^{\bullet-} + OH^- \tag{13}$$

$$M^n + S_2O_8^{2-} \rightarrow M^{(n+1)} + SO_4^{\bullet-} + SO_4^{2-} \tag{14}$$

$$M^n + S_2O_8^{2-} \rightarrow M^{(n+1)} + SO_4^{\bullet-} + SO_4^{2-} \tag{15}$$
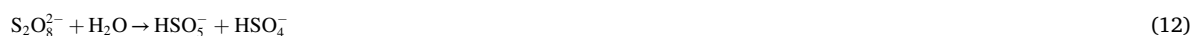
The degradation of pharmaceuticals and phenolic compounds using a persulfate-assisted photocatalytic system proceeds through free radical and non-radical pathway reaction mechanisms. Free radical pathway reaction consists of the generation of reactive oxidation species of sulfate (SO$_4^{\bullet-}$), hydroxyl (HO$^\bullet$), and superoxide radicals (O$_2^{\bullet-}$). The reaction rate constant (M^{-1}s^{-1}) of reactive oxidation species (ROS) were estimated with regard to scavenging agents of *tert*-butyl alcohol (TBA), ethanol, p-BQ and sodium azide (NaN$_3$), and they were determined to be 3.8–7.6 × 10^8 M^{-1}s^{-1} (HO$^\bullet$), 1.6–7.8 × 10^6 M^{-1}s^{-1} (SO$_4^{\bullet-}$), 9.4 × 10^8 M^{-1}s^{-1} (O$_2^{\bullet-}$) and 3.2 × 10^7 M^{-1}s^{-1} (^{1}O$_2$) [244,245]. The presence of radicals in the photocatalytic system is confirmed by scavenging experiments and electron spin resonance. Scavenging agents of para benzoquinone (P-BQ), EDTA, tert butyl alcohol (TBA), and isopropanol (IPA) were used to identify reactive oxidation species of O$_2^{\bullet-}$, h$^+$, HO$^\bullet$ and SO$_4^{\bullet-}$ in the photocatalytic system of CoFe$_2$O$_4$/Fe$_2$O$_3$/g-C$_3$N$_4$ for degradation of pharmaceuticals [237]. From experiments, it was observed that HO$^\bullet$ and SO$_4^{\bullet-}$ were responsible for the high degradation efficiency of tetracycline (TC; 99.7 %), sulfamethoxazole (SMX; 94.8 %), diclofenac (DC; 97 %), ibuprofen (IBU; 96.1 %) and ofloxacin (OFX; 96.5 %). This result was further observed via electron paramagnetic resonance (EPR), confirming the free radical pathway

Table 3
Persulfate-activated magnetic carbon-related materials for photodegradation of pharmaceuticals and phenolic compounds.

Ferrites	Type of catalyst	Comments	Ref
Fe_2O_3	Fe_2O_3/g-C_3N_4	Carbamazepine (2 mg dm^{-3}); Catalyst dosage (0.3 g dm^{-3}); 70 min irradiation time; High removal rate of carbamazepine; Vis light source ($\lambda < 400$ nm; 300 W Xenon lamp); PS Stable after 5 cycles. HO$^\bullet$ SO$_4^{\bullet-}$ (2 mM) SO$_3^{\bullet-}$ (5 mM)	[236]
$CoFe_2O_4$	$CoFe_2O_4/Fe_2O_3/g$-C_3N_4 (Z-Scheme); Self-assembly method	Tetracycline (TC); Bisphenol A (BPA); sulfamethoxazole (SMX); diclofenac (DFC); ibuprofen (IBP); ofloxacin (OFX) (30 mg dm^{-3}); Catalyst dosage (0.33 g dm^{-3}); Vis light source ($\lambda > 400$ nm); 500 W Xenon lamp; 80 min reaction time; PS [30 mg/30 mL]; High removal efficiency $\geq$95 %; Stable after 5 cycles. HO$^\bullet$ SO$_4^{\bullet-}$	[237]
$CuFe_2O_4$	$CuO/CuFe_2O_4/g$-C_3N_4; Calcination method	Tetracycline hydrochloride (20 mg dm^{-3}); Catalyst dosage (0.1 g dm^{-3}); 300 W Xenon lamp; PS concentration (1.0 mmol/L); High removal efficiency; Stable after 4 cycles. O$_2^{\bullet-}$; h$^+$ HO$^\bullet$	[238]
$CuFe_2O_4$	$CuFe_2O_4/g$-C_3N_4 Calcination; Sol-gel combustion method; Drying	Propranolol hydrochloride (0.02 mM); Catalyst dosage (1 g$\bullet$dm-3); Vis light source ($\lambda > 420$ nm); 350 W Xenon lamp; PS concentration (0.2 mM); High removal efficiency. O$_2^{\bullet-}$; h$^+$ HO$^\bullet$ $^1O_2$ SO$_4^{\bullet-}$	[239]
$CoFe_2O_4$	$rGO/CoFe_2O_4$; Hydrothermal method	4-Chlorophenol (10 mg dm^{-3}); Catalyst dosage (0.4 g dm^{-3}); Direct solar light; High removal rate; 120 min irradiation time; PMS (60 mg dm^{-3}); Stable catalyst after 3 cycles, HO$^\bullet$ SO$_4^{\bullet-}$	[240]
Fe_3O_4	Fe_3O_4/CNT; Chemical vapour deposition	Tetracycline (8 mg dm^{-3}); Catalyst dosage (0.4 g dm^{-3}); Sulfonamides (98.1 %) removal; 40 min irradiation time; Catalyst stable after 5 cycle. HO$^\bullet$ SO$_4^{\bullet-}$ O$_2^{\bullet-}$ k = 4.1 $\bullet10^5$ M^{-1}s^{-1}	[241]
$CuFe_2O_4$	$CQD/Ag/CuFe_2O_4$ Hydrothermal	Tetracycline (10 mg dm^{-3}); Catalyst dosage (0.3 g dm^{-3}); Vis light source (Xe-lamp 150 W); 5 cycle stability; O$_2^{\bullet-}$ h$^+$	[242]
Fe_2O_3	CQD/Fe_2O_3 Solvothermal	Sulfamethoxazole (10 mg dm^{-3}); Vis light source (Xe-lamp 300 W); High removal of SMX. HO$^\bullet$ SO$_4^{\bullet-}$	[243]

reaction mechanism for the degradation of pharmaceuticals. Successful degradation of tetracycline (99 %) was achieved in the presence of $CuFe_2O_4/g$-C_3N_4/CuO via a free radical pathway reaction mechanism assisted by oxidation species of HO$^\bullet$, O$_2^{\bullet-}$ and photoinduced holes (h$^+$) [238]. Additionally, the presence of HO$^\bullet$ and O$_2^{\bullet-}$ was confirmed using 5,5-dimethyl-1-pyrrolin-N-oxide (DMPO) as a trapping agent in electron spin resonance (ESR). No signals of DMPO-SO$_4^{\bullet-}$ were noticed, which can be explained by the implementation of SO$_4^{\bullet-}$ radicals to oxidize H_2O and produce HO$^\bullet$. A high degradation rate of propranolol hydrochloride via $CuFe_2O_4/g$-C_3N_4 was achieved via reactive oxidation species of HO$^\bullet$, O$_2^{\bullet-}$, SO$_4^{\bullet-}$, and h$^+$ [239]. The intense signals of DMPO-SO$_4^{\bullet-}$, DMPO-HO$^\bullet$, and DMPO-O$_2^{\bullet-}$ confirming the presence of reactive species were observed in ESR, and it further proved that the degradation mechanism occurred via free radical pathway reaction. Nevertheless, the presence of singlet oxygen ($^1O_2$) was also observed in spin-trapped peaks since the trapping agent of 4-oxo-2,2,6,6-tetramethylpiperidine (TEMP) and $^1O_2$ signal intensified from 0 to 10 min. The observation demonstrated that the reaction process occurs via a non-radical pathway along the free radical pathway. Data on PS-activated photocatalytic systems are presented in Table 3.

Non-radical pathway consists of singlet oxygen ($^1O_2$), electron transfer, and direct oxidation. In the reviewed literature, it was observed that non-radical pathways could occur along with free radical pathway reaction, and in most studies, the non-radical

Table 4

Fenton-like processes induced by magnetically modified carbon based materials and photocatalysis for degradation of pharmaceuticals and phenols.

Ferrites	Type of catalyst	Process	Ref
Fe_2O_3	Fe_2O_3/rGO-ATP (Hydrothermal method)	Ciprofloxacin (50 mg dm^{-3}) Catalyst dosage (1 g dm^{-3}); 60 min irradiation time; H_2O_2 (2.97 mmol/L); 90 % removal; Stable catalyst after 4 cycles; ROS (HO$^\bullet$); Fenton AOP	[251]
$CoFe_2O_4$	RGO/g-C_3N_4/CoFe$_2O_4$ (Hydrothermal method)	4-Nitrophenol (20 mg dm^{-3}); Catalyst dosage (0.25 g dm^{-3}); Vis light source; 40 W Led lamp; ($\lambda > 420$ nm); H_2O_2; 97 % removal; ROS (HO$^\bullet$); Fenton AOP	[252]
$ZnFe_2O_4$	CdS/r-GO/ZnFe$_2O_4$ (Hydrothermal method)	Tetracycline (50 mg dm^{-3}); Catalyst dosage (0.2 g dm^{-3}); Vis light source; 30 W LED lamp; (410 nm $< \lambda <$ 760 nm); 120 min irradiation time; 80 % removal rate; ROS (HO$^\bullet$); Fenton AOP	[253]
Fe_3O_4	Fe_3O_4/CNT (Bulk Milling strategy method)	Sulfonamides; Experiment was conducted under magnetic stirring. Catalyst dosage (1 g dm^{-3}); ROS (HO$^\bullet$), Fenton AOP	[254]
Fe_3O_4	Fe_3O_4/C/MWCNT (Coprecipitation method)	Paracetamol, Phenol (50–250 mg dm^{-3}) Catalyst dosage (0.05–0.10 g dm^{-3}); Irradiation source 4 UV lamps (15 W); H_2O_2 (5–25 mmol dm^{-3}); 99 % removal of pollutant; Stability after 5 cycle; Fenton AOP	[255]
$ZnFe_2O_4$	$Bi_2O_2CO_3$/CNT/ZnFe$_2O_4$ (Hydrothermal method)	2,4-dimethylphenol (1×10^{-4} mol dm^{-3}); Catalyst dosage (0.5 g dm^{-3}); Irradiation source 35 W LED lamps; H_2O_2; 94 % removal; Fenton AOP	[256]

Table 5

Reduction Potentials (V) and reaction rates of anions and their respective radical form.

Reactions of anions with hydroxyl radicals (HO$^\bullet$/2.8 V)				
Anions	Formed radical	Reduction Potential (V)	Reaction rate (M^{-1}s^{-1})	Ref.
Cl^-	$Cl^\bullet$	2.4	4.3×10^{10}	[260,261]
	$Cl_2^{\bullet-}$	2.0	1.1×10^5	
CO_3^{2-}	$CO_3^{\bullet-}$	1.59	3.9×10^8	[265]
HCO_3^-	$HCO_3^\bullet$	–	8.5×10^6	[273]
NO_3^-	$NO_3^\bullet$	2.3-2.5	–	[269]
PO_4^{3-}	$PO_4^{2-\bullet}$	1.54	1.1×10^9	[272,273]
SO_4^{2-}	$SO_4^{\bullet-}$	2.5-3.1	6.5×10^7	[274]

pathway was presented via singlet oxygen ($^1O_2$). An example of the co-existing free radical and non-radical pathway was reported by Zhang et al. [246] in the photodegradation of bisphenol (A) by MnFe$_2O_4$/g-C_3N_4/diatomite. It was observed that 99 % degradation was achieved within 40 min of irradiation, and responsible reactive species were found to be $^1O_2$, HO$^\bullet$, O$_2^{\bullet-}$, SO$_4^{\bullet-}$ and h$^+$, where $^1O_2$ and non-free radical pathway had the major role in photodegradation efficiency. A similar observation was reported by Yin et al. [247] for the photocatalytic system of rGO/Fe$_3O_4$ applied in the degradation of norfloxacin. Singlet oxygen species $^1O_2$ were found to be the main oxidation species, whereas hydroxyl HO$^\bullet$ and sulfate radicals SO$_4^{\bullet-}$ played a secondary role. The last reported pathways were related to electron transfer and adsorption. Bisphenol A (BPA) was efficiently removed in the presence of Fe$_2O_3$/g-C_3N_4, where singlet oxygen $^1O_2$ and electron transfer route were found responsible for pollutant degradation [248]. The existence of $^1O_2$ was proved by the recorded signal of TEMP-$^1O_2$ during ESR measurement and by the presence of $^1O_2$ scavenger of furfuryl alcohol (FFA), which showed significant singlet oxygen inhibition. Meanwhile, in the presence of potassium iodide (KI), an inhibition of electrons was observed, confirming that the electron transfer route was significant in the removal of BPA. The combination of CoFe$_2O_4$ and activated carbon (AC) led to the formation of a heterocomposite with high surface area and exposed active sites, which are responsible for facilitating the adsorption process [249]. Therefore, it was observed that the 60 % degradation of cefalexin (CEF) was associated with reactive oxidation species (HO$^\bullet$, O$_2^{\bullet-}$, SO$_4^{\bullet-}$) and 40 % with the adsorption mechanism.

Fenton reaction (Fe (II) and H$_2O_2$) is the advanced oxidation process responsible for the abundant generation of hydroxyl radicals (HO$^\bullet$). The heterogeneous Fenton process has been developed through the years to overcome the drawbacks of the homogeneous Fenton process. Homogeneous Fenton process suffers from sludge formation, a narrow pH range and high iron content [250]. Introducing a heterogeneous Fenton process with iron immobilized on solid catalysts reduces the leaching effect and increases photocatalytic efficiency and stability of photocatalysts. The role of heterogeneous Fenton processes, like photo-Fenton and nano-photo-Fenton, was investigated. The photo-Fenton reaction is defined as a hybrid process of photocatalysis and Fenton's reagent. The source of irradiation can be UV–Vis artificial light sources or sunlight. Introducing UV–Vis irradiation along with Fenton/Fenton-like reagents increases the efficiency of reactive oxygen species generation. The data related to Fenton processes induced via photocatalysis, liquid oxidant of hydrogen peroxide (H$_2O_2$) and magnetic carbon-related materials are presented in Table 4.

A combination of iron ferrites supported carbon-based catalysts and hydrogen peroxide (H$_2O_2$) generates hydroxyl radicals (HO$^\bullet$)

through heterogeneous Fenton and photo-Fenton reactions. Ferrous ions will be oxidised into ferric ions and generate hydroxyl radicals, further, they will be reduced into ferrous ions and renter the cycle of $HO^\bullet$ generation. The acidic pH media of 3.0 is required to avoid the precipitation of ferric ions (Fe^{2+}) and sludge formation. The Fenton's reaction is presented in the following equations Eqs 16–20 [257–259]:

$$Fe^{2+} + H_2O_2 \rightarrow Fe^{3+} + HO^\bullet + HO^- \quad k = 40 - 80 \; (L\bullet mol^{-1} s^{-1}) \tag{16}$$

$$Fe^{3+} + H_2O_2 \rightarrow Fe^{2+} + HO_2^\bullet + H^+ \quad k = 9.1 \times 10^7 \; (L\bullet mol^{-1} s^{-1}) \tag{17}$$

$$H_2O_2 + HO^\bullet \rightarrow HO_2^\bullet + H_2O \; k = 1.7 - 4.5 \times 10^7 \; (L\bullet mol^{-1} s^{-1}) \tag{18}$$

$$HO_2^\bullet + HO^\bullet \rightarrow O_2 + H_2O \; k = 1.4 \times 10^{10} \; (L\bullet mol^{-1} s^{-1}) \tag{19}$$

$$HO^\bullet + HO^\bullet \rightarrow H_2O_2 \; k = 5 - 8 \times 10^9 \; (L\bullet mol^{-1} s^{-1}) \tag{20}$$

The increased efficiency of contaminants degradation in the presence of the Fenton process can be explained through the oxidation of ferrous ions into ferric ions (Eq (14)), which, in further reactions with hydrogen peroxide, will generate an increased number of hydroxyl radicals. It was reported that a combination of Fe_3O_4/CNT and H_2O_2, yielded high removal rates of sulphonamide drugs (sulphanilamide, sulfamerazine, sulfadimethoxine, sulfadiazine, sulfamethazine and sulfamethoxydiazine) [254]. Coupled photo-Fenton like system of carbon/MWCNT/Fe_3O_4 composite nanofiber and H_2O_2, was demonstrated to give 99.9 % phenol and 99 % paracetamol degradation at pH 3.4, within 25 min irradiation time [255]. The designed system of CdS/rGO/$ZnFe_2O_4$ and H_2O_2 resulted in 80 % tetracycline removal and 59.2 % TOC mineralization rate within 60 min irradiation time [253].

4.2. Effect of water matrices, pH, natural organic matter (NOM), and temperature in the degradation of pollutants

The photocatalytic performance of heterocomposites in natural waters is highly affected by the presence of coexisting ions (Cl^-, CO_3^{2-}, HCO_3^-, NO_3^-, SO_4^{2-}, PO_4^{3-}), pH, natural organic matter, and temperature. Present ions may act as quenching factors in the degradation of pollutants due to the formation of reactive radicals such as $Cl^\bullet$, $CO_3^{\bullet-}$ (Table 5). This means that the type of oxidation pathway depicts whether the ions will impact contaminant degradation. The formed radicals will impact radical pathway systems more than nonradical pathway systems. Chlorine ions (Cl^-) in reaction with hydroxyl and sulfate radicals can be transformed into $Cl^\bullet$ (2.4 V) and $Cl_2^{\bullet-}$ (2.0 V) radicals that have lower reduction potentials as compared to $HO^\bullet$ (2.8 V) and $SO_4^{\bullet-}$ (2.5–3.1 V) [260,261]. Chlorine can react with hydroxyl radicals and decrease the degradation rate of organic pollutants, and they can be produced according to Eq 21–23 [262,263].

$$Cl^- + HO^\bullet \rightarrow ClOH^{\bullet-} \tag{21}$$

$$ClOH^{\bullet-} + H^+ \rightarrow Cl^\bullet + H_2O \tag{22}$$

$$SO_4^{\bullet-} + Cl^- \rightarrow SO_4^{2-} + Cl^\bullet \tag{23}$$

At the same time, chloride radicals may participate in the degradation of organic contaminants.

Degradation of ciprofloxacin (CIP) through radical pathway mechanism, demonstrated to be inhibited in the presence of HCO_3^- ions due to their interaction with hydroxyl radicals $HO^\bullet$ (2.8 V) that tend to form less reactive radicals like $CO_3^{\bullet-}$ (1.59 V) [264,265]. In the case of Fenton-like processes, bicarbonate ions HCO_3^- will directly react with the source of hydrogen peroxide (H_2O_2) and produce peroxymonocarbonate (HCO_4^-). In this way, bicarbonate ions reduce the amount of oxidant to convert into hydroxyl radicals ($HO^\bullet$) Eq (24) [266]. The same effect was observed in the PMS-activated photocatalytic system, where HCO_3^- reacted with PMS according to Eq (25) to produce peroxymonocarbonate ions (HCO_4^-) [267].

$$HCO_3^- + H_2O_2 \rightarrow HCO_4^- + H_2O \tag{24}$$

$$HSO_5^- + HCO_3^- \rightarrow HCO_4^- + HSO_4^- \tag{25}$$

Liu et al. [241] reported that in low concentrations, hydrogen carbonate ions (HCO_3^-) can also activate PDS; excess concentrations of HCO_3^- will capture $SO_4^{\bullet-}$ and $HO^\bullet$ to produce lower redox potential radicals of $CO_3^{\bullet-}$. The presence of a high concentration of $CO_3^{\bullet-}$ inhibits the oxidation process of pollutant, but in low concentration, it was reported to play the role of a single-electron oxidant that assists in electron transfer; hence, it was reported that it incited the degradation process of lomefloxacin (LFX) [268]. Nitrate ions can react with hydroxyl and sulfate radicals and produce nitrate radicals ($NO_3^\bullet$) that have lower reduction potential (2.3–2.5 V) as compared to hydroxyl radicals (2.8 V) and sulfate radicals (2.5–3.1 V); thus lower degradation rates can be observed in the presence of nitrate radicals [269,270]. The reaction of nitrate ions with sulfate radicals is demonstrated in the following equation Eq (26) [271].

$$NO_3^- + SO_4^{\bullet-} \rightarrow NO_3^\bullet + SO_4^{2-} \tag{26}$$

Reaction of phosphate ions (PO_4^{3-}) with hydroxyl radicals ($HO^\bullet$) and sulfate radicals ($SO_4^{\bullet-}$) leads to the formation of phosphate radicals ($PO_4^{\bullet 2-}$) and contributes to low photocatalytic activity of photocatalyst [272,273].

The next factor affecting the efficacy of contaminants removal is the pH of the reaction media. Actual wastewaters possess a variability of pH, and the pH of aqueous media influences the surface properties of photocatalysts, dissociation forms of contaminant molecules and reactive radicals. The optimal pH for the degradation of a contaminant is expected to be the pH at which the contaminant molecule exists in ionic form with the opposite charge as compared to the charge of the surface of the catalyst. Erim et al. [275] reported that using ternary photocatalyst of SWCNT/ZnO/Fe_3O_4, the highest degradation of cefixime (CFX) was achieved at pH 6, which is explained by electrostatic interactions of positively charged photocatalyst for pH < 7.69 (pzc = 7.69) and negatively charged CFX^{2-} (pH < 3.45). Removal of 2, 4-dimethylphenol using 20 % $Bi_2O_2CO_3$/CNT/$ZnFe_2O_4$ was observed to be higher under acidic pH media due to its zwitter ionic state that could be easily adsorbed on the positively charged surface of photocatalyst through HO^- interaction ion [256]. Another aspect of pH determination stands for the efficiency of combined photocatalysis and advanced oxidation processes (AOP) like the Fenton process and sulfate radical AOP process. Generation of hydroxyl radicals ($HO^\bullet$) during Fenton's reaction (iron salt + H_2O_2) takes place under acidic pH media [276]. The heterogeneous photo Fenton process results in the formation of hydroxyl radicals $HO^\bullet$ in acidic pH media and light irradiation (solar light or visible light) [277]. Maintenance of pH 3 is important to avoid Fe^{2+} precipitation. Heterogeneous photo-Fenton loaded on solid catalysts is an advantageous method as compared to the homogeneous Fenton process since it includes the use of ferrite/carbon materials based photocatalysts which are easily recovered, have low toxicity and good stability [250]. Utilization of 0.5 g dm^{-3} of TiO_2/GO/Fe_3O_4 (18 wt%) combined with H_2O_2 at pH 3 allowed to remove more than 90 % amoxicillin (AMX) within 120 min under visible light irradiation [278]. Lai et al. [279] reported that 95 % tetracycline was degraded at a natural pH of 5.5 using 0.5 g•dm^{-3} $MnFe_2O_4$/biochar and 100 mM H_2O_2 for 120 min irradiation time. Related to the SR-AOPs, the formation of reactive radical species is favoured in acidic (pH < 3) with predominating species of $SO_4^{\bullet-}$ or strongly alkaline media (pH > 13) with predomination of hydroxyl radicals $HO^\bullet$ [280]. However, it should be noted that such a significant pH correction (until pH of 3) will always limit the practical application of an advanced oxidation process in practice.

The concentration of organic pollutants is another parameter that determines the efficiency of photodegradation. For an optimal concentration value, the highest degradation yield can be obtained; below and beyond the threshold value, a decrease in degradation may be observed due to insufficient active sites of photocatalyst or a low number of generated reactive radicals. The highest degradation of sulfamethoxazole (SMX) by means of $NiFe_2O_4$/CNT and H_2O_2 was achieved at an optimum concentration of 1 mg dm^{-3} and decreased when the concentration of SMX was adjusted to 2.5 and 5 mg dm^{-3} [174].

Natural aqueous systems contain natural organic matter (NOM) that originates from biogeochemical cycles and consists of a range of organic substances disseminated in water bodies. The presence of NOM, may hinder the degradation of pollutants since the NOM tends to interact with reactive oxidation species, thus blocking oxidation of contaminants by reactive radicals [281]. In higher concentrations, NOM, may block active sites of photocatalysts, decreasing thus the active surface of photocatalysts for oxidation of pollutants. Since humic acid (HA) is widely used as a model of dissolved organic matter, it was reported that in the presence of HA, the degradation rate of pollutant, i.e., tetracycline (10 mg dm^{-3}) in the presence of Ag/CQD/$CuFe_2O_4$, decreased due to the quenching effect of HA [242].

In combined systems of photocatalysis and sulfate radical advanced oxidation processes (SR-AOP), temperature is an important factor, known as heat activation of persulfate (PS), that leads to an increased removal rate of studied pollutants. Zhang et al. [282] reported that the removal of diethyl phthalate (DEP), an endocrine disruptor, in the presence of a hybrid oxidation system of $CuFe_2O_4$/MWCNT + PS was significantly enhanced when the temperature was increased from 25 °C to 40 °C.

4.3. Economic evaluation

High stability and proper dispersion of magnetic carbon-related materials result in decreased treatment costs for removing organic pollutants from wastewater. From the reviewed literature, it was observed that there is a lack of studies concerning cost estimation related to the photocatalytic process and its scaling-up. Cost estimation includes many factors, such as cost of chemicals, equipment maintenance, labour costs and cost of energy. Acquiring this information is difficult; hence, the cost estimation of various studies was conducted with regard to the cost of energy and electrical energy per order (EEO). The price of electricity for industrial customers in Poland is 0.403 US dollars (USD) per 1 kWh (3600 kJ) [283]. The cost of treatment was firstly estimated for 1 dm^3 batch volume and then for 1 m^3 of treated effluent.

Electrical energy per order (EEO; kWh•m^{-3}•$order^{-1}$) is defined as the electrical energy necessary to achieve 90 % contaminant degradation (one order of magnitude) in a unit of volume effluent [295]. Electrical energy per order EEO was evaluated for the studies where more than 90 % pollutant degradation was achieved. EEO was calculated with the following equations: Eqs (27) and (28) [296].

$$EEO \left(kWh / m^3 order^1\right) = \frac{P_{el} \times t \times 1000}{V \times 60 \times \log\left(\frac{C}{C_t}\right)} \tag{27}$$

where, P_{el} and t represent electric power (kW) and reaction time (min). The volume of treated effluent is expressed in dm^3, whereas C and Ct stand for the initial and final concentration of studied pollutants. Since log (C/Ct) = kt, where k is the pseudo-first order rate constant, the equation (28) can be transformed in the following equation (29).

$$EEO \left(kWh / m^3 order^1\right) = \frac{38.4 \times P_{el}}{V \times k} \tag{28}$$

Table 6
Evaluation of cost of the treatment for different studies of magnetic ferrite combined carbon materials, in the photocatalytic degradation of various pollutants.

Nr	Heterocomposite	Time (min)	V (dm^{-3})	Energy consumption [kJ•dm^{-3}]	Total cost of treatment [USD•m^{-3}]	EEO [kWh •m^{-3} • order^{-1}]	Ref.
1	α-Fe$_2$O$_3$/C$_3$N$_4$	120	0.06	2160	4030	7440.48	[202]
2	Fe$_2$O$_3$/C$_3$N$_4$	60	0.10	1080	1209	4208.75	[284]
3	β-Fe$_2$O$_3$/C$_3$N$_4$	240	0.16	4320	9672	232.56	[285]
4	rGO/Fe$_2$O$_3$/g-C$_3$N$_4$	60	0.10	1800	2015	163.40	[286]
5	MnFe$_2$O$_4$/MWCNT	120	0.01	72	806	–	[287]
6	CoFe$_2$O$_4$/g-C$_3$N$_4$/ Fe$_2$O$_3$	80	0.03	960	2149	1754.39	[288]
7	CuFe$_2$O$_4$/g-C$_3$N$_4$	120	0.05	2520	5642	–	[289]
8	MgFe$_2$O$_4$/g-C$_3$N$_4$	120	0.10	2160	2418	–	[290]
9	ZnFe$_2$O$_4$/g-C$_3$N$_4$	40	0.10	720	806	1101.32	[291]
10	LaFe$_3$O$_4$/g-C$_3$N$_4$/ BiFeO$_3$	60	0.10	1080	241.80	172.41	[292]
11	CoFe$_2$O$_4$/rGO	80	0.10	0.36	0.40	1.45	[293]
12	ZnFe$_2$O$_4$/rGO	60	0.02	9	50.3	4960.32	[208]
13	ZnFe$_2$O$_4$/r-GO/CdS	120	0.05	5.4	12.09	434.78	[253]
14	CuNiFe$_2$O$_4$/MWCNT	120	0.10	12.96	14.5	52.17	[294]
15	NiFe$_2$O$_4$/MWCNT	120	0.04	36	100.75	4734.85	[174]

Table 7
Comparison of operational costs between photocatalytic processes and photocatalysis aided by AOPs (SR-AOP, Fenton-AOP). The economic evaluation was estimated as cost of energy and total cost (cost of energy + cost of oxidant). PS (111.67 USD/kg; Sigma Aldrich), PMS (145.46 USD/kg; Sigma Aldrich), H$_2$O$_2$ (31.97 USD/L) cost of electricity for industrial use (1 kWh = 0.403 USD).

Referred study	Cost of energy [USD/m^3]	Total cost [USD/m^3] (Cost of energy + oxidant]	Ref
SR-AOP	268.67	380.33	[237]
SR-AOP	60	86.57	[238]
SR-AOP	282	287.31	[239]
SR-AOP	(Direct solar light)	8.72	[240]
SR-AOP	300	459.46	[241]
Fenton-AOP	3	21.73	[255]
Fenton-AOP	107.47	107.48	[252]

From the calculations, it was noticed that the cost of treatment related to the photocatalytic systems of magnetic carbon-related materials ranged from 0.40 USD•m^{-3} (Table 6, Nr 11) to the highest energy consumption cost of 9672 USD•m^{-3} (Table 6, Nr 3). The lowest electrical energy per order (EEO) value was estimated to be 1.45 and 52.17 (kWh•m^{-3}•order^{-1}) (Table 6, Nr 11 and Nr 14).

The investigation identified the sulfate radical-based advanced oxidation process (SR-AOP) as the most cost-effective method (Table 7). The process utilised direct sunlight as the irradiation source, which consequently contributed to reduced cost of treatment with only 8.72 USD/m^3, positioning it as the most economically viable option [242]. With regard to Fenton-assisted AOP, the study conducted by Akhi et al. [257], demonstrated a low cost of treatment for operational conditions and total cost evaluated as cost of energy and oxidant with respective values of 3 USD/m^3 and 21.73 USD/m^3.

5. Conclusions and future prospects

Recently, advanced oxidation processes (AOPs), including photocatalysis, sulfate-based radical advanced oxidation processes (SR-AOP) and Fenton/Fenton-like reactions, are considered the most effective technologies for the treatment of waters containing trace amounts of emerging pollutants belonging to the group of pharmaceutical and phenolic compounds not susceptible to degradation.

Significant progress has been achieved in recent years in the field of heterogeneous photocatalysis, particularly in the application of carbon-related materials for improved degradation of organic pollutants. Graphitic carbon nitride (g-C$_3$N$_4$), graphene, graphene oxide (GO), reduced graphene oxide (rGO), carbon nanotubes (CNT), multi-wall carbon nanotubes (MWCNT) and carbon quantum dots (CQDs) were used for the preparation of heterocomposite with improved photocatalytic activity. Furthermore, the incorporation of *ferrite particles* into carbon-related materials may enhance the *separation* and recovery of nanosized photocatalysts after the water treatment process. Magnetic ferrites were predominately represented by spinel-type ferrites (MeFe$_2$O$_4$; Me- Cu, Zn, Fe, Cu, Ni, Mn, Mg), hematite (Fe$_2$O$_3$), magnetite (Fe$_3$O$_4$) and a few studies on orthoferrites (MeFeO$_3$; Me-La, Sr). Different types of heterojunction of carbon-related materials (CRM) and magnetic ferrites were described. These consisted of three main types of heterocomposites such as CRM/magnetic ferrite, CRM/magnetic ferrite/CRM, and magnetic ferrite/CRM/magnetic ferrite. Moreover, the combination of photocatalysis process in the presence of these types of heterocomposite with sulfate radical advanced oxidation process (SR-AOPs) and Fenton-type photocatalysis demonstrated to enhance the photodegradation of selected organic pollutants synergistically. Studied pharmaceuticals utilizing carbon-based materials modified with magnetic ferrite are classified antiepileptic drugs (carbamazepine), anti-inflammatory drugs (diclofenac, ibuprofen), analgesic (paracetamol), antimicrobial (sulphonamide), antibiotics (cefalexin, sul-famethoxazole, spiramycin, chloramphenicol, chloromycetin), penicillin-type antibiotics (amoxicillin, ampicillin), quinolone type antibiotics (ciprofloxacin, ofloxacin, norfloxacin, lomefloxacin) and B-blocker agent (propranolol hydrochloride). Regarding phenolic compounds, they belong to phenol, 2,4 dimethylphenol, 4-chlorophenol (para), 2-chlorophenol (ortho), 4-nitrophenol (para, and 2-nitrophenol (ortho). Additionally, all studied photocatalysts demonstrated to have remarkable recovery and stability properties, they exhibited to be stable from three up to eight consecutive cycles of pollutant photodegradation.

Despite the progress that was made related to the modification of carbon-related materials with magnetic ferrites, there are still significantly fewer studies focusing on the photodegradation of pharmaceuticals not susceptible to biodegradation and phenolic compounds compared to dyes photodegradation. The studies belong to the very recent years, suggesting that the topic is quite new for the photodegradation of discussed pollutants, and further efforts are needed in order to have a broad spectrum of the mechanism of these types of photocatalysts with active pharmaceutical ingredients and phenolic compounds. Additionally, toxicity assessments of used photocatalysts should be established and discussed. Many aspects are not fully covered yet, particularly low-cost preparation methods and the effect of sulfate ions presence when significant amounts of PMS or PS are used in SR-AOP process.

At the same time, new photoreactors with potential for implementation in industrial practice are an essential element of process development. There is also a need for gaining a better understanding of the effects of process indicators on the efficiency of pharmaceuticals and phenolic compounds degradation for elucidating the reaction kinetics with the view to optimising the photocatalytic process. The integrated water *treatment* system includes a photoreactor and *magnetic separator* for the recovery of the magnetic *photocatalyst* particles, which seems to be crucial for the technological application of photocatalysts. Therefore, future studies should focus on the development of new photoreactors as well on the economic feasibility of photocatalytic processes, whether they are efficient on laboratory scale or industrial scale processes.

CRediT authorship contribution statement

Elvana Çako: Conceptualization, Investigation, Methodology, Writing – original draft, Writing – review & editing. **Kumaravel Dinesh Gunasekaran:** Writing – review & editing. **Saravanan Rajendran:** Writing – review & editing. **Anna Zielińska-Jurek:** Funding acquisition, Writing – review & editing.

Declaration of competing interest

The authors declare that they have no known competing financial interests or personal relationships that could have appeared to influence the work reported in this paper.

Data availability

No data was used for the research described in the article.

Acknowledgement

The research was financially supported by the Polish National Science Centre grant no. NCN 2021/43/B/ST5/02983. The author acknowledges the support of Gdansk University of Technology within the Oxygenium Programme.

Appendix A. Supplementary data

Supplementary data to this article can be found online at https://doi.org/10.1016/j.wri.2024.100241.

References

[1] United Nations Environment Programme (UNEP), Global Chemicals Outlook II: from Legacies to Innovative Solutions - Implementing the 2030 Agenda for Sustainable Development, 2019. https://www.unep.org/resources/report/global-chemicals-outlook-ii-legacies-innovative-solutions.

[2] European Commission, Joint Research Centre, H. Hernández, N. Grassano, A. Tübke, S. Amoroso, Z. Csefalvay, P. Gkotsis, The 2019 EU Industrial R&D Investment Scoreboard, Publications Office of the European Union, 2019, https://doi.org/10.2760/04570.

[3] R. Cavicchioli, W.J. Ripple, K.N. Timmis, F. Azam, L.R. Bakken, M. Baylis, M.J. Behrenfeld, A. Boetius, P.W. Boyd, A.T. Classen, T.W. Crowther, R. Danovaro, C.M. Foreman, J. Huisman, D.A. Hutchins, J.K. Jansson, D.M. Karl, B. Koskella, D.B. Mark Welch, J.B.H. Martiny, M.A. Moran, V.J. Orphan, D.S. Reay, J. V. Remais, V.I. Rich, B.K. Singh, L.Y. Stein, F.J. Stewart, M.B. Sullivan, M.J.H. van Oppen, S.C. Weaver, E.A. Webb, N.S. Webster, Scientists' warning to humanity: microorganisms and climate change, Nat. Rev. Microbiol. 17 (2019) 569–586, https://doi.org/10.1038/s41579-019-0222-5.

[4] W.J. Sim, J.W. Lee, E.S. Lee, S.K. Shin, S.R. Hwang, J.E. Oh, Occurrence and distribution of pharmaceuticals in wastewater from households, livestock farms, hospitals and pharmaceutical manufactures, Chemosphere 82 (2011) 179–186, https://doi.org/10.1016/j.chemosphere.2010.10.026.

[5] N.H. Tran, K.Y.H. Gin, Occurrence and removal of pharmaceuticals, hormones, personal care products, and endocrine disrupters in a full-scale water reclamation plant, Sci. Total Environ. 599–600 (2017) 1503–1516, https://doi.org/10.1016/j.scitotenv.2017.05.097.

[6] K.M. Blum, S.H. Norström, O. Golovko, R. Grabic, J.D. Järhult, O. Koba, H. Söderström Lindström, Removal of 30 active pharmaceutical ingredients in surface water under long-term artificial UV irradiation, Chemosphere 176 (2017) 175–182, https://doi.org/10.1016/j.chemosphere.2017.02.063.

[7] R. Singh, I.S. Thakur, Cancer Treatment Drugs and Endocrine-Disrupting Chemicals Release and Fate in Hospital Wastewater, BV, 2020, https://doi.org/10.1016/b978-0-12-819722-6.00007-9.

[8] S. Obimakinde, O. Fatoki, B. Opeolu, O. Olatunji, Veterinary pharmaceuticals in aqueous systems and associated effects: an update, Environ. Sci. Pollut. Control Ser. 24 (2017) 3274–3297, https://doi.org/10.1007/s11356-016-7757-z.

[9] W.C. Li, Occurrence, sources, and fate of pharmaceuticals in aquatic environment and soil, Environ. Pollut. 187 (2014) 193–201, https://doi.org/10.1016/j.envpol.2014.01.015.

[10] W. Sanchez, W. Sremski, B. Piccini, O. Palluel, E. Maillot-Maréchal, S. Betoulle, A. Jaffal, S. Aït-Aïssa, F. Brion, E. Thybaud, N. Hinfray, J.M. Porcher, Adverse effects in wild fish living downstream from pharmaceutical manufacture discharges, Environ. Int. 37 (2011) 1342–1348, https://doi.org/10.1016/j.envint.2011.06.002.

[11] OECD, Pharmaceutical Residues in Freshwater: Hazards and Policy Responses, OECD Studies on Water, OECD Publishing, Paris, 2019, https://doi.org/10.1787/c936f42d-en.

[12] N. Pérez-Lemus, R. López-Serna, S.I. Pérez-Elvira, E. Barrado, Analytical methodologies for the determination of pharmaceuticals and personal care products (PPCPs) in sewage sludge: a critical review, Anal. Chim. Acta 1083 (2019) 19–40, https://doi.org/10.1016/j.aca.2019.06.044.

[13] H.B. Quesada, A.T.A. Baptista, L.F. Cusioli, D. Seibert, C. de Oliveira Bezerra, R. Bergamasco, Surface water pollution by pharmaceuticals and an alternative of removal by low-cost adsorbents: a review, Chemosphere 222 (2019) 766–780, https://doi.org/10.1016/j.chemosphere.2019.02.009.

[14] J.F.J.R. Pesqueira, M.F.R. Pereira, A.M.T. Silva, Environmental impact assessment of advanced urban wastewater treatment technologies for the removal of priority substances and contaminants of emerging concern: a review, J. Clean. Prod. 261 (2020), https://doi.org/10.1016/j.jclepro.2020.121078.

[15] F. Spataro, N. Ademollo, T. Pescatore, J. Rauseo, L. Patrolecco, Antibiotic residues and endocrine disrupting compounds in municipal wastewater treatment plants in Rome, Italy, Microchem. J. 148 (2019) 634–642, https://doi.org/10.1016/j.microc.2019.05.053.

[16] V. Phonsiri, S. Choi, C. Nguyen, Y.L. Tsai, R. Coss, S. Kurwadkar, Monitoring occurrence and removal of selected pharmaceuticals in two different wastewater treatment plants, SN Appl. Sci. 1 (2019), https://doi.org/10.1007/s42452-019-0774-z.

[17] T. aus der Beek, F.-A. Weber, A. Bergmann, G. Grüttner, A. Carius, Pharmaceuticals in the environment: global occurrence and potential cooperative action under the strategic approach to international chemicals management (SAICM), German Environment Agency (2016). http://www.umweltbundesamt.de/publikationen/.

[18] BIO Intelligence Service, Study on the environmental risks of medicinal products, Final Report, Executive Agency for Health and Consumers (2013). https://health.ec.europa.eu/system/files/2016-11/study_environment_0.pdf.

[19] G. Frascaroli, D. Reid, C. Hunter, J. Roberts, K. Helwig, J. Spencer, A. Escudero, Pharmaceuticals in wastewater treatment plants: a systematic review on the substances of greatest concern responsible for the development of antimicrobial resistance, Appl. Sci. (2021) 11, https://doi.org/10.3390/app11156670.

[20] I. Pugajeva, J. Rusko, I. Perkons, E. Lundanes, V. Bartkevics, Determination of pharmaceutical residues in wastewater using high performance liquid chromatography coupled to quadrupole-Orbitrap mass spectrometry, J. Pharm. Biomed. Anal. 133 (2017) 64–74, https://doi.org/10.1016/j.jpba.2016.11.008.

[21] R.R. Singh, L.F. Angeles, D.M. Butryn, J.W. Metch, E. Garner, P.J. Vikesland, D.S. Aga, Towards a harmonized method for the global reconnaissance of multi-class antimicrobials and other pharmaceuticals in wastewater and receiving surface waters, Environ. Int. 124 (2019) 361–369, https://doi.org/10.1016/j.envint.2019.01.025.

[22] D. Ramírez-Morales, M. Masís-Mora, J.R. Montiel-Mora, J.C. Cambronero-Heinrichs, S. Briceño-Guevara, C.E. Rojas-Sánchez, M. Méndez-Rivera, V. Arias-Mora, R. Tormo-Budowski, L. Brenes-Alfaro, C.E. Rodríguez-Rodríguez, Occurrence of pharmaceuticals, hazard assessment and ecotoxicological evaluation of wastewater treatment plants in Costa Rica, Sci. Total Environ. (2020) 746, https://doi.org/10.1016/j.scitotenv.2020.141200.

[23] X. Yu, F. Yu, Z. Li, J. Zhan, Occurrence, distribution, and ecological risk assessment of pharmaceuticals and personal care products in the surface water of the middle and lower reaches of the Yellow River (Henan section), J. Hazard Mater. 443 (2023), https://doi.org/10.1016/j.jhazmat.2022.130369.

[24] R.S. Davidson, The photodegradation of some naturally occurring polymers, J. Photochem. Photobiol., B 33 (1996) 3–25, https://doi.org/10.1016/1011-1344(95)07262-4.

[25] L. Onofrejová, J. Vašíčková, B. Klejdus, P. Stratil, L. Mišurcová, S. Kráčmar, J. Kopecký, J. Vacek, Bioactive phenols in algae: the application of pressurized-liquid and solid-phase extraction techniques, J. Pharm. Biomed. Anal. 51 (2010) 464–470, https://doi.org/10.1016/j.jpba.2009.03.027.

[26] O. Daniel, M.S. Meier, J. Schlatter, P. Frischknecht, Selected phenolic compounds in cultivated plants: ecologic functions, health implications, and modulation by pesticides, Environ. Health Perspect. 107 (1999) 109–114, https://doi.org/10.1289/ehp.99107s1109.

[27] W. Raza, J. Lee, N. Raza, Y. Luo, K.H. Kim, J. Yang, Removal of phenolic compounds from industrial wastewater based on membrane-based technologies, J. Ind. Eng. Chem. 71 (2019) 1–18, https://doi.org/10.1016/j.jiec.2018.11.024.

[28] N.V. Pradeep, S. Anupama, K. Navya, H.N. Shalini, M. Idris, U.S. Hampannavar, Biological removal of phenol from wastewaters: a mini review, Appl. Water Sci. 5 (2015) 105–112, https://doi.org/10.1007/s13201-014-0176-8.

[29] European Environment Agency, Contamination from Local Sources, 2019. https://www.eea.europa.eu/themes/soil/soil-threats.

[30] K.A. Mohamad Said, A.F. Ismail, Z. Abdul Karim, M.S. Abdullah, A. Hafeez, A review of technologies for the phenolic compounds recovery and phenol removal from wastewater, Process Saf. Environ. Protect. 151 (2021) 257–289, https://doi.org/10.1016/j.psep.2021.05.015.

[31] G. Crini, E. Lichtfouse, Advantages and disadvantages of techniques used for wastewater treatment, Environ. Chem. Lett. 17 (2019) 145–155, https://doi.org/10.1007/s10311-018-0785-9.

[32] A. Saravanan, P.S. Kumar, D.V.N. Vo, P.R. Yaashikaa, S. Karishma, S. Jeevanantham, B. Gayathri, V.D. Bharathi, Photocatalysis for removal of environmental pollutants and fuel production: a review, Environ. Chem. Lett. 19 (2021) 441–463, https://doi.org/10.1007/s10311-020-01077-8.

[33] B. Liu, H. Wu, I.P. Parkin, New insights into the fundamental principle of semiconductor photocatalysis, ACS Omega 5 (2020) 14847–14856, https://doi.org/10.1021/acsomega.0c02145.

[34] D. Robert, S. Malato, Solar photocatalysis: a clean process for water detoxification, Sci. Total Environ. 291 (2002) 85–97, https://doi.org/10.1016/S0048-9697(01)01094-4.

[35] S. Cao, J. Yu, Carbon-based H_2-production photocatalytic materials, J. Photochem. Photobiol. C Photochem. Rev. 27 (2016) 72–99, https://doi.org/10.1016/j.jphotochemrev.2016.04.002.

[36] A.O. Egbedina, O.P. Bolade, U. Ewuzie, E.C. Lima, Emerging trends in the application of carbon-based materials: a review, J. Environ. Chem. Eng. 10 (2022) 107260, https://doi.org/10.1016/j.jece.2022.107260.

[37] J. Yadav, Fullerene: Properties, Synthesis and Application, Research & Reviews: Journal of Physics 6 (3) (2017) 1–6.

[38] R.B. Onyancha, K.E. Ukhurebor, U.O. Aigbe, O.A. Osibote, H.S. Kusuma, H. Darmokoesoemo, Review article A methodical review on carbon-based nanomaterials in energy- related applications, Adsorpt. Sci. Technol. (2022) 1–21, https://doi.org/10.1155/2022/4438286.

[39] A. Dalla, M. Pelin, S. Sosa, L. Fusco, M. Prato, A. Tubaro, CARBON-BASED nanomaterials and SKIN : an overview, Carbon 196 (2022) 683–698, https://doi.org/10.1016/j.carbon.2022.05.036.

[40] R.F. Curl, Crystal structure of fullerene C_{60} & C_{70} – a theoretical approach, J. Pure Appl. Sci. Technol. 6 (1) (2016) 31–38.

[41] A. Astefanei, O. Núñez, M.T. Galceran, Characterisation and determination of fullerenes: a critical review, Anal. Chim. Acta 882 (2015) 1–21, https://doi.org/10.1016/j.aca.2015.03.025.

[42] N. Kosar, H. Tahir, K. Ayub, T. Mahmood, DFT studies of single and multiple alkali metals doped C_{24} fullerene for electronics and nonlinear optical applications, J. Mol. Graph. Model. 105 (2021) 107867, https://doi.org/10.1016/j.jmgm.2021.107867.

[43] S. Liu, F.W. Gao, H.L. Xu, Z.M. Su, Transition metals doped fullerenes: structures–NLO property relationships, Mol. Phys. 117 (2019) 705–711, https://doi.org/10.1080/00268976.2018.1538540.

[44] B. Gao, G. Chen, CO oxidization catalyzed by B, N, and their co-doped fullerenes: a first-principles investigation, RSC Adv. 9 (2019) 21626–21636, https://doi.org/10.1039/c9ra02172h.

[45] M.R. Benzigar, S. Joseph, G. Saianand, A.I. Gopalan, S. Sarkar, S. Srinivasan, D.H. Park, S. Kim, S.N. Talapaneni, K. Ramadass, A. Vinu, Highly ordered iron oxide-mesoporous fullerene nanocomposites for oxygen reduction reaction and supercapacitor applications, Microporous Mesoporous Mater. 285 (2019) 21–31, https://doi.org/10.1016/j.micromeso.2019.04.071.

[46] X. Bai, L. Wang, Y. Wang, W. Yao, Y. Zhu, Enhanced oxidation ability of g-C_3N_4 photocatalyst via C_{60} modification, Appl. Catal. B Environ. 152–153 (2014) 262–270, https://doi.org/10.1016/j.apcatb.2014.01.046.

[47] X. Ma, X. Li, M. Li, X. Ma, L. Yu, Y. Dai, Effect of the structure distortion on the high photocatalytic performance of C_{60}/g-C_3N_4 composite, Appl. Surf. Sci. 414 (2017) 124–130, https://doi.org/10.1016/j.apsusc.2017.04.019.

[48] Q. Li, L. Xu, K.W. Luo, W.Q. Huang, L.L. Wang, X.F. Li, G.F. Huang, Y. Bin Yu, Insights into enhanced visible-light photocatalytic activity of C_{60} modified g-C_3N_4 hybrids: the role of nitrogen, Phys. Chem. Chem. Phys. 18 (2016) 33094–33102, https://doi.org/10.1039/c6cp07046a.

[49] C. Ojeda-Aristizabal, E.J.G. Santos, S. Onishi, A. Yan, H.I. Rasool, S. Kahn, Y. Lv, D.W. Latzke, J. Velasco, M.F. Crommie, M. Sorensen, K. Gotlieb, C.Y. Lin, K. Watanabe, T. Taniguchi, A. Lanzara, A. Zettl, Molecular arrangement and charge transfer in C_{60}/graphene heterostructures, ACS Nano 11 (5) (2017) 4686–4693, https://doi.org/10.1021/acsnano.7b00551.

[50] A.V. Baskar, A.M. Ruban, J.M. Davidraj, G. Singh, A.H. Al-Muhtaseb, J.M. Lee, J. Yi, A. Vinu, Single-step synthesis of 2D mesoporous C_{60}/Carbon hybrids for supercapacitor and Li-Ion battery applications, Bull. Chem. Soc. Jpn. 94 (1) (2021) 133–140, https://doi.org/10.1246/BCSJ.20200265.

[51] A.V. Baskar, M.R. Benzigar, S.N. Talapaneni, G. Singh, A.S. Karakoti, J. Yi, A.H. Al-Muhtaseb, K. Ariga, P.M. Ajayan, A. Vinu, Self-assembled fullerene nanostructures: synthesis and applications, Advanced Functional Matrials 32 (6) (2021) 2106924, https://doi.org/10.1002/adfm.202106924.

[52] R. Dubey, D. Dutta, A. Sarkar, P. Chattopadhyay, Functionalized carbon nanotubes: synthesis, properties and applications in water purification, drug delivery, and material and biomedical sciences, Nanoscale Adv. 3 (20) (2021) 5722–5744, https://doi.org/10.1039/d1na00293g.

[53] A. Garg, H.D. Chalak, M.O. Belarbi, A.M. Zenkour, R. Sahoo, Estimation of carbon nanotubes and their applications as reinforcing composite materials–an engineering review, Compos. Struct. 272 (2021) 114234, https://doi.org/10.1016/j.compstruct.2021.114234.

[54] N. Anzar, R. Hasan, M. Tyagi, N. Yadav, J. Narang, Carbon nanotube - a review on Synthesis, Properties and plethora of applications in the field of biomedical science, Sensors International 1 (2020) 100003, https://doi.org/10.1016/j.sintl.2020.100003.

[55] F.J. Peón-Díaz, R.S. del Río, S. Hevia, F. Olivares, J.C. Expósito-Gálvez, R. Escalante, K. Valadez-Villalobos, A.J. Riquelme, G. Oskam, R. Henríquez, The effect of oxidative functionalization of carbon nanotubes on the morphological, optical, and photoelectrochemical properties of modified titanium dioxide photoanodes, J. Mater. Sci. 58 (12) (2023) 5372–5388, https://doi.org/10.1007/s10853-023-08351-4.

[56] J. Peng, Y. He, C. Zhou, S. Su, B. Lai, The carbon nanotubes-based materials and their applications for organic pollutant removal: a critical review, Chin. Chem. Lett. 32 (5) (2021) 1626–1636, https://doi.org/10.1016/j.cclet.2020.10.026.

[57] X. Xing, R. Liu, M. Anjass, K. Cao, U. Kaiser, G. Zhang, C. Streb, Bimetallic manganese-vanadium functionalized N,S-doped carbon nanotubes as efficient oxygen evolution and oxygen reduction electrocatalysts, Appl. Catal., B 277 (2020) 119195, https://doi.org/10.1016/j.apcatb.2020.119195.

[58] H. Guo, Q. Feng, J. Zhu, J. Xu, Q. Li, S. Liu, K. Xu, C. Zhang, T. Liu, Cobalt nanoparticle-embedded nitrogen-doped carbon/carbon nanotube frameworks derived from a metal-organic framework for tri-functional ORR, OER and HER electrocatalysis, J Mater Chem A Mater 7 (8) (2019) 3664–3672, https://doi.org/10.1039/c8ta11400e.

[59] S.M. Seyed Arabi, R.S. Lalehloo, M.R.T.B. Olyai, G.A.M. Ali, H. Sadegh, Removal of Congo red azo dye from aqueous solution by ZnO nanoparticles loaded on multiwall carbon nanotubes, Physica E Low Dimens Syst Nanostruct 106 (2019) 150–155, https://doi.org/10.1016/j.physe.2018.10.030.

[60] S. Liu, L. Mei, X. Liang, L. Liao, G. Lv, S. Ma, S. Lu, A. Abdelkader, K. Xi, Anchoring Fe3O4 nanoparticles on carbon nanotubes for microwave-induced catalytic degradation of antibiotics, ACS Appl. Mater. Interfaces 10 (35) (2018) 29467–29475, https://doi.org/10.1021/acsami.8b08280.

[61] Y. Zhang, X. Xia, B. Liu, S. Deng, D. Xie, Q. Liu, Y. Wang, J. Wu, X. Wang, J. Tu, Multiscale graphene-based materials for applications in sodium ion batteries, Adv. Energy Mater. 9 (8) (2019) 1–35, https://doi.org/10.1002/aenm.201803342.

[62] J. Wang, Y. Liu, Z. Fan, W. Wang, B. Wang, Z. Guo, Ink-based 3D printing technologies for graphene-based materials: a review, Adv. Compos. Hybrid Mater. 2 (2019) 1–33, https://doi.org/10.1007/s42114-018-0067-9.

[63] Y. Wu, J. Zhu, L. Huang, A review of three-dimensional graphene-based materials: synthesis and applications to energy conversion/storage and environment, Carbon N Y 143 (2019) 610–640, https://doi.org/10.1016/j.carbon.2018.11.053.

[64] M. Minale, Z. Gu, A. Guadie, D.M. Kabtamu, Y. Li, X. Wang, Application of graphene-based materials for removal of tetracyclines using adsorption and photocatalytic-degradation: a review, J. Environ. Manag. 276 (2020) 111310, https://doi.org/10.1016/j.jenvman.2020.111310.

[65] A. Razaq, F. Bibi, X. Zheng, R. Papadakis, S.H.M. Jafri, H. Li, Review on graphene-, graphene oxide-, reduced graphene oxide-based flexible composites: from fabrication to applications, Materials 15 (3) (2022) 1012, https://doi.org/10.3390/ma15031012.

[66] C. Kavitha, A review on reduced Graphene oxide hybrid nano composites and their prominent applications, Mater. Today Proc. 49 (2021) 811–816, https://doi.org/10.1016/j.matpr.2021.05.343.

[67] B.C. Brodie, Xiii. On the atomic weight of graphite, Phil. Trans. Roy. Soc. Lond. 149 (1859) 249–259, https://doi.org/10.1098/rstl.1859.0013.

[68] W.S. Hummers, R.E. Offeman, Preparation of graphite oxide, J. Am. Chem. Soc. 80 (6) (1958) 1339, https://doi.org/10.1021/ja01539a017.

[69] D.C. Marcano, D.V. Kosynkin, J.M. Berlin, A. Sinitskii, Z. Sun, A. Slesarev, L.B. Alemany, W. Lu, J.M. Tour, Improved synthesis of graphene oxide, ACS Nano 4 (8) (2010) 4806–4814, https://doi.org/10.1021/nn1006368.

[70] K.S. Obayomi, S.Y. Lau, M. Danquah, T. Chiong, M. Takeo, Advances in graphene oxide based nanobiocatalytic technology for wastewater treatment, Environ. Nanotechnol. Monit. Manag. 17 (2022) 100647, https://doi.org/10.1016/j.enmm.2022.100647.

[71] P. Sharma, N. Hussain, D.J. Borah, M.R. Das, Kinetics and adsorption behaviour of the methyl blue at the graphene oxide/reduced graphene oxide nanosheet-water interface: a comparative study, J. Chem. Eng. Data 58 (12) (2013) 3477–3488, https://doi.org/10.1021/je400743r.

[72] C. Chen, J. Zhang, B. Zhang, H. Ming Duan, Hydrogen adsorption of Mg-doped graphene oxide: a first-principles study, J. Phys. Chem. C 117 (9) (2013) 4337–4344, https://doi.org/10.1021/jp308271b.

[73] B. Li, T. Liu, Y. Wang, Z. Wang, ZnO/graphene-oxide nanocomposite with remarkably enhanced visible-light-driven photocatalytic performance, J. Colloid Interface Sci. 377 (1) (2012) 114–121, https://doi.org/10.1016/j.jcis.2012.03.060.

[74] G. Wang, Z. Li, M. Li, J. Liao, C. Chen, S. Lv, C. Shi, Enhanced field-emission of silver nanoparticle-graphene oxide decorated ZnO nanowire arrays, Phys. Chem. Chem. Phys. 17 (47) (2015) 31822–31829, https://doi.org/10.1039/c5cp05036g.

[75] S.P. Dubey, T.T.M. Nguyen, Y.N. Kwon, C. Lee, Synthesis and characterization of metal-doped reduced graphene oxide composites, and their application in removal of Escherichia coli, arsenic and 4-nitrophenol, J. Ind. Eng. Chem. 29 (2015) 282–288, https://doi.org/10.1016/j.jiec.2015.04.008.

[76] S. Liu, J. Tian, L. Wang, Y. Luo, X. Sun, One-pot synthesis of CuO nanoflower-decorated reduced graphene oxide and its application to photocatalytic degradation of dyes, Catal. Sci. Technol. 2 (2) (2012) 339–344, https://doi.org/10.1039/c1cy00374g.

[77] T.D. Nguyen-Phan, V.H. Pham, J.S. Chung, M. Chhowalla, T. Asefa, W.J. Kim, E.W. Shin, Photocatalytic performance of Sn-doped TiO2/reduced graphene oxide composite materials, Appl. Catal. Gen. 473 (2014) 21–30, https://doi.org/10.1016/j.apcata.2013.12.030.

[78] X. Zhou, T. Shi, H. Zhou, Hydrothermal preparation of ZnO-reduced graphene oxide hybrid with high performance in photocatalytic degradation, Appl. Surf. Sci. 258 (17) (2012) 6204–6211, https://doi.org/10.1016/j.apsusc.2012.02.131.

[79] K.O. Sodeinde, S.O. Olusanya, O.S. Lawal, M. Sriariyanun, A.A. Adediran, Enhanced adsorptional-photocatalytic degradation of chloramphenicol by reduced graphene oxide-zinc oxide nanocomposite, Sci. Rep. 12 (1) (2022) 17054, https://doi.org/10.1038/s41598-022-21266-5.

[80] U.A. Rani, L.Y. Ng, C.Y. Ng, E. Mahmoudi, A review of carbon quantum dots and their applications in wastewater treatment, Adv. Colloid Interface Sci. 278 (2020) 102124, https://doi.org/10.1016/j.cis.2020.102124.

[81] A.S. Rasal, S. Yadav, A. Yadav, A.A. Kashale, S.T. Manjunatha, A. Altaee, J.Y. Chang, Carbon quantum dots for energy applications: a review, ACS Appl. Nano Mater. 4 (7) (2021) 6515–6541, https://doi.org/10.1021/acsanm.1c01372.

[82] M.J. Molaei, Principles, mechanisms, and application of carbon quantum dots in sensors: a review, Anal. Methods 12 (10) (2020) 1266–1287, https://doi.org/10.1039/C9AY02696G.

[83] Y. Guo, R. Zhang, S. Zhang, H. Hong, Y. Zhao, Z. Huang, C. Han, H. Li, C. Zhi, Ultrahigh oxygen-doped carbon quantum dots for highly efficient H2O2 production via two-electron electrochemical oxygen reduction, Energy Environ. Sci. 15 (10) (2022) 4167–4174, https://doi.org/10.1039/d2ee01797k.

[84] R. Mohammadi, H. Naderi-Manesh, L. Farzin, Z. Vaezi, N. Ayarri, L. Samandari, M. Shamsipur, Fluorescence sensing and imaging with carbon-based quantum dots for early diagnosis of cancer: a review, J. Pharm. Biomed. Anal. 212 (2022) 114628, https://doi.org/10.1016/j.jpba.2022.114628.

[85] X. Xu, R. Ray, Y. Gu, H.J. Ploehn, L. Gearheart, K. Raker, W.A. Scrivens, Electrophoretic analysis and purification of fluorescent single-walled carbon nanotube fragments, J. Am. Chem. Soc. 126 (40) (2004) 12736–12737, https://doi.org/10.1021/ja040082h.

[86] Y.P. Sun, B. Zhou, Y. Lin, W. Wang, K.A.S. Fernando, P. Pathak, M.J. Meziani, B.A. Harruff, X. Wang, H. Wang, P.G. Luo, H. Yang, M.E. Kose, B. Chen, L. M. Veca, S.Y. Xie, Quantum-sized carbon dots for bright and colourful photoluminescence, J. Am. Chem. Soc. 128 (24) (2006) 7756–7757, https://doi.org/10.1021/ja062677d.

[87] D. Bu, H. Zhuang, G. Yang, X. Ping, An immunosensor designed for polybrominated biphenyl detection based on fluorescence resonance energy transfer (FRET) between carbon dots and gold nanoparticles, Sensor. Actuator. B Chem. 195 (2014) 540–548, https://doi.org/10.1016/j.snb.2014.01.079.

[88] P. Jana, A. Dev, Carbon quantum dots: a promising nanocarrier for bioimaging and drug delivery in cancer, Mater. Today Commun. 32 (2022) 104068, https://doi.org/10.1016/j.mtcomm.2022.104068.

[89] Y. Dong, R. Wang, H. Li, J. Shao, Y. Chi, X. Lin, G. Chen, Polyamine-functionalized carbon quantum dots for chemical sensing, Carbon 50 (8) (2012) 2810–2815, https://doi.org/10.1016/j.carbon.2012.02.046.

[90] R. Wang, K.Q. Lu, Z.R. Tang, Y.J. Xu, Recent progress in carbon quantum dots: synthesis, properties and applications in photocatalysis, J. Mater. Chem. A 5 (8) (2017) 3717–3734, https://doi.org/10.1039/c6ta08660h.

[91] Y. Yao, H. Zhang, K. Hu, G. Nie, Y. Yang, Y. Wang, S. Duan, S. Wang, Carbon dots based photocatalysis for environmental applications, J. Environ. Chem. Eng. 10 (2) (2022) 107336, https://doi.org/10.1016/j.jece.2022.107336.

[92] S.Y. Lim, W. Shen, Z. Gao, Carbon quantum dots and their applications, Chem. Soc. Rev. 44 (1) (2015) 362–381, https://doi.org/10.1039/c4cs00269e.

[93] J. Pan, Z. Zheng, J. Yang, Y. Wu, F. Lu, Y. Chen, W. Gao, A novel and sensitive fluorescence sensor for glutathione detection by controlling the surface passivation degree of carbon quantum dots, Talanta 166 (2017) 1–7, https://doi.org/10.1016/j.talanta.2017.01.033.

[94] Q. Xu, B. Li, Y. Ye, W. Cai, W. Li, C. Yang, Y. Chen, M. Xu, N. Li, X. Zheng, J. Street, Y. Luo, L. Cai, Synthesis, mechanical investigation, and application of nitrogen and phosphorus co-doped carbon dots with a high photoluminescent quantum yield, Nano Res. 11 (2018) 3691–3701, https://doi.org/10.1007/s12274-017-1937-0.

[95] X. Jia, J. Li, E. Wang, One-pot green synthesis of optically pH-sensitive carbon dots with upconversion luminescence, Nanoscale 4 (18) (2012) 5572–5575, https://doi.org/10.1039/c2nr31319g.

[96] X. Liu, H. Jiang, J. Ye, C. Zhao, S. Gao, C. Wu, C. Li, J. Li, X. Wang, Nitrogen-doped carbon quantum dot stabilized magnetic iron oxide nanoprobe for fluorescence, magnetic resonance, and computed tomography triple-modal in vivo bioimaging, Adv. Funct. Mater. 26 (47) (2016) 8694–8706, https://doi.org/10.1002/adfm.201603084.

[97] X. Liu, R. Ma, L. Zhuang, B. Hu, J. Chen, X. Liu, X. Wang, Recent developments of doped g-C3N4 photocatalysts for the degradation of organic pollutants, Crit. Rev. Environ. Sci. Technol. 51 (8) (2021) 751–790, https://doi.org/10.1080/10643389.2020.1734433.

[98] X. Wang, K. Maeda, A. Thomas, K. Takanabe, G. Xin, J.M. Carlsson, K. Domen, M. Antonietti, A metal-free polymeric photocatalyst for hydrogen production from water under visible light, Nat. Mater. 8 (1) (2009) 76–80, https://doi.org/10.1038/nmat2317.

[99] J. Su, L. Zhu, P. Geng, G. Chen, Self-assembly graphitic carbon nitride quantum dots anchored on TiO2 nanotube arrays: an efficient heterojunction for pollutants degradation under solar light, J. Hazard Mater. 316 (2016) 159–168, https://doi.org/10.1016/j.jhazmat.2016.05.004.

[100] H.J. Li, D.J. Qian, M. Chen, Templateless Infrared Heating Process for Fabricating carbon nitride nanorods with efficient photocatalytic H2 evolution, ACS Appl. Mater. Interfaces 7 (45) (2015) 25162–25170, https://doi.org/10.1021/acsami.5b06627.

[101] K. Zhang, L. Wang, X. Sheng, M. Ma, M.S. Jung, W. Kim, H. Lee, J.H. Park, Tunable bandgap energy and promotion of H2O2 oxidation for overall water splitting from carbon nitride nanowire bundles, Adv. Energy Mater. 6 (11) (2016) 1–7, https://doi.org/10.1002/aenm.201502352.

[102] J. Jiang, L. Zhu, J. Zou, L. Ou-Yang, A. Zheng, H. Tang, Micro/nano-structured graphitic carbon nitride-Ag nanoparticle hybrids as surface-enhanced Raman scattering substrates with much improved long-term stability, Carbon 87 (2015) 193–205, https://doi.org/10.1016/j.carbon.2015.02.025.

[103] Y. Cui, Y. Tang, X. Wang, Template-free synthesis of graphitic carbon nitride hollow spheres for photocatalytic degradation of organic pollutants, Mater. Lett. 161 (2015) 197–200, https://doi.org/10.1016/j.matlet.2015.08.106.

[104] B.D. Boruah, A. Mathieson, B. Wen, C. Jo, F. Deschler, M. De Volder, Photo-rechargeable zinc-ion capacitor using 2D graphitic carbon nitride, Nano Lett. 20 (8) (2020) 5967–5974, https://doi.org/10.1021/acs.nanolett.0c01958.

[105] S. Fujita, H. Habuchi, S. Takagi, H. Takikawa, Optical properties of graphitic carbon nitride films prepared by evaporation, Diam. Relat. Mater. 65 (2016) 83–86, https://doi.org/10.1016/j.diamond.2016.02.008.

[106] Q. Liang, Z. Li, X. Yu, Z.H. Huang, F. Kang, Q.H. Yang, Macroscopic 3D porous graphitic carbon nitride monolith for enhanced photocatalytic hydrogen evolution, Adv. Mater. 27 (31) (2015) 4634–4639, https://doi.org/10.1002/adma.201502057.

[107] K.I. Katsumata, R. Motoyoshi, N. Matsushita, K. Okada, Preparation of graphitic carbon nitride (g-C$_3$N$_4$)/WO$_3$ composites and enhanced visible-light-driven photodegradation of acetaldehyde gas, J. Hazard Mater. 260 (2013) 475–482, https://doi.org/10.1016/j.jhazmat.2013.05.058.

[108] S. Zhou, Y. Liu, J. Li, Y. Wang, G. Jiang, Z. Zhao, D. Wang, A. Duan, J. Liu, Y. Wei, Facile in situ synthesis of graphitic carbon nitride (g-C$_3$N$_4$)-N-TiO$_2$ heterojunction as an efficient photocatalyst for the selective photoreduction of CO$_2$ to CO, Appl. Catal., B 158 (2014) 20–29, https://doi.org/10.1016/j.apcatb.2014.03.037.

[109] T.Y. Ma, J. Ran, S. Dai, M. Jaroniec, S.Z. Qiao, Phosphorus-doped graphitic carbon nitrides grown in situ on carbon-fiber paper: flexible and reversible oxygen electrodes, Angew. Chem. 127 (15) (2015) 4729–4733, https://doi.org/10.1002/ange.201411125.

[110] A.A.S. Nair, R. Sundara, N. Anitha, Hydrogen storage performance of palladium nanoparticles decorated graphitic carbon nitride, Int. J. Hydrogen Energy 40 (8) (2015) 3259–3267, https://doi.org/10.1016/j.ijhydene.2014.12.065.

[111] H. Yan, Soft-templating synthesis of mesoporous graphitic carbon nitride with enhanced photocatalytic H$_2$ evolution under visible light, Chem. Commun. 48 (28) (2012) 3430–3432, https://doi.org/10.1039/c2cc00001f.

[112] G. Liu, X. Yang, T. Li, Y. She, S. Wang, J. Wang, M. Zhang, F. Jin, M. Jin, H. Shao, M. Shi, Preparation of a magnetic molecularly imprinted polymer using g-C$_3$N$_4$-Fe$_3$O$_4$ for atrazine adsorption, Mater. Lett. 160 (2015) 472–475, https://doi.org/10.1016/j.matlet.2015.07.157.

[113] Y.P. Yuan, W.T. Xu, L.S. Yin, S.W. Cao, Y. Sen Liao, Y.Q. Tng, C. Xue, Large impact of heating time on physical properties and photocatalytic H$_2$ production of g-C$_3$N$_4$ nanosheets synthesized through urea polymerization in Ar atmosphere, Int. J. Hydrogen Energy 38 (30) (2013) 13159–13163, https://doi.org/10.1016/j.ijhydene.2013.07.104.

[114] C. Xing, Z. Wu, D. Jiang, M. Chen, Hydrothermal synthesis of In$_2$S$_3$/g-C$_3$N$_4$ heterojunctions with enhanced photocatalytic activity, J. Colloid Interface Sci. 433 (2014) 9–15, https://doi.org/10.1016/j.jcis.2014.07.015.

[115] S. Yang, W. Zhou, C. Ge, X. Liu, Y. Fang, Z. Li, Mesoporous polymeric semiconductor materials of graphitic-C$_3$N$_4$: general and efficient synthesis and their integration with synergistic AgBr NPs for enhanced photocatalytic performances, RSC Adv. 3 (16) (2013) 5631–5638, https://doi.org/10.1039/c3ra22493g.

[116] Q. Huang, J. Yu, S. Cao, C. Cui, B. Cheng, Efficient photocatalytic reduction of CO$_2$ by amine-functionalized g-C$_3$N$_4$, Appl. Surf. Sci. 358 (2015) 350–355, https://doi.org/10.1016/j.apsusc.2015.07.082.

[117] L. Liu, Y. Qi, J. Yang, W. Cui, X. Li, Z. Zhang, An AgI@g-C$_3$N$_4$ hybrid core@ shell structure: stable and enhanced photocatalytic degradation, Appl. Surf. Sci. 358 (2015) 319–327, https://doi.org/10.1016/j.apsusc.2015.07.212.

[118] Y.P. Yuan, L.S. Yin, S.W. Cao, L.N. Gu, G.S. Xu, P. Du, H. Chai, Y. Sen Liao, C. Xue, Microwave-assisted heating synthesis: a general and rapid strategy for large-scale production of highly crystalline g-C$_3$N$_4$ with enhanced photocatalytic H$_2$ production, Green Chem. 16 (11) (2014) 4663–4668, https://doi.org/10.1039/c4gc01517g.

[119] F. Yang, D. Liu, Y. Li, L. Cheng, J. Ye, Salt-template-assisted construction of honeycomb-like structured g-C$_3$N$_4$ with tunable band structure for enhanced photocatalytic H$_2$ production, Appl. Catal., B 240 (2019) 64–71, https://doi.org/10.1016/j.apcatb.2018.08.072.

[120] S. Hu, F. Li, Z. Fan, F. Wang, Y. Zhao, Z. Lv, Band gap-tunable potassium doped graphitic carbon nitride with enhanced mineralization ability, Dalton Trans. 44 (3) (2014) 1084–1092, https://doi.org/10.1039/c4dt02658f.

[121] J. Zhang, S. Hu, Y. Wang, A convenient method to prepare a novel alkali metal sodium doped carbon nitride photocatalyst with a tunable band structure, RSC Adv. 4 (2014) 62912–62919, https://doi.org/10.1039/c4ra11377b.

[122] S. Tonda, S. Kumar, S. Kandula, V. Shanker, Fe-doped and-mediated graphitic carbon nitride nanosheets for enhanced photocatalytic performance under natural sunlight, J Mater Chem A Mater 2 (19) (2014) 6772–6780, https://doi.org/10.1039/c3ta15358d.

[123] M. Duan, G. Zeng, J. He, W. Wang, The design and preparation of Mg and Zn co-doped carbon nitride with enhancing photocatalytic degradation efficiency for methylene blue, Diam. Relat. Mater. 137 (2023) 110090, https://doi.org/10.1016/j.diamond.2023.110090.

[124] H. Chen, Y. Xie, X. Sun, M. Lv, F. Wu, L. Zhang, L. Li, X. Xu, Efficient charge separation based on type-II g-C$_3$N$_4$/TiO$_2$-B nanowire/tube heterostructure photocatalysts, Dalton Trans. 44 (29) (2015) 13030–13039, https://doi.org/10.1039/c5dt01757b.

[125] J. Wang, P. Ren, Y. Du, X. Zhao, Z. Chen, L. Pei, Y. Jin, Construction of tubular g-C$_3$N$_4$/TiO$_2$ S-scheme photocatalyst for high-efficiency degradation of organic pollutants under visible light, J. Alloys Compd. 947 (2023) 169659, https://doi.org/10.1016/j.jallcom.2023.169659.

[126] M. Ismael, The photocatalytic performance of the ZnO/g-C$_3$N$_4$ composite photocatalyst toward degradation of organic pollutants and its inactivity toward hydrogen evolution: the influence of light irradiation and charge transfer, Chem. Phys. Lett. 739 (2020) 136992, https://doi.org/10.1016/j.cplett.2019.136992.

[127] J. Zhang, J. Li, X. Liu, Ternary nanocomposite ZnO-g–C$_3$N$_4$–Go for enhanced photocatalytic degradation of RhB, Opt. Mater. 119 (2021) 111351, https://doi.org/10.1016/j.optmat.2021.111351.

[128] J. Chen, X. Xiao, Y. Wang, Z. Ye, Ag nanoparticles decorated WO$_3$/g-C$_3$N$_4$ 2D/2D heterostructure with enhanced photocatalytic activity for organic pollutants degradation, Appl. Surf. Sci. 467–468 (2019) 1000–1010, https://doi.org/10.1016/j.apsusc.2018.10.236.

[129] Y.O. Ibrahim, M.A. Gondal, Visible-light-driven photocatalytic performance of a Z-scheme based TiO$_2$/WO$_3$/g-C$_3$N$_4$ ternary heterojunctions, Mol. Catal. 505 (2021), https://doi.org/10.1016/j.mcat.2021.111494.

[130] M. Alhaddad, M.S. Amin, Removal of ciprofloxacin applying Pt@BiVO$_4$-g-C$_3$N$_4$ nanocomposite under visible light, Opt. Mater. 124 (2022) 111976, https://doi.org/10.1016/j.optmat.2022.111976.

[131] Z. Wang, J. Wang, W. Iqbal, L. Yang, M. Shi, N. Chang, C. Qin, Controllable fabrication and enhanced photocatalysis of Cu$_2$O NP@g-C$_3$N$_4$ NT composite on visible-light-driven degradation of organic dyes in water, Materials Today Sustainability 20 (2022) 100239, https://doi.org/10.1016/j.mtsust.2022.100239.

[132] X. Zhang, Y. Zhang, Z. Wang, N. Zhang, X. Jia, Construction of a novel Ag$_2$O/P-g-C$_3$N$_4$ p-n type heterojunction for efficient degradation of organic pollutants under visible light irradiation, Diam. Relat. Mater. 130 (2022) 109398, https://doi.org/10.1016/j.diamond.2022.109398.

[133] H. Wei, F. Meng, W. Yu, J. Li, H. Zhang, Highly efficient photocatalytic degradation of levofloxacin by novel S-scheme heterojunction Co$_3$O$_4$/Bi$_2$MoO$_6$@g-C$_3$N$_4$ hollow microspheres: performance, degradation pathway and mechanism, Sep. Purif. Technol. 318 (2023) 123940, https://doi.org/10.1016/j.seppur.2023.123940.

[134] X. Ma, C. Chen, J. Hu, M. Zheng, H. Wang, S. Dong, C. Huang, X. Chen, Evidence of direct Z-scheme g-C$_3$N$_4$/WS$_2$ nanocomposite under interfacial coupling: first-principles study, J. Alloys Compd. 788 (2019) 1–9, https://doi.org/10.1016/j.jallcom.2019.02.044.

[135] Q. Li, N. Zhang, Y. Yang, G. Wang, D.H.L. Ng, High efficiency photocatalysis for pollutant degradation with MoS$_2$/C$_3$N$_4$ heterostructures, Langmuir 30 (29) (2014) 8965–8972, https://doi.org/10.1021/la502033t.

[136] Y. Cui, L. Yang, J. Zheng, Z. Wang, B. Li, Y. Yan, M. Meng, Synergistic interaction of Z-scheme 2D/3D g-C$_3$N$_4$/BiOI heterojunction and porous PVDF membrane for greatly improving the photodegradation efficiency of tetracycline, J. Colloid Interface Sci. 586 (2021) 335–348, https://doi.org/10.1016/j.jcis.2020.10.097.

[137] P. Veisi, M.S. Seyed Dorraji, V. Vatanpour, M.H. Rasoulifard, Dimensional effect of ZnO-g-C$_3$N$_4$ heterostructures on hydrophilic and anti-fouling properties of the PVDF/PAN composite membrane: dye rejection, J. Environ. Chem. Eng. 11 (4) (2023) 110249, https://doi.org/10.1016/j.jece.2023.110249.

[138] M. Majdoub, Z. Anfar, A. Amedlous, Emerging chemical functionalization of g-C$_3$N$_4$: covalent/noncovalent modifications and applications, ACS Nano 14 (10) (2020) 12390–12466, https://doi.org/10.1021/acsnano.0c06116.

[139] D.W. Stephan, Frustrated Lewis pairs, J. Am. Chem. Soc. 137 (32) (2015) 10018–10032, https://doi.org/10.1021/JACS.5B06794.

[140] S. Zhang, Y. Liu, M. Zhang, Y. Ma, J. Hu, Y. Qu, Sustainable production of hydrogen with high purity from methanol and water at low temperatures, Nat. Commun. 13 (1) (2022) 5527, https://doi.org/10.1038/s41467-022-33186-z.

[141] D.W. Stephan, G. Erker, Frustrated Lewis pair chemistry: development and perspectives, Angew. Chem. Int. Ed. 54 (22) (2015) 6400–6441, https://doi.org/10.1002/ANIE.201409800.

[142] J. Chen, M. Yuan, W. Cai, J. Wei, J. Zhou, P. Liu, Z. Yang, J. Luo, Q. Xia, Z. Cai, Constructing the Frustrated Lewis Pairs within N,S-codoped carbon to reveal the role of adjacent heteroatom sites for highly effective removal of heavy metal ions, Chem. Eng. J. 422 (2021) 130153, https://doi.org/10.1016/j.cej.2021.130153.

[143] Y. Ma, S. Zhang, C.R. Chang, Z.Q. Huang, J.C. Ho, Y. Qu, Semi-solid and solid frustrated Lewis pair catalysts, Chem. Soc. Rev. 47 (15) (2018) 5541–5553, https://doi.org/10.1039/c7cs00691h.

[144] M. Trunk, J.F. Teichert, A. Thomas, Room-temperature activation of hydrogen by semi-immobilized frustrated Lewis pairs in microporous polymer networks, J. Am. Chem. Soc. 139 (10) (2017) 3615–3618, https://doi.org/10.1021/jacs.6b13147.

[145] H. Lee, Y.N. Choi, D.W. Lim, M. Rahman, Y. Kim, I.H. Cho, H.W. Kang, J.H. Seo, C. Jeon, K. B Yoon, Formation of frustrated Lewis pairs in pt$_x$-loaded zeolite NaY, Angew. Chem. 127 (44) (2015) 13017–13327, https://doi.org/10.1002/ange.201506790.

[146] X.Y. Sun, B. Li, T.F. Liu, J. Song, D.S. Su, Designing graphene as a new Frustrated Lewis Pair catalyst for hydrogen activation by co-doping, Phys. Chem. Chem. Phys. 18 (16) (2016) 11120–11124, https://doi.org/10.1039/c5cp07969a.

[147] Y. Ran, X. Yu, J. Liu, J. Cui, J. Wang, L. Wang, Y. Zhang, X. Xiang, J. Ye, Polymeric carbon nitride with frustrated Lewis pair sites for enhanced photofixation of nitrogen, J Mater Chem A Mater 8 (26) (2020) 13292–13298, https://doi.org/10.1039/d0ta03914d.

[148] Y. Zhang, Y. Mo, Z. Cao, Rational design of main group metal-embedded nitrogen-doped carbon materials as Frustrated Lewis Pair Catalysts for CO_2 hydrogenation to formic acid, ACS Appl. Mater. Interfaces 14 (1) (2022) 1002–1014, https://doi.org/10.1021/acsami.1c20230.

[149] Q. Wan, J. Li, R. Jiang, S. Lin, Construction of Frustrated Lewis Pairs on carbon nitride nanosheets for catalytic hydrogenation of acetylene, Phys. Chem. Chem. Phys. 23 (42) (2021) 24349–24356, https://doi.org/10.1039/d1cp03592d.

[150] S. Shyshkanov, T.N. Nguyen, A. Chidambaram, K.C. Stylianou, P.J. Dyson, Frustrated Lewis Pair-mediated fixation of CO_2 within a metal-organic framework, Chem. Commun. 55 (73) (2019) 10964–10967, https://doi.org/10.1039/c9cc04374h.

[151] X. Tan, H. Wang, Frustrated Lewis Pair catalysis: it takes two to make a thing go right, Chin. J. Chem. 39 (5) (2021) 1344–1352, https://doi.org/10.1002/CJOC.202000570.

[152] W. Lin, H. Chen, G. Lin, S. Yao, Z. Zhang, J. Qi, M. Jing, W. Song, J. Li, X. Liu, J. Fu, S. Dai, Creating Frustrated Lewis Pairs in defective boron carbon nitride for electrocatalytic nitrogen reduction to ammonia, Angew. Chem. Int. Ed. 61 (36) (2022) e202207807, https://doi.org/10.1002/anie.202207807.

[153] R.C. Pullar, Hexagonal ferrites: a review of the synthesis, properties and applications of hexaferrite ceramics, Prog. Mater. Sci. 57 (7) (2012) 1191–1334, https://doi.org/10.1016/j.pmatsci.2012.04.001.

[154] A. Houbi, Z.A. Aldashevich, Y. Atassi, Z. Bagasharova Telmanovna, M. Saule, K. Kubanych, Microwave absorbing properties of ferrites and their composites: a review, J. Magn. Magn Mater. 529 (2021) 167839, https://doi.org/10.1016/j.jmmm.2021.167839.

[155] K.K. Kefeni, B.B. Mamba, T.A.M. Msagati, Application of spinel ferrite nanoparticles in water and wastewater treatment: a review, Sep. Purif. Technol. 188 (2017) 399–422, https://doi.org/10.1016/j.seppur.2017.07.015.

[156] H. Qin, Y. He, P. Xu, D. Huang, Z. Wang, H. Wang, Z. Wang, Y. Zhao, Q. Tian, C. Wang, Spinel ferrites (MFe_2O_4): synthesis, improvement and catalytic application in environment and energy field, Adv. Colloid Interface Sci. 294 (2021) 102486, https://doi.org/10.1016/j.cis.2021.102486.

[157] C.M. Park, Y.M. Kim, K.H. Kim, D. Wang, C. Su, Y. Yoon, Potential utility of graphene-based nano spinel ferrites as adsorbent and photocatalyst for removing organic/inorganic contaminants from aqueous solutions: a mini review, Chemosphere 221 (2019) 392–402, https://doi.org/10.1016/j.chemosphere.2019.01.063.

[158] V.G. Harris, A. Geiler, Y. Chen, S.D. Yoon, M. Wu, A. Yang, Z. Chen, P. He, P.V. Parimi, X. Zuo, C.E. Patton, M. Abe, O. Acher, C. Vittoria, Recent advances in processing and applications of microwave ferrites, J. Magn. Magn Mater. 321 (14) (2009) 2035–2047, https://doi.org/10.1016/j.jmmm.2009.01.004.

[159] T. Kimura, Magnetoelectric Hexaferrites, Annual Review of Condensed Matter Physics 3 (1) (2012) 93–110, https://doi.org/10.1146/annurev-conmatphys-020911-125101.

[160] R.L. White, Review of recent work on the magnetic and spectroscopic properties of the rare-earth orthoferrites, J. Appl. Phys. 40 (3) (1969) 1061–1069, https://doi.org/10.1063/1.1657530.

[161] R. Sagayaraj, S. Aravazhi, G. Chandrasekaran, Review on structural and magnetic properties of (Co–Zn) ferrite nanoparticles, Int. Nano Lett. 11 (4) (2021) 307–319, https://doi.org/10.1007/s40089-021-00343-z.

[162] D.S. Mathew, R.S. Juang, An overview of the structure and magnetism of spinel ferrite nanoparticles and their synthesis in microemulsions, Chem. Eng. J. 129 (1–3) (2007) 51–65, https://doi.org/10.1016/j.cej.2006.11.001.

[163] W. Li, J.D. Fortner, (Super)paramagnetic nanoparticles as platform materials for environmental applications: from synthesis to demonstration, Front. Environ. Sci. Eng. 14 (77) (2020), https://doi.org/10.1007/s11783-020-1256-7.

[164] A. Goldman, Handbook of Modern Ferromagnetic Materials, Springer Science & Business Media, New York, 2012, p. 505, https://doi.org/10.1007/978-1-4615-4917-8.

[165] S. Palagummi, F.G. Yuan, Magnetic levitation and its application for low frequency vibration energy harvesting, in: Structural Health Monitoring (SHM) in Aerospace Structures, Woodhead Publishing, 2016, pp. 213–251, https://doi.org/10.1016/B978-0-08-100148-6.00008-1.

[166] C. Tapeinos, Magnetic nanoparticles and their bioapplications, in: Smart Nanoparticles for Biomedicine, Elsevier, 2018, pp. 131–142, https://doi.org/10.1016/B978-0-12-814156-4.00009-4.

[167] M.K. Zate, S.D. Raut, S.D. Shirsat, S. Sangale, A.S. Kadam, Ferrite nanostructures: synthesis methods, in: Spinel Ferrite Nanostructures for Energy Storage Devices, Micro and Nano Technologies, Elsevier, 2020, pp. 13–34, https://doi.org/10.1016/b978-0-12-819237-5.00002-x.

[168] S. Zhang, F. Rong, S. Huang, S. Zhao, M. Wang, L. He, Z. Zhang, M. Du, Atomic Fe sites embedded within carbon nanotubes for the efficient photodegradation of multiple tetracyclines, Sep. Purif. Technol. 287 (2022) 120530, https://doi.org/10.1016/j.seppur.2022.120530.

[169] J. Liu, Y. Song, H. Xu, X. Zhu, J. Lian, Y. Xu, Y. Zhao, L. Huang, H. Ji, H. Li, Non-metal photocatalyst nitrogen-doped carbon nanotubes modified mpg-C_3N_4: facile synthesis and the enhanced visible-light photocatalytic activity, J. Colloid Interface Sci. 494 (2017) 38–46, https://doi.org/10.1016/j.jcis.2017.01.010.

[170] N. Agasti, V. Gautam, Manju Priyanka, N. Pandey, M. Genwa, P.L. Meena, S. Tandon, R. Samantaray, Carbon nanotube based magnetic composites for decontamination of organic chemical pollutants in water: a review, Applied Surface Science Advances 10 (2022) 100270, https://doi.org/10.1016/j.apsadv.2022.100270.

[171] Y. Deng, Y.S. Ok, D. Mohan, C.U. Pittman, X. Dou, Carbamazepine removal from water by carbon dot-modified magnetic carbon nanotubes, Environ. Res. 169 (2019) 434–444, https://doi.org/10.1016/j.envres.2018.11.035.

[172] S. Das, S. Das, R.G. Nair, A. Chowdhury, Magnetically separable ZnFe$_2$O$_4$ grafted g-C_3N_4/rGO ternary nanocomposites for enhanced photo-Fenton catalytic activity under visible light, Materials Today Sustainability 21 (2023) 100263, https://doi.org/10.1016/j.mtsust.2022.100263.

[173] A. Sudhaik, P. Raizada, P. Shandilya, P. Singh, Magnetically recoverable graphitic carbon nitride and NiFe$_2$O$_4$ based magnetic photocatalyst for degradation of oxytetracycline antibiotic in simulated wastewater under solar light, J. Environ. Chem. Eng. 6 (4) (2018) 3874–3883, https://doi.org/10.1016/j.jece.2018.05.039.

[174] M. Nawaz, A. Shahzad, K. Tahir, J. Kim, M. Moztahida, J. Jang, M.B. Alam, S.H. Lee, H.Y. Jung, D.S. Lee, Photo-Fenton reaction for the degradation of sulfamethoxazole using a multi-walled carbon nanotube-NiFe$_2$O$_4$ composite, Chem. Eng. J. 382 (2020) 123053, https://doi.org/10.1016/j.cej.2019.123053.

[175] Y. Fu, P. Xiong, H. Chen, X. Sun, X. Wang, High photocatalytic activity of magnetically separable manganese ferrite-graphene heteroarchitectures, Ind. Eng. Chem. Res. 51 (2) (2012) 725–731, https://doi.org/10.1021/ie2026212.

[176] I.F. Waheed, M.A. Hamad, K.A. Jasim, A.J. Gesquiere, Degradation of methylene blue using a novel magnetic CuNiFe$_2$O$_4$/g-C_3N_4 nanocomposite as heterojunction photocatalyst, Diam. Relat. Mater. 133 (2023) 109716, https://doi.org/10.1016/j.diamond.2023.109716.

[177] A.S. Basaleh, Construction of mesoporous ZnFe$_2$O$_4$-g-C_3N_4 nanocomposites for enhanced photocatalytic degradation of acridine orange dye under visible light illumination adopting soft- and hard-template-assisted routines, J. Mater. Res. Technol. 11 (2021) 1260–1271, https://doi.org/10.1016/j.jmrt.2021.01.110.

[178] D. Xie, S. Zhang, T. Wu, M. He, Y. Cai, P. Zhao, F. Cheng, Efficient RhB degradation using MnFe$_2$O$_4$/g-C_3N_4 composites under visible light irradiation, Opt. Mater. 124 (2022) 111965, https://doi.org/10.1016/j.optmat.2021.111965.

[179] C. Aruljothi, P. Balaji, E. Vaishnavi, T. Pazhanivel, T. Vasuki, Magnetic recyclable CuFe2O4/rGO nanocomposite for the degradation of tetracycline under sunlight irradiation, J. Chem. Technol. Biotechnol. 98 (8) (2023) 1908–1917, https://doi.org/10.1002/jctb.7408.

[180] S. Shenoy, C. Chuaicham, T. Okumura, K. Sekar, K. Sasaki, Simple tactic polycondensation synthesis of Z-scheme quasi-polymeric g-C3N4/CaFe2O4 composite for enhanced photocatalytic water depollution via p-n heterojunction, Chem. Eng. J. 453 (2023) 139758, https://doi.org/10.1016/j.cej.2022.139758.

[181] J. Kaur, M. Kaur, Facile fabrication of ternary nanocomposite of MgFe2O4/TiO2@GO for synergistic adsorption and photocatalytic degradation studies, Ceram. Int. 45 (7) (2019) 8646–8659, https://doi.org/10.1016/j.ceramint.2019.01.185.

[182] S. Huang, Y. Xu, M. Xie, H. Xu, M. He, J. Xia, L. Huang, H. Li, Synthesis of magnetic CoFe2O4/g-C3N4 composite and its enhancement of photocatalytic ability under visible-light, Colloids Surf. A Physicochem. Eng. Asp. 478 (2015) 71–80, https://doi.org/10.1016/j.colsurfa.2015.03.035.

[183] S. Vignesh, S. Suganthi, J. Kalyana Sundar, V. Raj, Construction of α-Fe2O3/CeO2 decorated g-C3N4 nanosheets for magnetically separable efficient photocatalytic performance under visible light exposure and bacterial disinfection, Appl. Surf. Sci. 488 (2019) 763–777, https://doi.org/10.1016/j.apsusc.2019.05.147.

[184] Y. Wu, H. Luo, X. Jiang, H. Wang, J. Geng, Facile synthesis of magnetic Bi25FeO40/rGO catalyst with efficient photocatalytic performance for phenolic compounds under visible light, RSC Adv. 5 (7) (2015) 4905–4908, https://doi.org/10.1039/c4ra11355a.

[185] P. Zhou, F. Chen, X. Su, T. Zhang, S. Meng, M. Xie, Y. Song, X. Yan, Y. Xu, Ag2O modified magnetic BaFe12O19/C3N4 photocatalysts with enhanced antibiotic removal: photocatalytic mechanism and toxicity evaluation, Adv. Powder Technol. 34 (6) (2023) 104015, https://doi.org/10.1016/j.apt.2023.104015.

[186] Y. Lu, B. Ren, S. Chang, W. Mi, J. He, W. Wang, Achieving effective control of the photocatalytic performance for CoFe2O4/MoS2 heterojunction via exerting external magnetic fields, Mater. Lett. 260 (2020) 126979, https://doi.org/10.1016/j.matlet.2019.126979.

[187] Y. Bian, Z. Zheng, W. Ding, L. Hu, Z. Sheng, Magnetic field effect on the photocatalytic degradation of methyl orange by commercial TiO2 powder, RSC Adv. 11 (11) (2021) 6284–6291, https://doi.org/10.1039/d0ra08359c.

[188] X. Li, W. Wang, F. Dong, Z. Zhang, L. Han, X. Luo, J. Huang, Z. Feng, Z. Chen, G. Jia, T. Zhang, Recent advances in noncontact external-field-assisted photocatalysis: from Fundamentals to applications, ACS Catal. 11 (2021) 4739–4769, https://doi.org/10.1021/acscatal.0c05354.

[189] Y. Wu, T. Li, X. Ren, Y. Fu, H. Zhang, X. Xie, H. Huang, R. Xie, Magnetic field assisted α-Fe2O3/Zn1−xFexO heterojunctions for accelerating antiviral agents degradation under visible-light, J. Environ. Chem. Eng. 10 (2022), https://doi.org/10.1016/j.jece.2021.106990.

[190] Y. Li, Z. Wang, Y. Wang, A. Kovács, C. Foo, R.E. Dunin-Borkowski, Y. Lu, R.A. Taylor, C. Wu, S.C.E. Tsang, Local magnetic spin mismatch promoting photocatalytic overall water splitting with exceptional solar-to-hydrogen efficiency, Energy Environ. Sci. 15 (2022) 265–277, https://doi.org/10.1039/d1ee02222a.

[191] H. Okumura, S. Endo, S. Joonwichien, E. Yamasue, K.N. Ishihara, Magnetic field effect on heterogeneous photocatalysis, Catal. Today 258 (2015) 634–647, https://doi.org/10.1016/j.cattod.2014.12.048.

[192] J. Li, Q. Pei, R. Wang, Y. Zhou, Z. Zhang, Q. Cao, D. Wang, W. Mi, Y. Du, Enhanced photocatalytic performance through magnetic field boosting carrier transport, ACS Nano 12 (4) (2018) 3351–3359, https://doi.org/10.1021/acsnano.7b08770.192.

[193] U.E. Steiner, T. Ulrich, Magnetic field effects in chemical kinetics and related phenomena, Chem. Rev. 89 (1) (1989) 51–147, https://doi.org/10.1021/cr00091a003.

[194] R. Marschall, Semiconductor composites: strategies for enhancing charge carrier separation to improve photocatalytic activity, Adv. Funct. Mater. 24 (17) (2014) 2421–2440, https://doi.org/10.1002/adfm.201303214.

[195] L. Zhang, J. Zhang, H. Yu, J. Yu, Emerging S-Scheme photocatalyst, Adv. Mater. 34 (11) (2022) 2107668, https://doi.org/10.1002/adma.202107668.

[196] J. Low, J. Yu, C. Jiang, Design and fabrication of direct Z-scheme photocatalysts, Interface Science and Technology 31 (2020) 193–229, https://doi.org/10.1016/B978-0-08-102890-2.00006-3.

[197] S.A. Hassanzadeh-Tabrizi, Synthesis of NiFe2O4/Ag nanoparticles immobilized on mesoporous g-C3N4 sheets and application for degradation of antibiotics, J. Photochem. Photobiol. Chem. 418 (2021) 113398, https://doi.org/10.1016/j.jphotochem.2021.113398.

[198] V.D. Dang, T. Annadurai, A.P. Khedulkar, J.Y. Lin, J. Adorna, W.J. Yu, B. Pandit, T.V. Huynh, R.A. Doong, S-scheme N-doped carbon dots anchored g-C3N4/Fe2O3 shell/core composite for photoelectrocatalytic trimethoprim degradation and water splitting, Appl. Catal., B 320 (2023), https://doi.org/10.1016/j.apcatb.2022.121928.

[199] Y. Shi, L. Li, Z. Xu, H. Sun, S. Amin, F. Guo, W. Shi, Y. Li, Engineering of 2D/3D architectures type II heterojunction with high-crystalline g-C3N4 nanosheets on yolk-shell ZnFe2O4 for enhanced photocatalytic tetracycline degradation, Mater. Res. Bull. 150 (2022) 111789, https://doi.org/10.1016/j.materresbull.2022.111789.

[200] A.A.P. Khan, P. Singh, P. Raizada, A.M. Asiri, Synthesis of magnetically separable Bi2O2CO3/carbon nanotube/ZnFe2O4 as Z-scheme heterojunction with enhanced photocatalytic activity for water purification, J. Sol. Gel Sci. Technol. 95 (2) (2020) 408–422, https://doi.org/10.1007/s10971-020-05336-6.

[201] M. Danish, M. Saud Athar, I. Ahmad, M.Z.A. Warshagha, Z. Rasool, M. Muneer, Highly efficient and stable Fe2O3/g-C3N4/GO nanocomposite with Z-scheme electron transfer pathway: role of photocatalytic activity and adsorption isotherm of organic pollutants in wastewater, Appl. Surf. Sci. 604 (2022), https://doi.org/10.1016/j.apsusc.2022.154604.

[202] V. Van Pham, T.K. Truong, L.V. Hai, H.P.P. La, H.T. Nguyen, V.Q. Lam, H.D. Tong, T.Q. Nguyen, A. Sabbah, K.H. Chen, S.J. You, T.M. Cao, S-Scheme α-Fe2O3/g-C3N4 nanocomposites as heterojunction photocatalysts for antibiotic degradation, ACS Appl. Nano Mater. 5 (3) (2022) 4506–4514, https://doi.org/10.1021/acsanm.2c00741.

[203] R. Acharya, K. Parida, A review on TiO2/g-C3N4 visible-light-responsive photocatalysts for sustainable energy generation and environmental remediation, J. Environ. Chem. Eng. 8 (4) (2020) 103896, https://doi.org/10.1016/j.jece.2020.103896.

[204] S. Shanavas, S. Mohana Roopan, A. Priyadharsan, D. Devipriya, S. Jayapandi, R. Acevedo, P.M. Anbarasan, Computationally guided synthesis of (2D/3D/2D) rGO/Fe2O3/g-C3N4 nanostructure with improved charge separation and transportation efficiency for degradation of pharmaceutical molecules, Appl. Catal., B 255 (2019) 117758, https://doi.org/10.1016/j.apcatb.2019.117758.

[205] K. Saravanakumar, C.M. Park, Rational design of a novel LaFeO3/g-C3N4/BiFeO3 double Z-scheme structure: photocatalytic performance for antibiotic degradation and mechanistic insight, Chem. Eng. J. 423 (2021) 130076, https://doi.org/10.1016/j.cej.2021.130076.

[206] Y. Shi, L. Li, Z. Xu, H. Sun, S. Amin, F. Guo, W. Shi, Y. Li, Engineering of 2D/3D architectures type II heterojunction with high-crystalline g-C3N4 nanosheets on yolk-shell ZnFe2O4 for enhanced photocatalytic tetracycline degradation, Mater. Res. Bull. 150 (2022) 111789, https://doi.org/10.1016/j.materresbull.2022.111789.

[207] M.C. Shibu, M.D. Benoy, S. Shanavas, M.A. Haija, J. Duraimurugan, G.S. Kumar, T. Ahamad, P. Maadeswaran, Q. Van Le, White LED active α-Fe2O3/rGO photocatalytic nanocomposite for an effective degradation of tetracycline and ibuprofen molecules, Environ. Res. 212 (2022) 113301, https://doi.org/10.1016/j.envres.2022.113301.

[208] A. Behera, D. Kandi, S. Mansingh, S. Martha, K. Parida, Facile synthesis of ZnFe2O4@RGO nanocomposites towards photocatalytic ciprofloxacin degradation and H2 energy production, J. Colloid Interface Sci. 556 (2019) 667–679, https://doi.org/10.1016/j.jcis.2019.08.109.

[209] A. Behera, S. Mansingh, K.K. Das, K. Parida, Synergistic ZnFe2O4-carbon allotropes nanocomposite photocatalyst for norfloxacin degradation and Cr (VI) reduction, J. Colloid Interface Sci. 544 (2019) 96–111, https://doi.org/10.1016/j.jcis.2019.02.056.

[210] F. Liu, W. Zhang, W. Chen, J. Wang, Q. Yang, W. Zhu, J. Wang, One-pot synthesis of NiFe2O4 integrated with EDTA-derived carbon dots for enhanced removal of tetracycline, Chem. Eng. J. 310 (2017) 187–196, https://doi.org/10.1016/j.cej.2016.10.116.

[211] P. Xiong, Y. Fu, L. Wang, X. Wang, Multi-walled carbon nanotubes supported nickel ferrite: a magnetically recyclable photocatalyst with high photocatalytic activity on degradation of phenols, Chem. Eng. J. 195–196 (2012) 149–157, https://doi.org/10.1016/j.cej.2012.05.007.

[212] R. Foroutan, S.J. Peighambardoust, P. Latifi, A. Ahmadi, M. Alizadeh, B. Ramavandi, Carbon nanotubes/β-cyclodextrin/MnFe2O4 as a magnetic nanocomposite powder for tetracycline antibiotic decontamination from different aqueous environments, J. Environ. Chem. Eng. 9 (6) (2021) 106344, https://doi.org/10.1016/j.jece.2021.106344.

[213] H. Wang, L. Zhang, Z. Chen, J. Hu, S. Li, Z. Wang, J. Liu, X. Wang, Semiconductor heterojunction photocatalysts: design, construction, and photocatalytic performances, Chem. Soc. Rev. 43 (15) (2014) 5234–5244, https://doi.org/10.1039/c4cs00126e.

[214] M.I. Litter, Heterogeneous photocatalysis: transition metal ions in photocatalytic systems, Appl. Catal., B 23 (2–3) (1999) 89–114, https://doi.org/10.1016/S0926-3373(99)00069-7.

[215] S. Wacławek, H.V. Lutze, K. Grübel, V.V.T. Padil, M. Černík, D.D. Dionysiou, Chemistry of persulfates in water and wastewater treatment: a review, Chem. Eng. J. 330 (2017) 44–62, https://doi.org/10.1016/j.cej.2017.07.132.

[216] Z. Zhou, X. Liu, K. Sun, C. Lin, J. Ma, M. He, W. Ouyang, Persulfate-based advanced oxidation processes (AOPs) for organic-contaminated soil remediation: a review, Chem. Eng. J. 372 (2019) 836–851, https://doi.org/10.1016/j.cej.2019.04.213.

[217] C. Yao, Y. Zhang, M. Du, X. Du, S. Huang, Insights into the mechanism of non-radical activation of persulfate via activated carbon for the degradation of p-chloroaniline, Chem. Eng. J. 362 (2019) 262–268, https://doi.org/10.1016/j.cej.2019.01.040.

[218] D.L. Ball, J.O. Edwards, The kinetics and mechanism of the decomposition of Caro's acid. I, J. Am. Chem. Soc. 78 (6) (1956) 1125–1129, https://doi.org/10.1021/ja01587a011.

[219] S. Wacławek, K. Grübel, M. Černík, Simple spectrophotometric determination of monopersulfate, Spectrochim. Acta: Mol Biomol Spectrosc. 149 (2015) 928–933, https://doi.org/10.1016/j.saa.2015.05.029.

[220] Q. Gao, G. Wang, Y. Chen, B. Han, K. Xia, C. Zhou, Utilizing cobalt-doped materials as heterogeneous catalysts to activate peroxymonosulfate for organic pollutant degradation: a critical review, Environ. Sci. 7 (7) (2021) 1197–1211, https://doi.org/10.1039/d0ew01042a.

[221] S. Giannakis, K.Y.A. Lin, F. Ghanbari, A review of the recent advances on the treatment of industrial wastewaters by sulfate radical-based advanced oxidation processes (SR-AOPs), Chem. Eng. J. 406 (2021) 127083, https://doi.org/10.1016/j.cej.2020.127083.

[222] Y. Gao, Q. Wang, G. Ji, A. Li, Degradation of antibiotic pollutants by persulfate activated with various carbon materials, Chem. Eng. J. 429 (2022) 132387, https://doi.org/10.1016/j.cej.2021.132387.

[223] R.L. Johnson, P.G. Tratnyek, R.O.B. Johnson, Persulfate persistence under thermal activation conditions, Environ. Sci. Technol. 42 (2008) 9350–9356, https://doi.org/10.1021/es8019462.

[224] A. Ghauch, A.M. Tuqan, Oxidation of bisoprolol in heated persulfate/H2O systems: kinetics and products, Chem. Eng. J. 183 (2012) 162–171, https://doi.org/10.1016/j.cej.2011.12.048.

[225] Z. Wei, F.A. Villamena, L.K. Weavers, Kinetics and mechanism of ultrasonic activation of persulfate: an in situ EPR spin trapping study, Environ. Sci. Technol. 51 (6) (2017) 3410–3417, https://doi.org/10.1021/acs.est.6b05392.

[226] Y.Q. Gao, N.Y. Gao, Y. Deng, Y.Q. Yang, Y. Ma, Ultraviolet (UV) light-activated persulfate oxidation of sulfamethazine in water, Chem. Eng. J. 195–196 (2012) 248–253, https://doi.org/10.1016/j.cej.2012.04.084.

[227] S.X. Liang, Z. Jia, W.C. Zhang, W.M. Wang, L.C. Zhang, Rapid malachite green degradation using Fe73.5Si13.5B9Cu1Nb3 metallic glass for activation of persulfate under UV–Vis light, Mater. Des. 119 (2017) 244–253, https://doi.org/10.1016/j.matdes.2017.01.039.

[228] Y. Shi, H. Chen, Y. Wu, W. Dong, Degradation of atenolol via heterogeneous activation of persulfate by using BiOCl@Fe3O4 catalyst under simulated solar light irradiation, Environ. Sci. Pollut. Control Ser. 25 (2018) 693–703, https://doi.org/10.1007/s11356-017-0256-z.

[229] Y. Li, W. Xiang, T. Zhou, M. Huang, C. Wang, X. Wu, J. Mao, P. Wang, Visible light induced efficient activation of persulfate by a carbon quantum dots (CQDs) modified γ-Fe2O3 catalyst, Chin. Chem. Lett. 31 (2020) 2757–2761, https://doi.org/10.1016/j.cclet.2020.01.032.

[230] F. Gao, Y. Li, B. Xiang, Degradation of bisphenol A through transition metals activating persulfate process, Ecotoxicol. Environ. Saf. 158 (2018) 239–247, https://doi.org/10.1016/j.ecoenv.2018.03.035.

[231] S. Yan, Y. Shi, Y. Tao, H. Zhang, Enhanced persulfate-mediated photocatalytic oxidation of bisphenol A using bioelectricity and a g-C3N4/Fe2O3 heterojunction, Chem. Eng. J. 359 (2019) 933–943, https://doi.org/10.1016/j.cej.2018.11.093.

[232] Y.Y. Ahn, E.T. Yun, Heterogeneous metals and metal-free carbon materials for oxidative degradation through persulfate activation: a review of heterogeneous catalytic activation of persulfate related to oxidation mechanism, Kor. J. Chem. Eng. 36 (2019) 1767–1779, https://doi.org/10.1007/s11814-019-0398-4.

[233] P.F. Xiao, L. An, D.D. Wu, The use of carbon materials in persulfate-based advanced oxidation processes: a review, N. Carbon Mater. 35 (6) (2020) 667–683, https://doi.org/10.1016/S1872-5805(20)60521-2.

[234] F. Ghanbari, M. Moradi, Application of peroxymonosulfate and its activation methods for degradation of environmental organic pollutants: review, Chem. Eng. J. 310 (2017) 41–62, https://doi.org/10.1016/j.cej.2016.10.064.

[235] Z. Zhou, X. Liu, K. Sun, C. Lin, J. Ma, M. He, W. Ouyang, Persulfate-based advanced oxidation processes (AOPs) for organic-contaminated soil remediation: a review, Chem. Eng. J. 372 (2019) 836–851, https://doi.org/10.1016/j.cej.2019.04.213.

[236] P. Gan, Z. Zhang, Y. Hu, Y. Li, J. Ye, M. Tong, J. Liang, Insight into the role of Fe in the synergetic effect of persulfate/sulfite and Fe2O3@g-C3N4 for carbamazepine degradation, Sci. Total Environ. 819 (2022) 152787, https://doi.org/10.1016/j.scitotenv.2021.152787.

[237] S.W. Lv, J.M. Liu, N. Zhao, C.Y. Li, F.E. Yang, Z.H. Wang, S. Wang, MOF-derived CoFe2O4/Fe2O3 embedded in g-C3N4 as high-efficient Z-scheme photocatalysts for enhanced degradation of emerging organic pollutants in the presence of persulfate, Sep. Purif. Technol. 253 (2020) 117413, https://doi.org/10.1016/j.seppur.2020.117413.

[238] L. Wang, X. Ma, G. Huang, R. Lian, J. Huang, H. She, Q. Wang, Construction of ternary CuO/CuFe2O4/g-C3N4 composite and its enhanced photocatalytic degradation of tetracycline hydrochloride with persulfate under simulated sunlight, J. Environ. Sci. (China) 112 (2021) 59–70, https://doi.org/10.1016/j.jes.2021.04.026.

[239] R. Li, M. Cai, Z. Xie, Q. Zhang, Y. Zeng, H. Liu, G. Liu, W. Lv, Construction of heterostructured CuFe2O4/g-C3N4 nanocomposite as an efficient visible light photocatalyst with peroxydisulfate for the organic oxidation, Appl. Catal., B 244 (2019) 974–982, https://doi.org/10.1016/j.apcatb.2018.12.043.

[240] L.G. Devi, M. Srinivas, Hydrothermal synthesis of reduced graphene oxide-CoFe2O4 heteroarchitectures for high visible light photocatalytic activity: exploration of efficiency, stability and mechanistic pathways, J. Environ. Chem. Eng. 5 (4) (2017) 3243–3255, https://doi.org/10.1016/j.jece.2017.06.023.

[241] B. Liu, W. Song, W. Zhang, X. Zhang, S. Pan, H. Wu, Y. Sun, Y. Xu, Fe3O4@CNT as a high-effective and steady chainmail catalyst for tetracycline degradation with peroxydisulfate activation: performance and mechanism, Sep. Purif. Technol. 273 (2021) 118705, https://doi.org/10.1016/j.seppur.2021.118705.

[242] R. Amiri, A. Rezaei, N. Fattahi, M. Pirsaheb, J. Rodríguez-Chueca, M. Moradi, Carbon quantum dots decorated Ag/CuFe2O4 for persulfate-assisted visible light photocatalytic degradation of tetracycline: a comparative study, J. Water Proc. Eng. 47 (2022) 102742, https://doi.org/10.1016/j.jwpe.2022.102742.

[243] Y. Li, W. Xiang, T. Zhou, M. Huang, C. Wang, X. Wu, J. Mao, P. Wang, Visible light induced efficient activation of persulfate by a carbon quantum dots (CQDs) modified γ-Fe2O3 catalyst, Chin. Chem. Lett. 31 (10) (2020) 2757–2761, https://doi.org/10.1016/j.cclet.2020.01.032.

[244] T. Zhang, H. Zhu, J.P. Croué, Production of sulfate radical from peroxymonosulfate induced by a magnetically separable CuFe2O4 spinel in water: efficiency, stability, and mechanism, Environ. Sci. Technol. 47 (6) (2013) 2784–2791, https://doi.org/10.1021/es304721g.

[245] S. Zhu, W. Wang, Y. Xu, Z. Zhu, Z. Liu, F. Cui, Iron sludge-derived magnetic Fe0/Fe3C catalyst for oxidation of ciprofloxacin via peroxymonosulfate activation, Chem. Eng. J. 365 (2019) 99–110, https://doi.org/10.1016/j.cej.2019.02.011.

[246] X. Zhang, C. Li, T. Chen, Y. Tan, X. Liu, F. Yuan, S. Zheng, Z. Sun, Enhanced visible-light-assisted peroxymonosulfate activation over MnFe2O4 modified g-C3N4/diatomite composite for bisphenol A degradation, Int. J. Min. Sci. Technol. 31 (2021) 1169–1179, https://doi.org/10.1016/j.ijmst.2021.11.008.

[247] F. Yin, C. Wang, K.Y.A. Lin, S. Tong, Persulfate activation for efficient degradation of norfloxacin by a rGO-Fe3O4 composite, J. Taiwan Inst. Chem. Eng. 102 (2019) 163–169, https://doi.org/10.1016/j.jtice.2019.05.022.

[248] S. Zuo, D. Xia, Z. Guan, F. Yang, B. Zhang, H. Xu, M. Huang, X. Guo, D. Li, The polarized electric field on Fe2O3/g-C3N4 for efficient peroxymonosulfate activation: a synergy of 1O2, electron transfer and pollutant oxidation, Sep. Purif. Technol. 269 (2021), https://doi.org/10.1016/j.seppur.2021.118717.

[249] N. Olfatmehr, B. Kakavandi, S.M. Khezri, Peroxydisulfate activation by enhanced catalytic activity of CoFe2O4 anchored on activated carbon: a new sulfate radical-based oxidation study on the Cefixime degradation, Sep. Purif. Technol. 302 (2022), https://doi.org/10.1016/j.seppur.2022.121991.

[250] A. Kumar, A. Rana, G. Sharma, M. Naushad, P. Dhiman, A. Kumari, F.J. Stadler, Recent advances in nano-Fenton catalytic degradation of emerging pharmaceutical contaminants, J. Mol. Liq. 290 (2019) 111177, https://doi.org/10.1016/j.molliq.2019.111177.

[251] T. Zhang, C. Qian, P. Guo, S. Gan, L. Dong, G. Bai, Q. Guo, A novel reduced graphene oxide-attapulgite (RGO-ATP) supported Fe2O3 catalyst for heterogeneous Fenton-like oxidation of ciprofloxacin : degradation mechanism and pathway, Catalysts 10 (2) (2020) 189, https://doi.org/10.3390/catal10020189.

[252] B. Palanivel, M. Lallimathi, B. Arjunkumar, M. Shkir, T. Alshahrani, K.S. Al-Namshah, M.S. Hamdy, S. Shanavas, M. Venkatachalam, G. Ramalingam, rGO supported g-C_3N_4/$CoFe_2O_4$heterojunction: visible-light-active photocatalyst for effective utilization of H_2O_2 to organic pollutant degradation and OH radicals production, J. Environ. Chem. Eng. 9 (1) (2021) 104698, https://doi.org/10.1016/j.jece.2020.104698.

[253] W. Shi, L. Wang, J. Wang, H. Sun, Y. Shi, F. Guo, C. Lu, Magnetically retrievable CdS/reduced graphene oxide/$ZnFe_2O_4$ ternary nanocomposite for self-generated H_2O_2 towards photo-Fenton removal of tetracycline under visible light irradiation, Sep. Purif. Technol. 292 (2022) 120987, https://doi.org/10.1016/j.seppur.2022.120987.

[254] Y. Liu, X. Zhang, J. Deng, Y. Liu, A novel CNTs-Fe_3O_4 synthetized via a ball-milling strategy as efficient Fenton-like catalyst for degradation of sulfonamides, Chemosphere 277 (2021) 130305, https://doi.org/10.1016/j.chemosphere.2021.130305.

[255] Y. Akhi, M. Irani, M.E. Olya, Simultaneous degradation of phenol and paracetamol using carbon/MWCNT/Fe_3O_4 composite nanofibers during photo-like-Fenton process, J. Taiwan Inst. Chem. Eng. 63 (2016) 327–335, https://doi.org/10.1016/j.jtice.2016.03.028.

[256] A.A.P. Khan, P. Singh, P. Raizada, A.M. Asiri, Synthesis of magnetically separable $Bi_2O_2CO_3$/carbon nanotube/$ZnFe_2O_4$ as Z-scheme heterojunction with enhanced photocatalytic activity for water purification, J. Sol. Gel Sci. Technol. 95 (2020) 408–422, https://doi.org/10.1007/s10971-020-05336-6.

[257] J.A. Z, J.J.R.P. Bautista, A.F. Mohedano, J.A. Casas, An overview of the application of Fenton oxidation to industrial wastewaters treatment, J. Chem. Technol. Biotechnol. 83 (10) (2008) 1323–1338, https://doi.org/10.1002/jctb.1988.

[258] J.J. Pignatello, E. Oliveros, A. MacKay, Advanced oxidation processes for organic contaminant destruction based on the Fenton reaction and related chemistry, Crit. Rev. Environ. Sci. Technol. 36 (1) (2006) 1–84, https://doi.org/10.1080/10643380500326564.

[259] A. Babuponnusami, K. Muthukumar, A review on Fenton and improvements to the Fenton process for wastewater treatment, J. Environ. Chem. Eng. 2 (1) (2014) 557–572, https://doi.org/10.1016/j.jece.2013.10.011.

[260] Y. Yang, J.J. Pignatello, J. Ma, W.A. Mitch, Comparison of halide impacts on the efficiency of contaminant degradation by sulfate and hydroxyl radical-based advanced oxidation processes (AOPs), Environ. Sci. Technol. 48 (4) (2014) 2344–2351, https://doi.org/10.1021/es404118q.

[261] J.E. Grebel, J.J. Pignatello, W.A. Mitch, Effect of halide ions and carbonates on organic contaminant degradation by hydroxyl radical-based advanced oxidation processes in saline waters, Environ. Sci. Technol. 44 (17) (2010) 6822–6828, https://doi.org/10.1021/es1010225.

[262] J. De Laat, T.G. Le, Effects of chloride ions on the iron (III)-catalyzed decomposition of hydrogen peroxide and on the efficiency of the Fenton-like oxidation process, Appl. Catal., B 66 (1–2) (2006) 137–146, https://doi.org/10.1016/j.apcatb.2006.03.008.

[263] M. Mahdi Ahmed, S. Barbati, P. Doumenq, S. Chiron, Sulfate radical anion oxidation of diclofenac and sulfamethoxazole for water decontamination, Chem. Eng. J. 197 (2012) 440–447, https://doi.org/10.1016/j.cej.2012.05.040.

[264] A. Kumar, G. Sharma, M. Naushad, T. Ahamad, R.C. Veses, F.J. Stadler, Highly visible active Ag_2CrO_4/Ag/$BiFeO_3$@RGO nano-junction for photoreduction of CO_2 and photocatalytic removal of ciprofloxacin and bromate ions: the triggering effect of Ag and RGO, Chem. Eng. J. 370 (2019) 148–165, https://doi.org/10.1016/j.cej.2019.03.196.

[265] R.E. Huie, C.L. Clifton, P. Neta, Equilibria of the carbonate and sulfate radical anions, Int. J. Radiat. Appl. Instrum. C Radiat. Phys. Chem. 38 (5) (1991) 477–481, https://doi.org/10.1016/1359-0197(91)90065-A.

[266] A. Eslami, F. Mahdipour, H.S. Maleksari, G. Varank, S.M. Ghasemi, P. Nejatian, A. Bagheri, S. Madihi-Bidgoli, Enhanced degradation of 2,4-dichlorphe-noxyacetic acid herbicide by CaO_2 activated by Fe(II) and ultrasound irradiation: practical insight and mineralization, Kor. J. Chem. Eng. 40 (2023) 2866–2875, https://doi.org/10.1007/s11814-023-1405-3.

[267] M. Ahmadi, F. Ghanbari, Organic dye degradation through peroxymonosulfate catalyzed by reusable graphite felt/ferriferrous oxide: mechanism and identification of intermediates, Mater. Res. Bull. 111 (2019) 43–52, https://doi.org/10.1016/j.materresbull.2018.10.027.

[268] H.B. Truong, B.T. Huy, S.K. Ray, G. Gyawali, Y.I. Lee, J. Cho, J. Hur, Magnetic visible-light activated photocatalyst $ZnFe_2O_4$/$BiVO_4$/g-C_3N_4 for decomposition of antibiotic lomefloxacin: photocatalytic mechanism, degradation pathway, and toxicity assessment, Chemosphere 299 (2022) 134320, https://doi.org/10.1016/j.chemosphere.2022.134320.

[269] K. Thomas, A. Volz-Thomas, D. Mihelcic, H.G.J. Smit, D. Kley, On the exchange of NO_3 radicals with aqueous solutions: solubility and sticking coefficient, J. Atmos. Chem. 29 (1998) 17–43, https://doi.org/10.1023/A:1005860312363.

[270] P. Neta, R.E. Huie, A.B. Ross, Rate constants for reactions of inorganic radicals in aqueous solution, J. Phys. Chem. Ref. Data 1 7 (3) (1988) 1027–1284, https://doi.org/10.1063/1.555808.

[271] R. Feizi, M. Ahmad, S. Jorfi, F. Ghanbari, Sunset yellow degradation by ultrasound/peroxymonosulfate/$CuFe_2O_4$: influential factors and degradation processes, Kor. J. Chem. Eng. 36 (2019) 886–893, https://doi.org/10.1007/s11814-019-0268-0.

[272] E.D. Black, E. Hayon, Pulse radiolysis of phosphate anions $H_2PO_4^-$, HPO_4^{2-}, PO_4^{3-}, and $P_2O_7^{4-}$ in aqueous solutions, J. Phys. Chem. 74 (17) (1970) 3199–3203, https://doi.org/10.1021/j100711a007.

[273] J. Ma, Y. Yang, X. Jiang, Z. Xie, X. Li, C. Chen, H. Chen, Impacts of inorganic anion and natural organic matter on thermally activated persulfate oxidation of BTEX in waters, Chemosphere 190 (2018) 296–306, https://doi.org/10.1016/j.chemosphere.2017.09.148.

[274] J. Wang, S. Wang, Activation of persulfate (PS) and peroxymonosulfate (PMS) and application for the degradation of emerging contaminants, Chem. Eng. J. 334 (2018) 1502–1517, https://doi.org/10.1016/j.cej.2017.11.059.

[275] B. Erim, Z. Ciğeroğlu, S. Şahin, Y. Vasseghian, Photocatalytic degradation of cefixime in aqueous solutions using functionalized SWCNT/ZnO/Fe_3O_4 under UV-A irradiation, Chemosphere 291 (2022), https://doi.org/10.1016/j.chemosphere.2021.132929.

[276] J.J. Pignatello, D. Liu, P. Huston, Evidence for an additional oxidant in the photoassisted Fenton reaction, Environ. Sci. Technol. 33 (1999) 1832–1839, https://doi.org/10.1021/es980969b.

[277] J. He, X. Yang, B. Men, D. Wang, Interfacial mechanisms of heterogeneous Fenton reactions catalyzed by iron-based materials: a review, J. Environ. Sci. 39 (2016) 97–109, https://doi.org/10.1016/j.jes.2015.12.003.

[278] Q. Li, H. Kong, P. Li, J. Shao, Y. He, Photo-Fenton degradation of amoxicillin via magnetic TiO_2-graphene oxide-Fe_3O_4 composite with a submerged magnetic separation membrane photocatalytic reactor (SMSMPR), J. Hazard Mater. 373 (2019) 437–446, https://doi.org/10.1016/j.jhazmat.2019.03.066.

[279] C. Lai, F. Huang, G. Zeng, D. Huang, L. Qin, M. Cheng, C. Zhang, B. Li, H. Yi, S. Liu, L. Li, L. Chen, Fabrication of novel magnetic $MnFe_2O_4$/bio-char composite and heterogeneous photo-Fenton degradation of tetracycline in near neutral pH, Chemosphere 224 (2019) 910–921, https://doi.org/10.1016/j.chemosphere.2019.02.193.

[280] U. Ushani, X. Lu, J. Wang, Z. Zhang, J. Dai, Y. Tan, S. Wang, W. Li, C. Niu, T. Cai, N. Wang, G. Zhen, Sulfate radicals-based advanced oxidation technology in various environmental remediation: a state-of-the–art review, Chem. Eng. J. 402 (2020) 126232, https://doi.org/10.1016/j.cej.2020.126232.

[281] A. Matilainen, M. Sillanpää, Removal of natural organic matter from drinking water by advanced oxidation processes, Chemosphere 80 (4) (2010) 351–365, https://doi.org/10.1016/j.chemosphere.2010.04.067.

[282] X. Zhang, M. Feng, R. Qu, H. Liu, L. Wang, Z. Wang, Catalytic degradation of diethyl phthalate in aqueous solution by persulfate activated with nano-scaled magnetic $CuFe_2O_4$/MWCNTs, Chem. Eng. J. 301 (2016) 1–11, https://doi.org/10.1016/j.cej.2016.04.096.

[283] Global Petrol Prices, 2023. https://www.globalpetrolprices.com/electricity_prices/.

[284] Q. Yu, J. Pan, X. Ren, Q. Wang, N. Shi, Y. Li, Influence of preparation methods in the structure and properties of Fe_2O_3/g-C_3N_4 composite catalysts, Mater. Sci. Semicond. Process. 148 (2022), https://doi.org/10.1016/j.mssp.2022.106800.

[285] K.C. Christoforidis, T. Montini, E. Bontempi, S. Zafeiratos, J.J.D. Jaén, P. Fornasiero, Synthesis and photocatalytic application of visible-light active β-Fe_2O_3/g-C_3N_4 hybrid nanocomposites, Appl. Catal., B 187 (2016) 171–180, https://doi.org/10.1016/j.apcatb.2016.01.013.

[286] S. Shanavas, S. Mohana Roopan, A. Priyadharsan, D. Devipriya, S. Jayapandi, R. Acevedo, P.M. Anbarasan, Computationally guided synthesis of (2D/3D/2D) rGO/Fe_2O_3/g-C_3N_4 nanostructure with improved charge separation and transportation efficiency for degradation of pharmaceutical molecules, Appl. Catal., B 255 (2019), https://doi.org/10.1016/j.apcatb.2019.117758.

[287] M. Hazarika, P. Chinnamuthu, J.P. Borah, MWCNT decorated $MnFe_2O_4$ nanoparticles as an efficient photo-catalyst for phenol degradation, J. Mater. Sci. Mater. Electron. 29 (2018) 12231–12240, https://doi.org/10.1007/s10854-018-9334-3.

[288] P. Guo, X. Hu, ZIF-derived CoFe$_2$O$_4$/Fe$_2$O$_3$ combined with g-C$_3$N$_4$ as high-efficient photocatalysts for enhanced degradation of levofloxacin in the presence of peroxymonosulfate, J. Alloys Compd. 914 (2022) 165338, https://doi.org/10.1016/j.jallcom.2022.165338.

[289] R. Li, M. Cai, Z. Xie, Q. Zhang, Y. Zeng, H. Liu, G. Liu, W. Lv, Construction of heterostructured CuFe$_2$O$_4$/g-C$_3$N$_4$ nanocomposite as an efficient visible light photocatalyst with peroxydisulfate for the organic oxidation, Appl. Catal., B 244 (2019) 974–982, https://doi.org/10.1016/j.apcatb.2018.12.043.

[290] M.W. Kadi, R.M. Mohamed, D.W. Bahnemann, MgFe$_2$O$_4$ decoration of g-C$_3$N$_4$ nanosheets to enhance CIP oxidation in visible-light photocatalysis, Opt. Mater. 121 (2021), https://doi.org/10.1016/j.optmat.2021.111598.

[291] J. Yan, B. Chai, Y. Liu, G. Fan, G. Song, Construction of 3D/2D ZnFe$_2$O$_4$/g-C$_3$N$_4$ S-scheme heterojunction for efficient photo-Fenton degradation of tetracycline hydrochloride, Appl. Surf. Sci. 607 (2023) 155088, https://doi.org/10.1016/j.apsusc.2022.155088.

[292] K. Saravanakumar, C.M. Park, Rational design of a novel LaFeO$_3$/g-C$_3$N$_4$/BiFeO$_3$ double Z-scheme structure: photocatalytic performance for antibiotic degradation and mechanistic insight, Chem. Eng. J. 423 (2021) 130076, https://doi.org/10.1016/j.cej.2021.130076.

[293] A. Hassani, P. Eghbali, F. Mahdipour, S. Wacław, K.Y.A. Lin, F. Ghanbari, Insights into the synergistic role of photocatalytic activation of peroxymonosulfate by UVA-LED irradiation over CoFe$_2$O$_4$-rGO nanocomposite towards effective Bisphenol A degradation: performance, mineralization, and activation mechanism, Chem. Eng. J. 453 (2023) 139556, https://doi.org/10.1016/j.cej.2022.139556.

[294] T.J. Al-Musawi, P. Rajiv, N. Mengelizadeh, F. Sadat Arghavan, D. Balarak, Photocatalytic efficiency of CuNiFe$_2$O$_4$ nanoparticles loaded on multi-walled carbon nanotubes as a novel photocatalyst for ampicillin degradation, J. Mol. Liq. 337 (2021) 116470, https://doi.org/10.1016/j.molliq.2021.116470.

[295] O. Keen, J. Bolton, M. Litter, K. Bircher, T. Oppenländer, Standard reporting of electrical energy per order (EEO) for UV/H$_2$O$_2$ reactors (IUPAC technical report), in: Pure and Applied Chemistry, De Gruyter, 2018, pp. 1487–1499, https://doi.org/10.1515/pac-2017-0603.

[296] P. Asaithambi, E. Alemayehu, B. Sajjadi, A.R.A. Aziz, Electrical energy per order determination for the removal pollutant from industrial wastewater using UV/Fe^{2+}/H$_2$O$_2$ process: optimization by response surface methodology, Water Resour. Ind. (2017), https://doi.org/10.1016/j.wri.2017.06.002.